CHAPTER 7

DRUG PARAMETERS

> "It is much easier to make measurements than to know exactly what you are measuring."
>
> —J. W. N. Sullivan

It is critically important to prepare high quality input data for high quality biopharmaceutical modeling. Even though it might look easy, the experiments are actually very difficult and meticulous care is required to obtain high quality data. More than twofold error could occur easily. Considering the propagation of error, even a small error in each parameter could pile up to a significant error in the final output. It is important to understand the specification of each experiment, pros and cons of each method, and accuracy level of each data. In this section, experimental methods to obtain the drug parameters for biopharmaceutical modeling are discussed.

7.1 DISSOCIATION CONSTANT (pK_a)

The dissociation constant (K_a) of a drug is one of the most important parameter for biopharmaceutical modeling. pK_a affects solubility (Henderson–Hasselbalch equation; Section 2.3.2), the dissolution rate (solid surface pH; Section 3.2.6), and permeability (pH partition theory; Section 4.8). Even though computational prediction from the chemical structure is available, it is highly recommended

Biopharmaceutics Modeling and Simulations: Theory, Practice, Methods, and Applications, First Edition. Kiyohiko Sugano.

to use a measured pK_a value for biopharmaceutical modeling. Computational prediction often has circa 1 pK_a unit error (10-fold error as K_a) [1, 2]. The pH titration, pH–UV shift, and capillary electrophoresis methods are most often used in drug discovery and development. In the case of compounds with low solubility, pK_a should also be obtained from the pH–solubility profile and compared with the values from other methods.

7.1.1 pH Titration

The pH titration method is one of the authentic methods to obtain pK_a values [3]. When the solution containing a drug is titrated by an acid or an alkali such as HCl or KOH solution, the pH change becomes less sensitive to the titrated amount around the pK_a of a drug because of the buffering effect of the drug molecules. The advantage of this method is that the pK_a of a dissociable group, which is not near the chromosphere, can be measured. The disadvantage is that this method requires 5–10 mg sample. For drugs with low solubility, an organic solvent can be added to the test solution and the pK_a values at each percentage of organic solvent are extrapolated to 0%. Automated instruments are commercially available.

7.1.2 pH–UV Shift

When a dissociable group is within or close to the chromophore of a drug, the UV spectrum changes when pH is shifted [4]. The advantages of this method are that this method requires less than 1 mg sample and a DMSO sample stock solution can be used. The disadvantage of this method is that the pK_a of a dissociable group not near the chromosphere cannot be measured. Automated instruments are commercially available. Impurities in a sample can affect the result when it has a strong chromophore.

Similar concept can be used with NMR spectroscopy, but the pK_a of a dissociable group not near the chromophore can also be measured.

7.1.3 Capillary Electrophoresis

The capillary electrophoresis method is becoming more popular recently [5–7]. When a charged molecule is put in an electric field, it migrates toward the electrode of the opposite charge. The migration index at each pH depends on f_z and z. From the pH migration index relationship (usually 10–20 pH points between pH 2–11), the pK_a value of a drug can be obtained. The advantages of this method are that this method requires less than 0.1 mg sample, a DMSO sample stock solution can be used, and this method is suitable for less pure samples. The pK_a of samples with low solubility can be measured as far as it is detectable. The 96-well format and the pressure-supported method have been implemented to increase the throughput of this method [5, 8–11].

7.1.4 pH–Solubility Profile

The pK_a of a drug can be calculated from the pH–solubility profile (Fig. 2.11) [12]. For a drug with low solubility, this method is very useful. Usually, the pH–solubility profile data becomes available at the late discovery stage [13, 14]. Because the other method can have an error in pK_a for a drug with low solubility, this method should always be applied when the pH–solubility profile is available.

7.1.5 Calculation from Chemical Structure

Even though calculation from the chemical structure is still not accurate enough to be an alternative to experimental measurements, it can support pK_a assignment. Assignment of pK_a to a functional group is often not obvious for heterocyclic drugs and other structurally complex drugs. The most often encountered misunderstandings are "nitrogen is always a base," "p$K_a > 7$ always denoted basicity," "p$K_a < 7$ always denoted acidity," etc. Some programs predict both macro- and micro-pK_as for multivalent drugs.

7.1.6 Recommendation

The pK_a data is the most crucial data for biopharmaceutical modeling. It affects solubility, dissolution rate, permeability, cytosol concentration, etc. Therefore, pK_a should be obtained with good precision (<0.1 log unit error is preferable). To increase the robustness, two or more methods can be used and the pK_a values can be compared. In real drug discovery, it is often the case that a discrepancy between the methods is observed, especially for drugs with low solubility.

7.2 OCTANOL–WATER PARTITION COEFFICIENT

The octanol–water partition coefficient of a drug is one of the most reliably obtainable data in drug discovery and should be experimentally measured before starting biopharmaceutical modeling. The importance of log P_{oct} is often underestimated. This is the key parameter not only for biopharmaceutical modeling but also for understanding the pharmacokinetics of a drug, for example, distribution to each organ (including CNS and liver) [15–17] and renal reabsorption. Furthermore, log P_{oct} is often related to the toxicity of a drug, for example, phospholipidosis [18]. In biopharmaceutical modeling, log P_{oct} is used for estimating $P_{trans,0}$, intrinsic solubility, K_{bm}, etc. log P_{oct} value is the most consistent data obtained from laboratories. log P_{oct} is a common language among many disciplines in drug discovery and development. We have a huge wealth of knowledge about log P_{oct}. Therefore, as the *de facto* standard lipophilicity parameter, log P_{oct} has an irreplaceable value in drug discovery.

Even though there are many *in silico* log P_{oct} prediction programs, the prediction accuracy for a newly synthesized compound is usually not sufficient

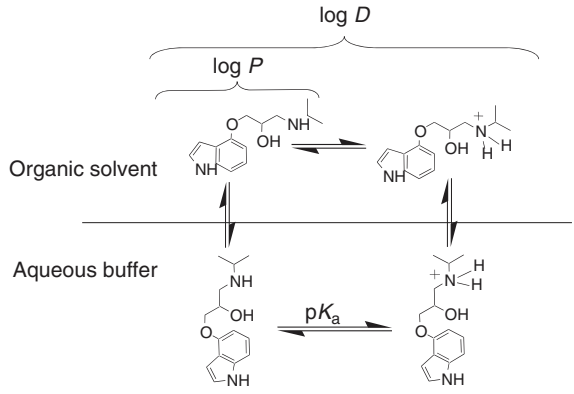

Figure 7.1 log P_{oct} and log D_{oct}.

(on average, circa 10-fold error) [19, 20]. Therefore, it is highly recommended to use an experimental log P_{oct} data for biopharmaceutical modeling.

Figure 7.1 explains the difference between log P_{oct} and log D_{oct}. log P_{oct} is the logarithm of the partition coefficient of undissociated (unionized) drug molecules between octanol and water, whereas log D_{oct} is the logarithm of the distribution coefficient as the sum of undissociated and ionized species at a pH.

To measure log P_{oct}, a pH in which the drug does not dissociate is used. log P_{oct} can be also back-calculated from log D_{oct}, pK_a, and pH (cf. $D_{oct} = f_0 P_{oct}$). When using the latter method, the ion pair partitioning of the dissociated species should be kept at a minimum [21].

For zwitterions, it is impossible to separately measure the concentration of neutral and zwitterionic species. Therefore, log D_{oct} should be measured at a physiological pH of interest [22]. The lipophilicity of zwitterion species is usually higher than that of the monoanionic and monocationic species and the pH–lipophilicity profile becomes bell shaped. Even when the zwitterionic species is predominant at a physiological pH, many zwitterionic drugs have good membrane permeability, for example, fluoroquinolones [23]. It should be noted that some software calculate log P_{oct} as of the undissociated species ([AH-B] in Figure 2.5), while the others calculate it as of the total of neutral species ([AHB] + [A-BH$^+$]).

7.2.1 Shake Flask Method

The shake flask (SF) method is the gold standard method to experimentally determine log P_{oct} and log D_{oct}. With a standard SF method, log D_{oct} can be reliably measured within $-2 < \log D_{oct} < 4$ range ($0.01 < D_{oct} < 10,000$). This dynamic range is significantly wider than that of an *in vitro* membrane permeability assay such as Caco-2 ($0.1–20 \times 10^{-6}$ cm/s for P_{ep} measurement). However, when log $D_{oct} > 4$, standard experimental methods could have significant artifact as a result

of the contamination of octanol and water phases. An improved method to avoid the octanol-phase contamination has been reported [24, 25].

7.2.2 HPLC Method

HPLC-based methods have been extensively investigated [26–28]. The retention time of reverse phase HPLC correlates with the lipophilicity of a drug. However, the chemical selectivity largely depends on the characteristics of the stationary and mobile phases. Therefore, the stationary and mobile phases have to be carefully selected so that the chemical selectivity of an HPLC method becomes similar to that of real octanol–water partitioning. The advantage of this method is that it can be applied for high log P_{oct} range. The disadvantage of this method is that the chemical selectivity is not perfectly identical to octanol–water partitioning, especially for acidic compounds. Micelle capillary electrophoresis has also been used to estimate log P_{oct} [29–32].

7.2.3 Two-Phase Titration Method

The pH titration curve shifts with and without the coexistence of organic phase [33, 34]. The two-phase titration method can be used to obtain the partition coefficient of both unionized and ionized species.

7.2.4 PAMPA-Based Method

Recently, a PAMPA (parallel artificial membrane permeation assay)-based method was reported (Section 7.9.4). The PAMPA setup enables HTS (high throughput screening) measurement. To measure log P_{oct} by PAMPA [35], octanol is impregnated into the filter membrane for permeability measurement. The permeability value is then converted to the partition coefficient.

7.2.5 *In Silico* Method

Various algorithms have been investigated to calculate the octanol–water partition coefficient from the chemical structure. However, the prediction accuracy is still often more than 10-fold (>1 log unit) for a newly synthesized compound [19]. If two or more software are available, it would be a good practice to compare the results. If the prediction values from different algorithms converge to a similar value, the estimated value would be more reliable. This consensus-based approach was found to predict the log P_{oct} value more accurately compared to the sole use of a software [19].

7.2.6 Recommendation

As an authentic method, the SF method is recommended as the first choice. This data is often used for regulatory submission. An *in silico* method can be

helpful for experimental design and sanity check of the experiment. For the drugs with log $D_{oct} > 4$, the standard SF method cannot be applied. On the other hand, *in silico* prediction tends to be more reliable for compounds with high lipophilicity, as they have less intramolecular hydrogen bonds [19]. Therefore, for the drugs with log $D_{oct} > 4$, *in silico* log P_{oct} prediction could be more reliable than the experimental ones unless otherwise a specialized experimental method is used. In biopharmaceutical modeling, when log $D_{oct} > 3$, the prediction error of log D_{oct} has little impact on P_{eff} prediction.

7.3 BILE-MICELLE PARTITION COEFFICIENT (K_{BM})

Bile-micelles affect not only the solubility and dissolution rate but also the effective permeability of a drug. Without considering bile-micelle binding, P_{eff} cannot be appropriately estimated. The bile-micelle binding is especially important to estimate the food effect (both positive and negative food effects). Owing to the amphiphilic nature of bile micelles, even a hydrophilic drug such as nadolol can bind to bile micelles.

Prediction of K_{bm} from log P_{oct} is discussed in Section 2.2.5. In this section, experimental methods are discussed. As the bile micelles do not have a distinct critical micelle concentration and as a dynamic equilibrium exist between monomer, aggregates, and micelles, equilibrium dialysis and ultrafiltration are not suitable to separate free monomer molecules from bile-micelle-bound molecules.

7.3.1 Calculation from Solubility in Biorelevant Media

K_{bm} can be calculated from the experimental solubility data in a biorelevant media and a simple buffer [36, 37]. This method is useful for compounds with low solubility. For dissociable compounds, $K_{bm,z}$ of cation and anion species can be estimated as one-tenth and one-hundredth of $K_{bm,0}$, respectively [38, 39].

Example The $K_{bm,0}$ for a base with $pK_a = 7$ from the solubility in 3 mM bile-micelle media $S_{dissolv} = 40$ μg/ml and $S_0 = 2.4$ μg/ml can be calculated as follows. By assuming K_{bm+} is one-tenth of the K_{bm0}, Equation 2.27 can be rearranged to

$$K_{bm,0} = \left[\frac{S_{dissolv}}{S_0} - \left(1 + \frac{[H^+]}{K_a}\right)\right]\left(\frac{\text{Water}}{\text{Bile acid}}\right)\left(1 + \frac{[H^+]}{K_a}\frac{1}{10}\right)^{-1}$$

$$= \left[\frac{40}{2.4} - \left(1 + \frac{10^{-6.5}}{10^{-7}}\right)\right]\frac{55600}{3}\left(1 + \frac{10^{-6.5}}{10^{-7}}\frac{1}{10}\right)^{-1} = 1.8 \times 10^5$$

7.3.2 Spectroscopic Method

The UV and fluorescent spectroscopies can be used to obtain K_{bm} [40]. When a chromophore is put in different environments, such as water and bile micelles, its spectrum changes. Therefore, like the pH–UV titration method for pK_a measurement, a bile micelle titration curve can be obtained. This method is useful for compounds with high solubility. Even though it is often neglected in the literature, many hydrophilic bases such as nadolol and atenolol can bind to bile micelles, resulting in reduction of the effective permeability [41–43].

7.3.3 Recommendations

For drugs with low solubility, the solubility method is most appropriate. The solubility data in the blank media and biorelevant media such as the fasted state simulated intestinal fluid (FaSSIF) is usually readily available in drug discovery and development. For drugs with high solubility, the solubility method might not be suitable. In this case, the spectroscopic method would be suitable.

7.4 PARTICLE SIZE AND SHAPE

Particle size is one of the most important information for biopharmaceutical modeling. There are several methods to define the size of a particle (Fig. 7.2).

In biopharmaceutical modeling, weight-based particle size distribution is used, as it is straightforward to apply for the dissolution equations. D50 is the accumulative value at which it becomes 50% of the weight. D50 and D90 are often used to characterize the particle size distribution. D[4, 3] is also used as a representative diameter. The definitions of these parameters are illustrated in Figure 7.3 and Table 7.1.

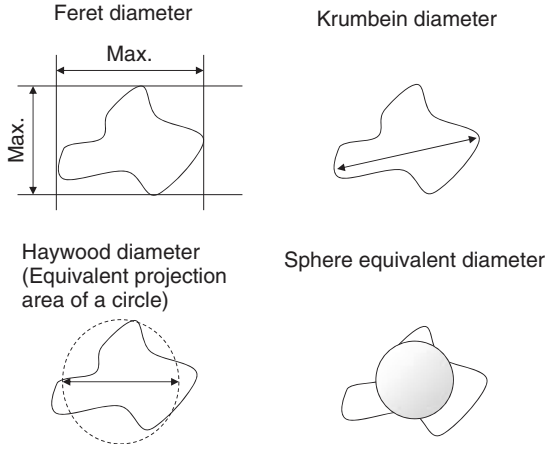

Figure 7.2 Definition of particle diameter.

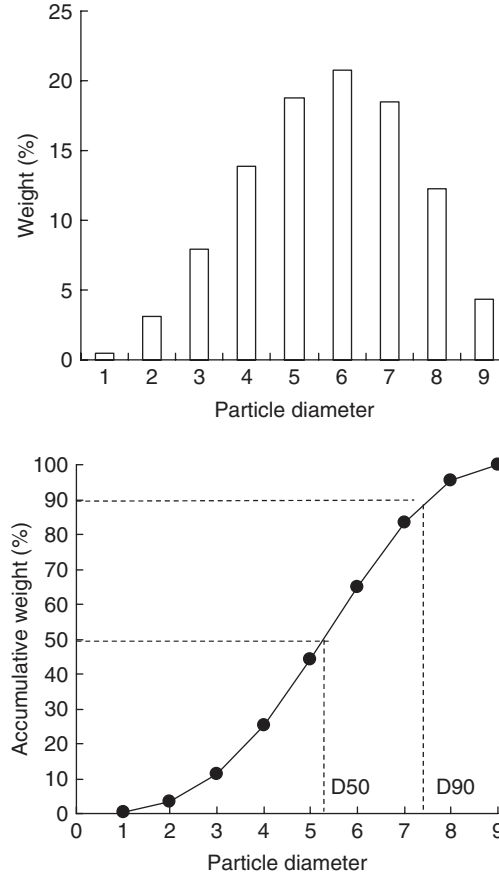

Figure 7.3 Definition of D50 and D90.

Aerodynamic diameter (d_{AD}) is also used to characterize an inhalation formulation.

$$d_{AD} = d\frac{\rho}{\rho_0} \quad (\rho_0 = 1\text{g/ml}) \tag{7.1}$$

7.4.1 Microscope

Even though it is the most classical method, microscopic observation is of great importance. A small amount of sample (<0.1 mg) is required for microscopic analysis. To increase the visibility of the sample, the drug powder is often mixed with an inert oil such as silicon oil. The particle size can be easily calculated using graphical analysis software.

The flow particle image analyzer (FPIA) is an application of this method. A dilute suspension of particles is passed through a measurement cell where

TABLE 7.1 Example of D[4,3] Calculation

Diameter of Particle Bin, $d(=2r)$	Particle Number in Each Bin, n	Volume per Particle, $v_p = 4/3\pi r^3 n$	Weight in Particle Size Bin, $v_p \times \rho$	Weight, %	Accumulative Weight, %	$d \times n$	$d^2 \times n$	$d^2 \times n$	$d^4 \times n$
1	81	0.523	42	0.49	0.49	81	81	81	81
2	64	4.187	268	3.07	3.56	128	256	512	1024
3	49	14.130	692	7.94	11.50	147	441	1323	3969
4	36	33.493	1206	13.83	25.32	144	576	2304	9216
5	25	65.417	1635	18.75	44.07	125	625	3125	15625
6	16	113.040	1809	20.74	64.81	96	576	3456	20736
7	9	179.503	1616	18.52	83.34	63	441	3087	21609
8	4	267.947	1072	12.29	95.63	32	256	2048	16384
9	1	381.510	382	4.37	100.00	9	81	729	6561
Total —	285	—	8721	100	—	D[1,0]	D[2,1]	D[3,2]	D[4,3]
—	—	—	—	—	—	$\sum dn/\sum n$	$\sum d^2n/\sum dn$	$\sum d^3n/\sum d^2n$	$\sum d^4n/\sum d^3n$
—	—	—	—	—	—	2.894737	4.04	5	5.712871

images of each particle are captured using stroboscopic illumination and a CCD camera.

7.4.2 Laser Diffraction

The laser diffraction method is widely used in drug discovery and development as a convenient and robust method. This method is suitable for one to several hundred micrometer range, covering most of the API particle size. This method assumes a spherical particle shape.

7.4.3 Dynamic Laser Scattering (DLS)

Dynamic laser scattering (DLS) is used to measure the particle size less than the micrometer range, such as nanomilled particle, emulsions, and micelles. The measurement is very simple and easy, and it is routinely used in formulation investigations. Figure 7.4 shows the size of bile micelles measured by DLS. This method can be combined with the zeta potential (surface charge) measurement.

7.4.4 Recommendations

Microscopic observation should be performed every time a new batch of API is synthesized. The particle size can change during formulation preparation. Therefore, the particle size should be monitored before and after the formulation process.

7.5 SOLID FORM

Even though the information about the solid form of a drug is not directly used in biopharmaceutical modeling, this information is critically important to interpret the results of biopharmaceutical modeling. Different solid forms show different apparent solubility and dissolution profiles. The information about the solid form must be presented together with the results of biopharmaceutical modeling. Therefore, this subject is briefly discussed in this section to cover the minimum knowledge required for biopharmaceutical modeling. This knowledge would also enhance the communication among the biopharmaceutical scientists, solid state chemists, and formulation scientists.

7.5.1 Nomenclature

7.5.1.1 Crystalline and Amorphous. Figure 7.5 illustrates the difference between amorphous and crystalline forms. In crystalline forms, the atoms of a drug have defined positions in a crystal lattice. On the other hand, the amorphous form has little regularity in the arrangement of the atoms. The solid form is diagnosed as crystalline by (i) sharp peaks of powder X-ray diffraction (PXRD), (ii) defined melting point, (iii) sharply defined particle shape, and (iv) birefringence under polarized light microscopy (PLM). An amorphous form does not have

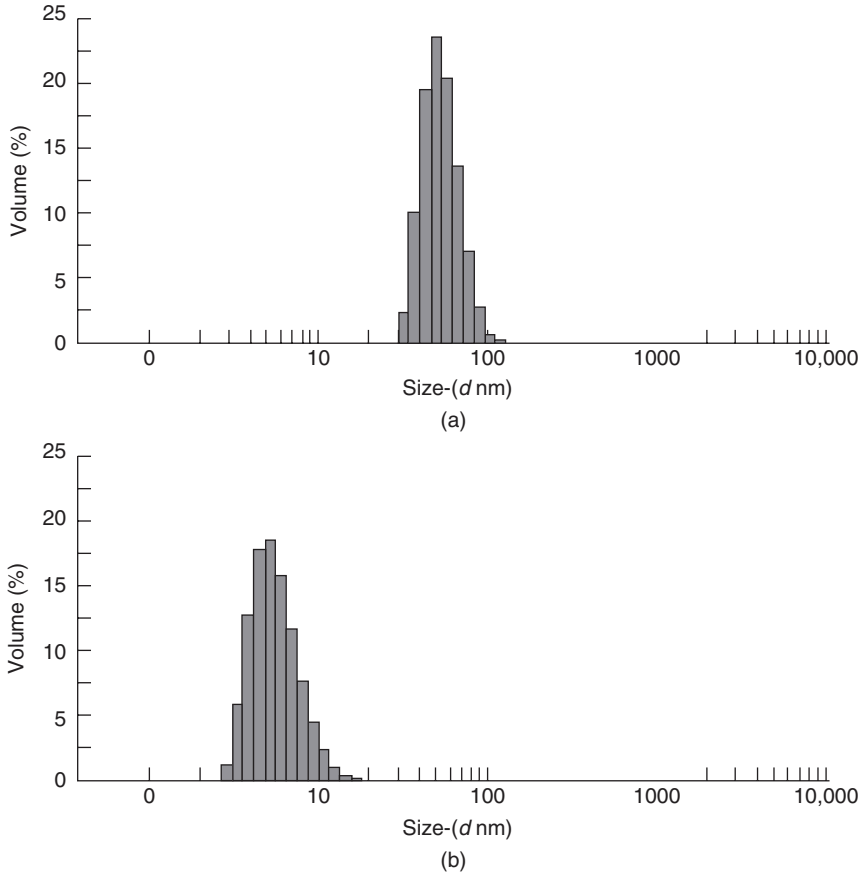

Figure 7.4 DLS data of (a) fasted and (b) fed state simulated intestinal fluids (FaSSIF and FeSSIF).

these characteristics. Even though an amorphous form shows no sharply defined melting point, it has a glass-transition temperature (T_g). Below T_g, the amorphous form has certain properties of a crystalline solid, such as plastic deformation, and is referred to as *glassy*, whereas above T_g, it has certain properties of a liquid, such as molecular mobility, and is referred to as *rubbery* [44].

7.5.1.2 Salts, Cocrystals, and Solvates. Salts, cocrystals, and solvates are binary- or multiple-component systems. The difference between a salt and cocrystal is the nature of the chemical bond. In the salt form, the chemical bond between the drug and the cofactor is an ionic bond, whereas in cocrystals, it is the hydrogen bond and other intermolecular interactions. When the countercomponent of a cocrystal is a solvent, it is referred to as a *solvate*. Except ethanolate and hydrate, no solvate has been marketed.

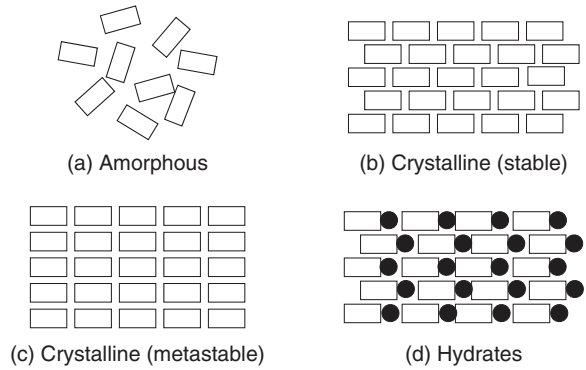

Figure 7.5 Crystalline and amorphous forms.

7.5.1.3 Hydrate. Hydrate is a kind of solvate. Many of the marketed drugs are manufactured as hydrates. In water, a hydrate has lower solubility than an anhydrate [45]. To find a hydrate, the drug is suspended as a slurry in various solvents with different water activity and the conversion of the solid form is monitored. Dynamic vapor sorption (DVS) data is also useful to identify and characterize a hydrate form. To measure the critical relative humidity, long-term sample weight monitoring would be suitable. The samples are stored in humidity-controlled chambers and the sample weight and solid form are monitored. The use of saturated salt solution is a convenient and inexpensive method to control the humidity in a chamber.

In a suspension formulation, an anhydrate can transform into a hydrate during formulation preparation and storage. Therefore, when using a suspension formulation for preclinical and clinical PK studies, the solid form of API particles in the suspension formulation should be confirmed.

7.5.2 Crystal Polymorph

7.5.2.1 True Polymorph and Pseudopolymorph. When solid forms of a drug have the same molecular component but different stacking patterns, the relationship between these solids is "true polymorph" (Fig. 7.5b and c). On the other hand, when the solids have the additional molecular component, the relationship between these solids is "pseudopolymorph" (Fig. 7.5d), for example, hydrates and cocrystalline forms.

7.5.2.2 Kinetic Resolution versus Stable Form. When solid forms of a drug show multiple polymorphs, the most stable form is usually selected for drug development to mitigate the risks of polymorph change during the manufacture processes and long-term storage. When discussing the thermodynamic stability of solid forms, the following two perspectives should be kept in mind: kinetic resolution and enantiotropy.

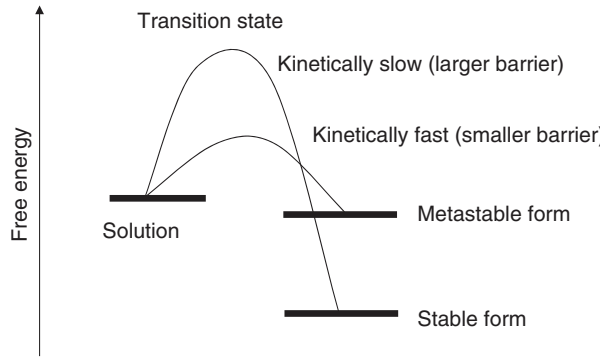

Figure 7.6 Kinetic resolution and stable form.

When various solvents are used for recrystallization, different solids form can be recrystallized from different solvents. However, the most stable form is basically always the same even in different solvents and atmosphere (except pseudopolymorphs).[1] The reason for having different polymorphs from recrystallization with different solvents is that the free energy barrier at the transition state of crystallization is different from that at equilibrium (Fig. 7.6). A metastable form can precipitate out faster than a more stable form via a kinetically favored route (with lower free energy barrier). The Ostwald rule of stage suggests that a less stable form tends to precipitate out faster [46]. The less stable form first generated in a recrystallization process would then eventually become a more stable form, leading to the most stable form if we wait for infinite time.

7.5.2.3 Dissolution Profile Advantages of Less Stable Forms. A less stable form of a drug can induce a supersaturated dissolved drug concentration in the GI tract, which eventually settles down to the equilibrium solubility of more stable forms. An amorphous form can induce a significantly higher dissolved drug concentration compared to a crystal form [47]. Therefore, a less stable form is advantageous compared to a more stable form for oral absorption. However, it is disadvantageous for manufacturing and long-term storage.

The difference in solubility between amorphous and crystalline forms could reach 10,000-fold [47]. On the other hand, the difference between polymorphs is less than fourfold in more than 80% cases [45].

7.5.2.4 Enantiotropy. In the case of enantiotropic polymorphs, the rank order of the stability of each solid form switches as temperature changes. The more stable form can be different at room temperature and a higher temperature (e.g., at a melting point; Fig. 7.7). Therefore, a polymorph with the highest melting point is not always the most stable form at room temperature. To compare the stability of polymorphs at room temperature, two polymorphs are put together

[1]So the solvent slurry method can be used to identify a more stable form in the air atmosphere.

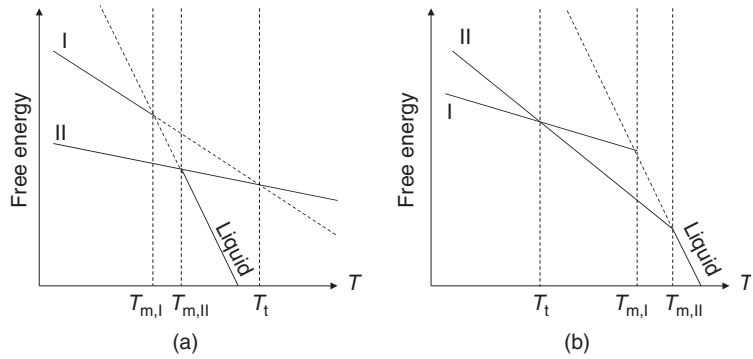

Figure 7.7 Free energy relationships of (a) monotropic and (b) enantiotropic crystalline forms.

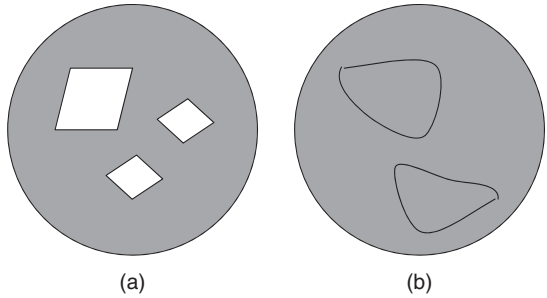

Figure 7.8 PLM image of (a) crystalline and (b) amorphous forms.

in a solvent as a slurry [48]. A less stable form eventually converts to a more stable form at room temperature.

7.5.3 Solid Form Characterization

7.5.3.1 Polarized Light Microscopy (PLM). The first step to characterize the solid form of a drug would be PLM (Fig. 7.8). Under the cross-polarized light, the crystalline forms look bright, whereas amorphous forms look dark. Crystalline/amorphous form can be also judged from the sharpness of the edge of particles. Owing to its convenience and small sample requirement, PLM is usually used as the first measure to diagnose crystalline/amorphous form.

7.5.3.2 Powder X-Ray Diffraction (PXRD). PXRD is most often used as a definitive method to identify a solid form. When the difference between the path length ($d \sin\theta$, where d is the spacing between the plains of crystal lattice and θ is the incident angle) and the wavelength of the X-ray (λ) satisfy the Bragg equation, $2d \sin\theta = n\lambda$, interference of the X-ray occurs (Fig. 7.9).

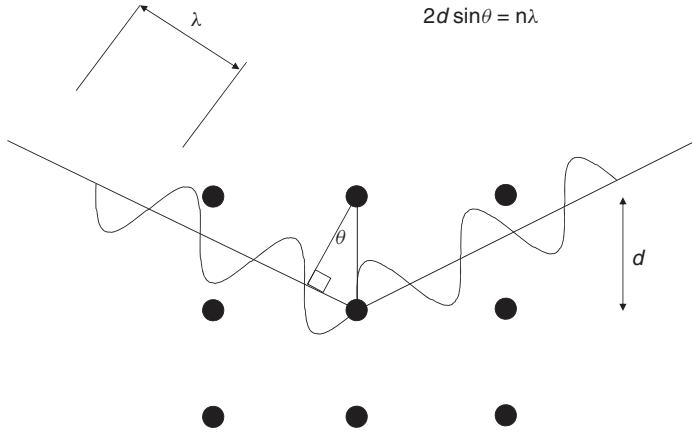

Figure 7.9 Bragg's equation.

The PXRD chart of an API is interpreted as a fingerprint of polymorphs (an example can be found in Figure 11.4). The position, but not the intensity, of the peak is used to identify the crystal form. The PXRD pattern can be used to diagnose the crystalline/amorphous form. The PXRD spectrum of a crystal shows multiple sharp peaks, whereas that of an amorphous form shows a broad halo spectrum.

Usually, a small amount of the solid sample (>1–5 mg) is put on a sample plate. The inlet beam angle of (2θ in $5^\circ \sim 35^\circ$ range) is usually used for solid form identification. Depending on the difference in crystal habit and sample orientation, the relative intensity of each peak can be changed (even a peak can appear or disappear). The amorphous content can be semiquantitatively estimated from the PXRD data, for example, by the Ruland method [49].

7.5.3.3 Differential Scanning Calorimeter (DSC) and Thermal Gravity (TG). Differential scanning calorimeter (DSC) and thermal gravity (TG) are used to characterize the thermal behavior of a solid form. The DSC methods are further categorized as power compensation DSC and heat flow DSC. TG is often coupled with differential thermal analysis (TG/DTA).

The analytical principles of heat flow DSC and DTA are the same, but the former is designed to enhance quantitative analysis. Figure 7.10 is the schematic of a DSC instrument. The reference material and the analytical sample (~5 mg) are put in the heater chamber. The chamber is then heated gradually (e.g., 10°C/min). The temperature of the sample and the reference is recorded. When the sample melts, the temperature of the sample becomes lower than that of the reference. In the case of power compensation DSC, as a temperature difference between the sample and the reference is detected, the sample is heated to maintain identical temperatures (Fig. 7.11).

From the DSC data, the melting point (T_m) and heat of fusion (ΔH_m, the area of the peak) can be obtained. As the free energy (G) of the solid and melt

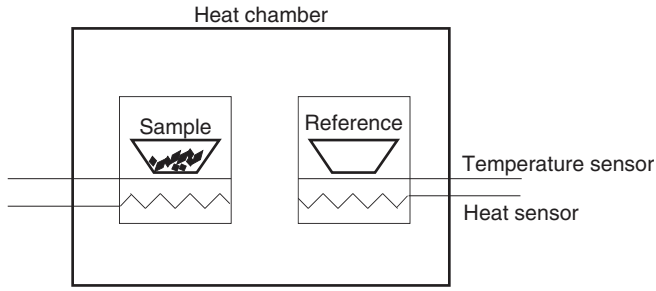

Figure 7.10 Differential scanning calorimeter.

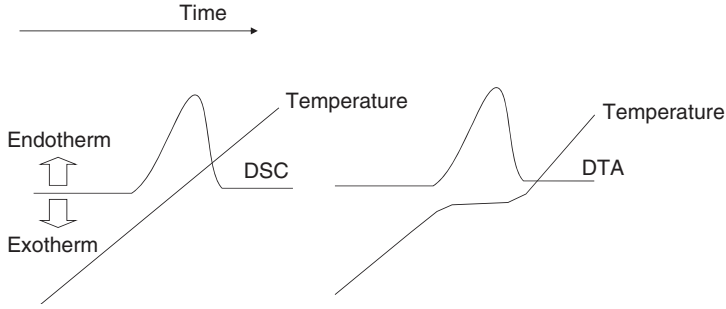

Figure 7.11 DSC and DTA charts.

material becomes the same at the melting point temperature (i.e., $\Delta G = 0$),[2] the entropy of melting (ΔS_m) can be calculated as

$$\Delta S_m = \frac{\Delta H_m}{T_m} \qquad (\text{cf.} \Delta G = T_m \Delta S_m - \Delta H_m) \tag{7.2}$$

ΔS_m is used to estimate the difference in solubility between crystalline and amorphous forms (Section 2.3.8).

From the TG data, information about solvates (e.g., hydrates) can be obtained. In addition, decomposition of a drug by heating is often observed as an exothermic event.

7.5.3.4 High Throughput Solid Form Screening. It is preferable to find the most stable form at ambient temperatures. However, it is challenging to arrive at a concrete conclusion about the possibility of finding a new and more stable form. Structure-based computational approach and high throughput solid form screening would be helpful to increase the success rate in finding the most stable form. Recent advances in laboratory automation enabled fast screening of a vast number of crystallization conditions [50–52]. To maximize the chance of finding

[2]In other words, the solid and liquid states are in equilibrium at the melting point temperature.

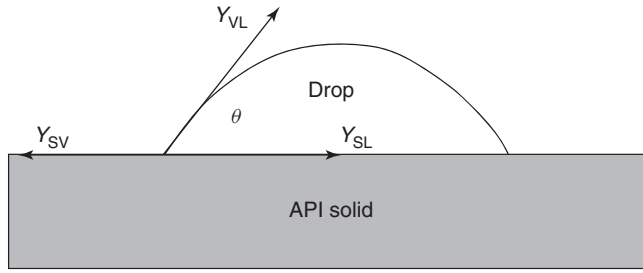

Figure 7.12 Sessile drop method.

the most stable form, a set of solvents with a variety of solvent characters can be selected.

7.5.4 Wettability and Surface Free Energy

The initial wetting process of the surface of drug particles is an important determinant of the dissolution profile in an aqueous media. In most cases, the wettability issue can be fixed during the formulation process. Therefore, wettability is rarely considered in the API form selection process. The formulation process has a significant impact on the API wetting process, and the wettability data of a pure API cannot be directly applied for the API in a formulation.

The sessile drop method (Fig. 7.12) is most often used, although it is not a robust and convenient method. The surface energy between (i) solid and liquid (γ_{SL}), (ii) solid and vapor (γ_{SV}), and (iii) liquid and vapor (γ_{LV}) and the contact angle (θ) are related by the Young equation.

$$\gamma_{SV} = \gamma_{SL} + \gamma_{LV} \cos\theta \tag{7.3}$$

7.5.5 True Density

The true density of an API is used to calculate the dissolution rate in biopharmaceutical modeling. It affects the surface area per weight of drug particles (Section 3.2.3). In addition, true density affects the sedimentation terminal velocity of API particles and hence the UWL thickness on API particles (Section 3.2.4).

The true density[3] of drugs (ρ_p) is in the 1.1–1.5 g/cm^3 range in most cases, and 1.2 g/cm^3 is often used as the average value. Girolami developed a simple "back of the envelope" method to calculate true density from a chemical formula [53, 54].

$$\rho_p(\text{g/cm}^3) = \frac{\text{MW}}{v_m} \tag{7.4}$$

where v_m is the molecular volume (Section 2.3.9).

[3]This should not be confused with bulk density and tap density, which are usually less than 1 g/cm^3.

7.6 SOLUBILITY

Solubility of a drug plays one of the central roles in biopharmaceutical modeling. In this section, we start with the terminology of solubility and then move toward the experimental methods. The definition of "solution" or "dissolved state" is discussed in Section 2.1.

7.6.1 Terminology

Most scientists are familiar with the word "solubility," and it is often used carelessly, leading to various misconceptions. These misconceptions may be caused by unclear terminology.

7.6.1.1 Definition of Solubility. Solubility is an equilibrium value per se. However, to avoid confusion, in this book, the term *equilibrium solubility* is used when needed. Equilibrium solubility is defined as the concentration of a compound in a solution that is in contact with an excess amount of the solid compound (equilibrium maker) when the concentration and the solid form do not change over time (i.e., the system is at equilibrium). A time course measurement is essential to confirm that the system reached equilibrium.

7.6.1.2 Intrinsic Solubility. In the literature, the term *intrinsic solubility* implicitly refers to the equilibrium solubility of a free form. Therefore, strictly speaking, it should be referred to as *intrinsic solubility of a free form*. The same definition is used in this book unless otherwise noted. The intrinsic solubility of a stable free form can be measured at a pH at which the drug does not dissociate (Fig. 2.9).

As discussed in Chapter 2, the intrinsic solubilities of a salt, a cocrystal, a metastable form, an anhydrate, and an amorphous form can be "theoretically" defined. In this book, these are referred as the intrinsic solubility of the form, for example, "the *intrinsic solubility of HCl salt*".

7.6.1.3 Solubility in Media. The solubility of a drug in a medium, such as a phosphate buffer and FaSSIF, is also defined as an equilibrium value. However, in this case, the solid form can convert to a different form that is more stable in the media. For example, in the pH-controlled region, a salt form dissociates to a free form. Therefore, the *equilibrium solubility* in the pH-controlled region becomes identical regardless of the starting material being a salt or a free form.[4] Therefore, when we measure the solubility of a drug, the final solid form should always be checked and this information should always be associated with the solubility value when interpreting the data (Section 16.3).

[4]One of the most often observed mistakes in biopharmaceutical modeling is that a salt form and a free form are considered to have different equilibrium solubility at a pH in a buffer.

7.6.1.4 Initial pH and Final pH. When measuring the equilibrium solubility of a drug, an excess amount of the drug is added to the media. In the case of a dissociable drug, the pH can be shifted from the initial pH by the dissolving drug, especially when a buffer with weak buffer capacity is used.[5] In this book, the pH after achieving equilibrium (i.e., the final pH) is used unless otherwise noted.

7.6.1.5 Supersaturable API. In this book, salts, cocrystals, anhydrates, amorphous forms, and other metastable forms are called *supersaturable API*. As discussed above, regardless of the starting material being a salt or a free form, in the pH-controlled region (as final pH), the "experimental" equilibrium solubility of a drug usually becomes the same (strictly speaking, after infinite time, but usually within 24 h). In other words, salt formation does not increase the equilibrium solubility of a drug in the pH-controlled region. The reason a salt form increases the oral absorption of a drug is that (i) it increases the dissolution rate and (ii) it can induce the supersaturated drug concentration.[6] This point is discussed in detail in Section 11.1.

7.6.1.6 Critical Supersaturation Concentration and Induction Time. The degree of supersaturation can be defined as the drug concentration over the equilibrium solubility of a solid form ($C_{\mathrm{dissolv}}/S_{\mathrm{dissolv}}$). Critical supersaturation concentration (CSSC) is the dissolved drug concentration where nucleation of the solid form (or liquid droplet) occurs during the timescale of interest, which is several hours in biopharmaceutical modeling. Usually, the nucleation rate is steeply dependent on the degree of supersaturation (Section 3.3). Therefore, the CSSC of a drug can be defined as a characteristic value for the timescale of interest.[7]

In the literature, the term *kinetic solubility* is often used. However, literally speaking, the terms *kinetic* and *solubility* are contradictory concepts, as solubility is an equilibrium value per se. In most cases,[8] the kinetic solubility of a drug refers to the transient concentration of dissolved drug molecules immediately after the addition of a concentrated sample solution (e.g., in DMSO) to an aqueous media (typically within the timescale of several minutes to 1–2 h) [55–58]. Therefore, kinetic solubility represents the precipitation tendency in a short period of time [59]. To avoid confusion, "kinetic solubility" is not used in this book. Instead, we use "critical supersaturation concentration."

[5]In a transporter inhibition study, this point should be remembered. The concentration of inhibitor is often higher than the buffer capacity of incubation media such as Hank's balanced solution. This can result in an artifact reduction of the permeability of a dissociable drug.

[6]The experimental equilibrium solubility of a salt (which is usually the same as that of the free form) is often used in biopharmaceutical modeling for a salt. This can result in underestimation of oral absorption.

[7]Even when the degree of supersaturation is very small, after a very long time (e.g., several hundred million years), nucleation occurs at some time point and the dissolved drug concentration settles down to the equilibrium solubility. Therefore, if the timescale of interest is longer, CSSR becomes lower (Figure 11.1).

[8]Interestingly, some people use this term as "dissolution rate."

7.6.1.7 Dissolution Rate and Dissolution Profile. The dissolution rate is the rate of a drug dissolving into a media and is measured in units of amount/time (this is different from the dissolution rate coefficient (k_{diss})). In this book, the term *dissolution profile* is used as a comprehensive term, which includes equilibrium solubility, dissolution rate, supersaturation, etc.

7.6.2 Media

As the real human intestinal fluid is difficult to obtain, an artificial fluid is usually used in solubility measurements.

7.6.2.1 Artificial Stomach Fluids. As an artificial fluid for the stomach, simple HCl solutions at pH 1.2–2 are often used. More advanced media has been proposed [60].

7.6.2.2 Artificial Small Intestinal Fluids. The FaSSIF and FeSSIF (fed state simulated intestinal fluid) have been most widely used as a surrogate for the real human intestinal fluid [61, 62]. The composition of FaSSIF and FeSSIF is shown in Table 7.2. These simulated fluids contain phosphatidylcholine (PC) and taurocholic acid (TC) to mimic the bile micelles in the small intestine. When PC purified from a natural source is used, it could cause a laboratory to laboratory variation. In addition, the preparation method has a significant effect on the solubility of a drug in these media. During the preparation of FaSSIF, after dissolving PC and TC powders in a buffer, the obtained media often becomes slightly turbid. To avoid this, a concentrated FaSSIF (e.g., 30–300 mM) can be first prepared. This solution usually becomes transparent. This solution is then diluted with a blank buffer to prepare FaSSIF. After dilution, the diameter of bile micelles grows to an equilibrium value in a few hours (Fig. 3.2) [63]. This preparation process mimics the dilution of bile juice secreted from the gall bladder into the small intestine.

As a variation of FaSSIF, the bile concentration can be increased to 5 mM for dogs [64].

7.6.3 Solubility Measurement

7.6.3.1 Standard Shake Flask Method. To measure the solubility of a drug, an excess amount of the drug that would exceed the solubilization capacity (solubility × fluid volume) is added to the medium [12, 65–67]. The fluid and the undissolved solid drug are then separated by filtration (< 0.45 μm mesh size) or sedimentation.[9] When using sedimentation (usually with centrifuge), contamination of floating particles should be avoided. The first supernatant can be recentrifuged to avoid contamination (double centrifuge method).

Filter binding is often observed especially when the drug concentration is less than 10 μg/ml, resulting in an artifact low solubility. The first portion of the filtrate

[9]These methods cannot be used for nanoparticles.

TABLE 7.2 Artificial Intestinal Fluids

	Fasted State		Fed State (Snapshot Media for Fed State)				
	FaSSIF	FaSSIF-V2	Early	Middle	Late	FeSSIF	FeSSIF-V2
Sodium taurocholate, mM	3	3	10	7.5	4.5	15	10
Lecithin, mM	0.75	0.2	3	2	0.5	3	2
Glyceryl monooleate, mM	0	0	6.5	5	1	0	5
Sodium oleate, mM	0	0	40	30	0.8	0	0.8
Buffer, mM	28[a]	19.12[b]	28.6[b]	44[b]	58.09[b]	144[c]	55.02[b]
Sodium chloride, mM	—	68.62	145.2	122.8	51	—	125.5
pH	6.5	6.5	6.5	5.8	5.4	5.0	5.8
Osmolality, mOsm/kg	270	180 ± 10	400 ± 10	390 ± 10	240 ± 10	635	390 ± 10
Buffer capacity, mM/ΔpH	—	10	25	25	15	—	25

[a] Phosphate.
[b] Maleic acid.
[c] Acetate.

should be discarded to ensure that the filter binding is saturated. In the case of compounds with very low solubility (typically <1 μg/ml), the compound could bind to the test tube, pipette, etc. A recovery process with an organic solvent can be used to avoid the artifacts of these nonspecific bindings.

The dissolved drug concentration is then measured by the UV, HPLC, or LC-MS method. Usually, the detection limit of LC-MS or HPLC (<0.05 μg/ml for many cases) does not become an issue because a solubility value less than 0.1 μg/ml is practically not reliable due to significant experimental artifacts.

It is critically important to assure that the system reached equilibrium. A time course measurement is preferable to confirm equilibrium. After adding an aqueous media to a drug powder sample, it should be strongly agitated for more than 24 h. The final pH and the solid form of the undissolved drug at equilibrium must be recorded [68].

7.6.3.2 Measurement from DMSO Sample Stock Solution. It is preferable to use a solid drug material (preferably crystalline) as starting material. However, a sample stock solution is often used in early drug discovery due to its availability and ease of handling.

A sample stock solution in a rich solvent such as DMSO (>10 mM) is mixed with aqueous media. The precipitant is then separated by filtration or centrifuge. In the turbidity detection method, the stock solution is titrated into an aqueous media and the concentration at which turbidity is first observed is recorded as the solubility of the drug. A long incubation time, for example, more than 24 h, is highly recommended.

The solubility measured using a sample stock solution could be significantly higher than that measured from a solid crystalline material [69]. Three reasons have been suggested for this discrepancy: (i) the solubilization effect of DMSO, (ii) the short incubation time, and (iii) the effect of the solid state. Sugaya et al. [70] suggested that the discrepancy might be due to the difference in the solid form.

If 30 mM stock solution is available, 2 μl DMSO stock solution +200 μl aqueous media would give an upper limit of 300 μM (for MW = 400, 120 μg/ml). When a dilute DMSO stock solution is used, it can be concentrated using a centrifuge vacuum evaporator. This process might also stimulate the nucleation and increase the portion of the crystalline precipitant.

PLM analysis can be combined with this assay to obtain crystalline/amorphous information of precipitants [69]. PLM gives rapid and reasonably accurate crystalline/amorphous information. Using reversed microscope with an automatic stage, the microscopic pictures of precipitants can be taken automatically. It can be further combined with automatic graphical analysis. A disposable 96-well glass bottom plate is commercially available (<$10 per plate). On the basis of our experience, during the drug discovery stage, the drug precipitants become crystalline in about 36% cases.

7.6.3.3 Solid Surface Solubility. The surface solubility ($S_{surface}$) of a drug determines the dissolution rate of the drug. In the case of dissociable drugs, because of the buffering effect of drug molecules dissolving from the solid surface, the pH near the solid surface deviates from the bulk fluid solubility during the dissolution process. $S_{surface}$ can be lower (for free base and acid) or higher (for salts) than the equilibrium bulk solubility of the drug at a pH.

The slurry pH method can be used to estimate the solid surface solubility [71–73]. The pH values of the concentrated drug slurry in water (20–40% w/w) represent the solid surface pH.

7.6.3.4 Method for Nanoparticles. The baseline conclusion is that standard nanomization (>100 nm) does not increase the solubility of a drug.[10] The Ostwald–Freundlich equation predicts that a particle size of much less than 100 nm is required to increase the solubility of a drug (Section 2.3.9). This theoretical prediction was recently confirmed by carefully designed experiments for drugs [74]. In a standard solubility measurement method, the use of filtration and centrifuge can cause an artifactual increase in solubility by nanomization, as they cannot completely separate nanoparticles from a fluid.

The solid drug titration method would be suitable for solubility measurements of nanoparticles [74]. In this method, a suspension of nanoparticles is gradually titrated into an aqueous media and the DLS signals or turbidity signals are monitored. When the added drug amount is smaller than the solubilization capacity (solubility × volume), the drug particles completely dissolve and there is no increase in the signals. As the added amount increases, it exceeds the solubilization capacity and the signals increase. The point at which the signal starts to appear is the solubility of a drug. Using this method, it was found that by nanomizing, the increase in solubility of typical low solubility drugs[11] is only 15%, which is in good agreement with the Ostwald–Freundlich equation (Section 2.3.9). Even if we assume a very high interfacial tension of 50 mN/m, the solubility increase would be up to 20% in the greater than 100 nm range. As it is practically difficult to reduce the particle size to less than 100 nm, the effect of nanomizing on the solubility of a drug would be basically negligibly small.

7.6.4 Recommendation

The quality of solubility data is one of the key factors that affects the accuracy of biopharmaceutical modeling. When considering the cost-effectiveness, the following method would be recommended for use in drug discovery and development. Currently, computational prediction from the chemical

[10] A mechanism that explains why nanomilling increases the oral absorption of solubility-permeability limited cases is discussed in Section 4.7.2.

[11] Itraconazole (interfacial tension (mN/m) = 20, hereinafter the same), loviride (27.5), phenytoin (24.4), and naproxen (23.6).

structure has significant error and cannot be used for biopharmaceutical modeling [75].

7.6.4.1 Early Drug Discovery Stage (HTS to Early Lead Optimization). Considering the throughput required at this stage, the DMSO sample stock solution would be the starting material. The 96-well format is usually used at this stage. Even in this format, PLM, PXRD, and Raman spectroscopy can be used to determine the solid forms of precipitants with a practical throughput. Owing to the quality of the data, simple classification or mapping of drugs would be the practical use of the data at this stage. When the precipitant is crystalline, the solubility of a drug will not drop dramatically (within fourfold in 80% cases [45]) even if a more stable form appears in the later stages of drug discovery. Without the information whether the precipitant is crystalline/amorphous, a structure–solubility relationship study will be meaningless.

7.6.4.2 Late Lead Optimization Stage. At the stage before one candidate compound is selected, medium throughput/medium contents screening would be preferable. At this stage, compounds are synthesized in a singleton manner rather than combinatorially. The solubility data is used for structure design as well as to interpret the *in vivo* data. At this stage, a preclinical PK study is often performed in animals.

Considering the above situations, a miniaturized SF method would be appropriate for this stage. When more than 5 mg is available, the powder sample can be weighed into a small test tube. Simulated gastric and intestinal fluids can be used as the media. The solid state of samples should be confirmed before and after incubation. Cross-validation with the Yalkowsky equation would be useful if the melting point of a drug is available (Section 2.3.7).

These data can be used to perform biopharmaceutical modeling. As both the solid form and the dose strength for drug development are not yet known at this stage, Fa% prediction using the approximate analytical Fa% equation would be sufficient (Section 5.3.3). This would give us the minimum absorbable dose with a standard formation effort.

7.6.4.3 Transition Stage between Discovery and Development. After one or a few candidate compounds are selected, a detailed solubility profiling should be performed. Usually, detailed solid form information becomes available at this stage. A few hundred milligrams to a few grams of drug material become available for solubility measurements and the other pharmaceutical profiling (often called *preformulation*).

The pH–solubility profile (pH 1–11) with the solid form characterization should be performed at this stage [13, 14]. The pK_a and S_0 values of a drug can be estimated from this data. In addition, the solubility in FaSSIF and FeSSIF should be measured. The K_{bm} value of a drug can be estimated from this data. The pH–solubility profile data is also useful for parenteral formulation development and the other purposes in drug development.

7.7 DISSOLUTION RATE/RELEASE RATE

7.7.1 Intrinsic Dissolution Rate

The intrinsic dissolution rate (IDR) of an API is the dissolution rate per surface area per time (unit: amount/surface area/time). To measure IDR, an API powder is filled into a hole with a defined opening area and compressed to make a flat surface. The Wood apparatus has been used to measure the IDR. Recently, a miniaturized apparatus is available, such as μDISS (Fig. 7.13) [76]. It is sometimes difficult to compress the pure API into a tablet in a hole. The wetting process of the drug surface can cause a lag time.

The IDR data can be useful to differentiate between the dissolution rates of API polymorphs and salts. During the IDR experiments, conversion of the solid form is sometimes observed on the disk surface. In this case, the dissolution rate changes during the experiment.

7.7.2 Paddle Method

The paddle method is most often used as a dissolution test. Comparing the paddle apparatus with the real GI tract for their shapes, the agitation patterns, and the dynamic changes of chemical environments, it is rather fair to admit that

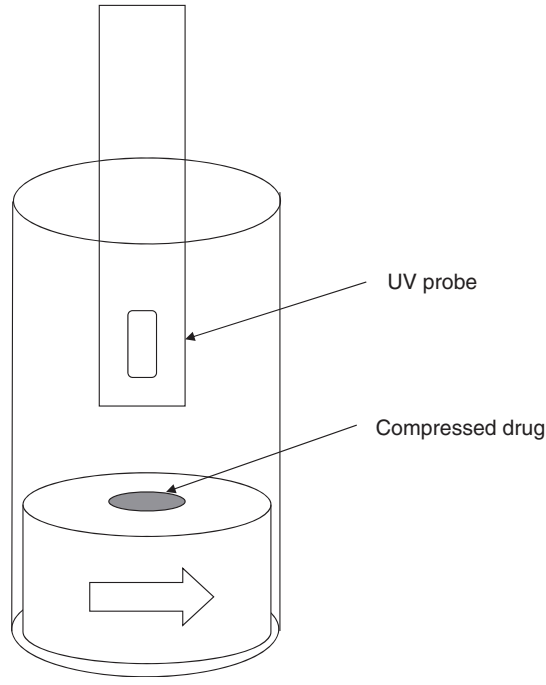

Figure 7.13 μDISS apparatus.

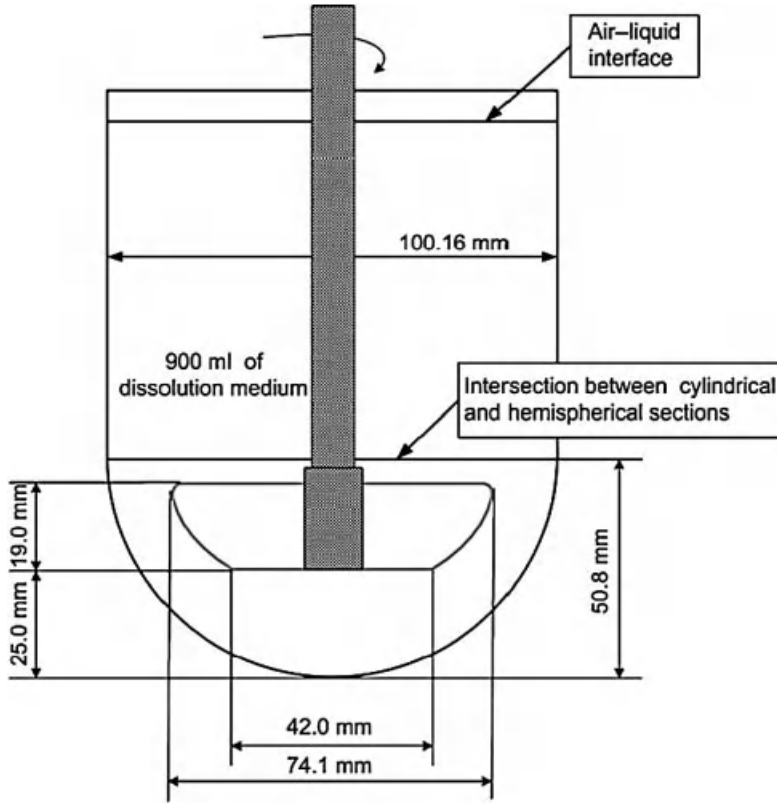

Figure 7.14 Basic geometry of USP Dissolution Testing Apparatus II. *Source:* Adapted from Reference 77 with permission.

quantitative *in vitro–in vivo* correlation is unlikely to be attainable per se using the paddle method. This notion has led to investigations for more physiological dissolution tests. However, the paddle apparatus is well standardized and the interexperimental variation is usually very small. Therefore, this method is currently used as the de facto standard method for quality control purposes.

7.7.2.1 Apparatus. The bottom of the flask is usually round, and the paddle is a semicircular plane (Fig. 7.14). In most pharmacopeias, circa 1-l flask is used for the paddle method. A miniscale paddle method (50–200 ml scale) can be used to measure the dissolution rate of API particle in drug discovery and early development.

7.7.2.2 Fluid Condition. A compendium dissolution test is usually performed under a sink condition (<30% of the saturated solubility). About 900 ml of a buffer with pH 1–7.4 is most often used. In the case of compounds with low solubility, SDS is often used to enhance the dissolution profile (up

to 9% found in the FDA dissolution database). High salt concentration is not compatible with SDS, as it forms insoluble material. The temperature is maintained at 37°C. The monographs of the dissolution test are available at http://www.fda.gov/Drugs/InformationOnDrugs/ucm135742.htm.

7.7.2.3 Agitation. The agitation strength is of great importance for the disintegration of a formulation and the dissolution of a large particle (D50 > 50 μm). The paddle speed for a compendium paddle method is usually 50, 75, or 100 rpm. However, in humans, the agitation strength is relatively weak, corresponding to less than 50 rpm in the compendium paddle method (Section 6.2.3.2).

In the minipaddle method, even when the same paddle speed is used, the agitation strength is much smaller compared to a standard paddle method. Equation 3.39 can be used to calculate the agitation strength in each system. For example, with a paddle size of 2.5 cm, a paddle speed of 50 rpm, and a fluid volume of 50 ml in the minipaddle method, the agitation strength corresponds to circa 10–25 rpm in the compendium paddle method.

The fluid dynamics in the USP (US Pharmacopeia) paddle method has been extensively investigated [77–80]. Figure 7.15 shows the distribution of fluid velocity at the flask bottom. The shear stress is high near the paddle and the flask wall. There is an upward flow around the flask bottom; however, there is a dead-flow region where the coning phenomenon is often observed. The coning results in a slower dissolution profile. The coning effect is observed when the dosage form contains a high amount of insoluble excipients. To avoid coning, usage of a peak bottom flask has been reported [81].

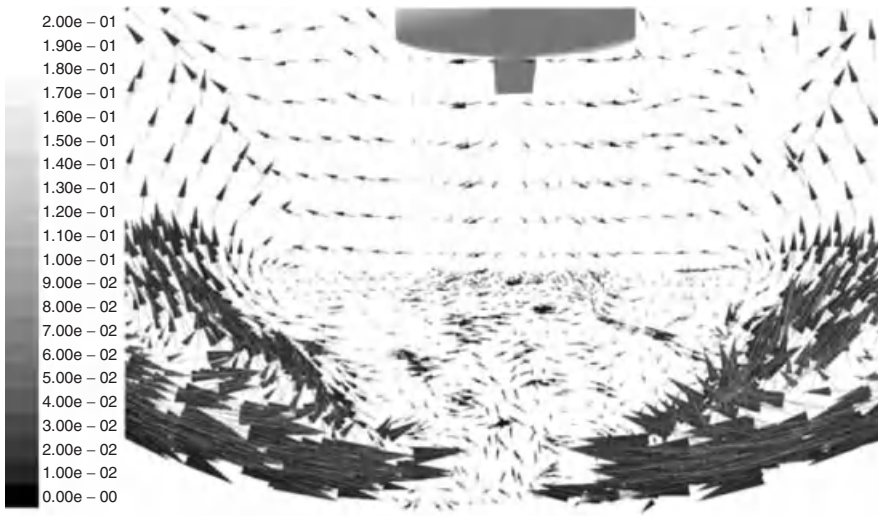

Figure 7.15 Distribution of fluid velocity in the USP paddle method. Numerically predicted velocity vectors (m/s) on the plane perpendicular to the impeller plane at the vessel bottom. *Source:* Adapted from Reference 77 with permission.

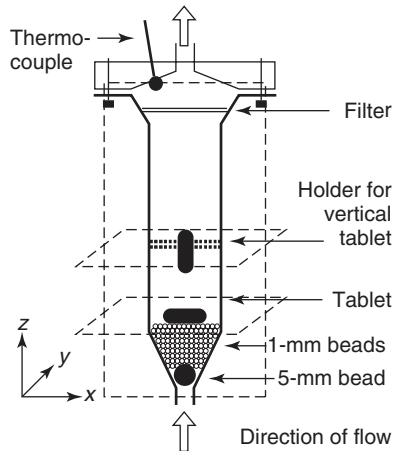

Figure 7.16 Geometry of the USP 4 flow-through method. *Source:* Adapted from Reference 82 with permission.

7.7.3 Flow-Through Method

Figure 7.16 shows the flow-through dissolution test apparatus [82]. The advantage of the flow-through method is that the dissolution media can be changed continuously, for example, from pH 1.2 to 6.8. In addition, a sink condition can be consistently maintained. Therefore, the flow-through method is suitable especially for controlled-release formulations and drugs with poor solubility (dissolution rate limited cases).

7.7.4 Multicompartment Dissolution System

Several multicompartment dissolution systems have been developed to represent the effect of gastric pH on the oral absorption of a drug. In these systems, a gastric compartment was sequentially connected to an intestinal compartment [83–86]. Furthermore, a membrane can be attached to the intestinal compartment [87]. These systems are especially useful for investigating the oral absorption of poorly soluble free bases, for example, ketoconazole, albendazole, cinnarizine, and dipyridamole. The bioavailability of these drugs was largely affected by the gastric pH (Table 12.4).

7.7.5 Dissolution Permeation System

Simultaneous assessment of dissolution and permeation is required to evaluate the performance of special formulations such as solid dispersion and self-emulsifying drug delivery systems (SEDDS), since the molecular state of a drug released from these formulations has not been well characterized. Therefore, the concentration of a drug available for permeation cannot be well defined for biopharmaceutical modeling (Section 4.4).

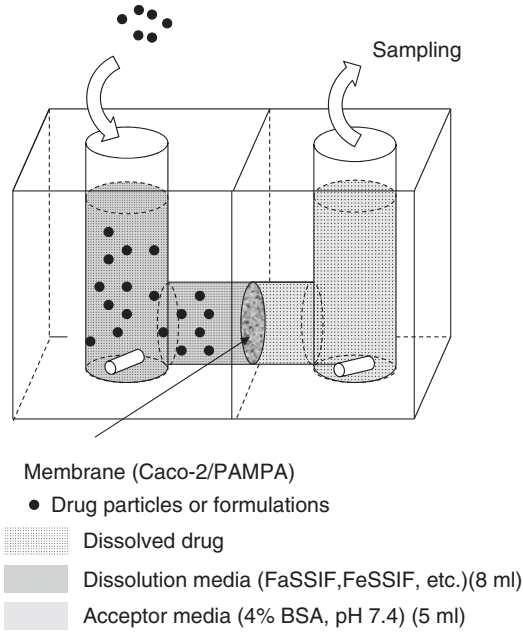

Figure 7.17 The D/P system.

Several types of *in vitro* systems in which the dissolution and permeation processes were combined were reported [87–89]. Kataoka et al. developed a dissolution/permeation (D/P) system (Fig. 7.17). The D/P system can evaluate the food effect and has the potential to be applied for the evaluation of prototype formulations as well [90].

The D/P system consists of two half-chambers and a Caco-2 monolayer (1.77 cm^2) mounted between them. Both sides of the monolayer are filled with transport media (apical side, pH 6.5, 8 ml (circa 6% of the intestinal fluid volume) and basal side, pH 7.4, 5 ml) and are constantly mixed by magnetic stirrers. Compounds are applied to the apical side as a solid, suspension, or solution. One-hundredth of the clinical dose is applied to the system. Compared to the *in vivo* situation, due to its small surface area/volume ratio (0.22 in the D/P system vs circa 2.3 in humans), the permeation clearance provided by the Caco-2 membrane is quite low. However, the fluid volume/dose ratio is sixfold higher in the D/P system than that *in vivo*. This excess fluid volume provides an additional clearance of a drug equivalent to $Pn = 6$.

By the D/P system, the food effect was correctly evaluated. The modified FaSSIF and FeSSIF with isotonic osmolality were used as the apical side fluid [88]. The applicability for lipid-based formulation was confirmed by albendazole and danazol formulations [89]. The D/P system was also found to be useful to evaluate various formulations [90, 91], including nanoparticles [92]. PAMPA membrane can be used as an alternative to Caco-2 membrane [93].

Sugano and Sakai [94] suggested the possibility of constructing a D/P system in a 96-well format. Their method is an application of the PAMPA (Section 7.9.4). One disadvantage of PAMPA for the formulation study is the lack of the mucous layer. Without the mucous layer, the formulations (particles, micelles, etc.) can directly interact with the membrane. To attach the mucous layer onto the artificial lipid membrane, the hot molten agarose/mucin gel (1% (w/v)) was impregnated into the hydrophilic fiber scaffold, which is physically attached on the membrane. The hydrophilic scaffold enables the formation of a thin mucous layer. Without the hydrophilic scaffold, the agarose/mucin mixture makes a droplet on the hydrophobic PAMPA membrane and does not form a uniform thin layer. They demonstrated that the food effect can be adequately assessed by the mucous-layer-adhered PAMPA.

7.7.6 Recommendation

There is no versatile technology for all stages in drug discovery. The minipaddle method is suitable for the early stages of drug discovery and development. μDISS can be also used in these stages. The USP method is most often used in the late stages of drug development. The main purpose of a dissolution test is to measure the dissolution rate of a drug rather than the saturated solubility. In most cases, a sink condition is used. The dissolution rate is then used in biopharmaceutical modeling (Section 8.5.1). The biopharmaceutical modeling can be modified to emulate the D/P system. As the D/P system can experimentally evaluate the effective concentration of a drug for membrane permeation, it can be used to validate a modeling hypothesis for the absorption mechanism of a special formulation such as solid dispersion.

7.8 PRECIPITATION

Development of an *in vitro* method, which correctly reflects an *in vivo* supersaturation profile, has not been successful so far. In most cases, an *in vitro* method underestimates the supersaturation of a drug *in vivo*, probably because of the difference in the chemical composition of the fluids, the containers (glass vs mucus), the pH neutralization processes, the agitation methods (stirring bar/paddle vs wall movement), etc. Therefore, the methods introduced here should be understood as a qualitative measure of supersaturation profiles.

7.8.1 Kinetic pH Titration Method

A kinetic pH titration method can be used to assess the ability of a drug to supersaturate in an aqueous solution [95]. A drug is first dissolved at a pH where it is dissolved predominantly in its ionized form, and then the pH is changed by titrating HCl or KOH. As pH shifts to the range close to the pK_a of a drug, the portion of undissociated form (f_0) increases. In the case when a drug is supersaturable

(Fig. 7.18b),[12] the dissolved drug concentration of the undissociated form in the solution ($C_{\text{dissolv},0}$) transiently exceeds the intrinsic solubility (S_0). Once $C_{\text{dissolv},0}$ hits the critical supersaturation ratio ($C_{\text{dissolv},0}/S_0 > \text{CSSR}$),[13] nucleation occurs. Subsequently, the rate of pH change by precipitation or dissolution of the drug is monitored. In the case when a drug is not supersaturable (Fig. 7.18a), the pH titration curve simply follows that of the pH–equilibrium solubility profile.

7.8.2 Serial Dilution Method

When a series of concentrated stock solutions of a drug in a rich solvent (such as DMSO or DMA (dimethylacetamide)) was diluted with an aqueous buffer, precipitation of the drug is observed when the dissolved drug concentration exceeds the CSSC (Fig. 7.19). Figure 7.20 shows the plot of dissolved drug concentration against the initially added drug amount [96].

7.8.3 Two-Chamber Transfer System

A two-chamber transfer system was used to investigate the precipitation of a base [83]. A base drug was first completely dissolved in a HCl solution and then infused into a neutral pH solution with sufficient buffer capacity to maintain the neutral pH. a paddle apparatus was used as the neutral pH chamber. Figures 7.21 and 7.22 show the dissolved drug concentration–time profile of dipyridamole and AZ0865, respectively.

However, this *in vitro* method was found to overestimate the precipitation *in vivo* (underestimate supersaturation) (Fig. 7.23) [97]. Figure 7.24 shows the dissolved drug concentration (C_{dissolv}) of AZ0865 in the small intestine after oral solution administration simulated by the S1I7C1 model. It was suggested that C_{dissolv} exceeded the critical supersaturated concentration in the *in vitro* method (Figs. 7.22 and 7.23). However, precipitation was not observed in clinical trials. The discrepancy was much smaller when a paddle stirrer was used compared to a magnetic stirrer.

7.8.4 Nonsink Dissolution Test

A nonsink dissolution test may be able to discriminate the effects of formulation components on the supersaturation and precipitation rate of a drug. Gu et al. showed that the use of appropriate dose/volume ratio is critical to evaluate the supersaturation and precipitation of a drug [98].

[12] As supersaturable compounds chase the equilibrium, it is called *chaser* by the investigators.

[13] CSSR can change depending on the titration speed. In addition, the local pH near the dispenser tip can be different from the bulk pH. Furthermore, mechanical stirring can stimulate nucleation. Therefore, the CSSR observed in this method does not necessarily quantitatively correlate with the *in vivo* supersaturation profile.

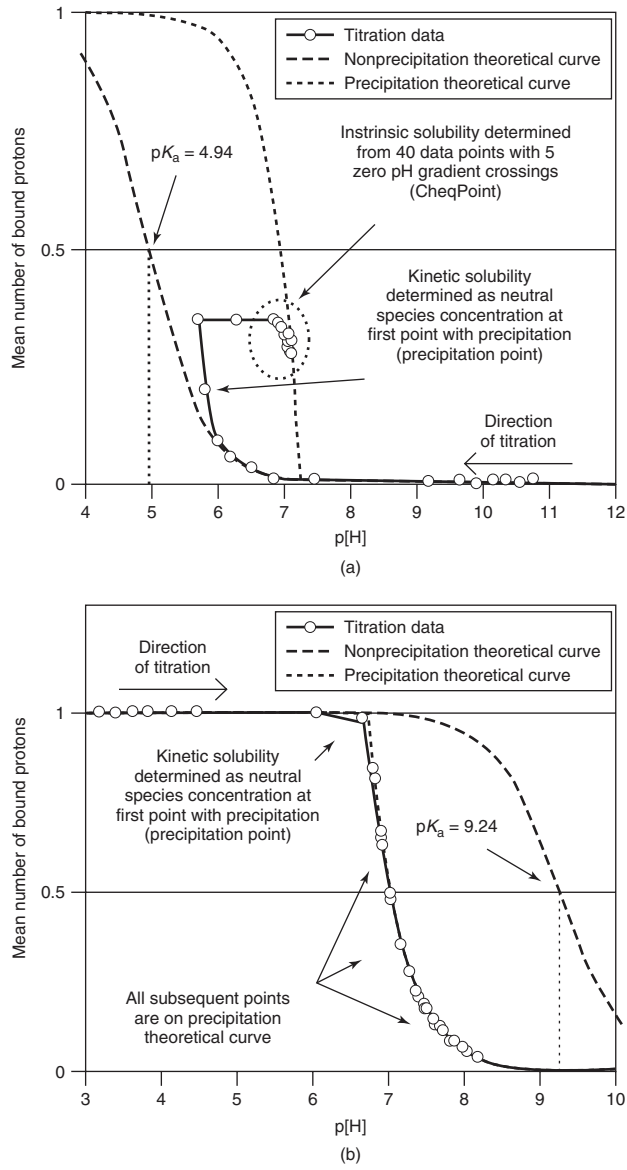

Figure 7.18 pH-supersaturation profile. (a) Bjerrum curve for warfarin. While the sample is fully dissolved, the experimental data fit well with the nonprecipitation theoretical curve. After precipitation, the points lie close to the precipitation theoretical curve at the CheqPoint. The precipitation point, when precipitation was first observed, lies a long way from the CheqPoint. The fact that the precipitation point does not lie on the precipitation theoretical curve indicates that the solution was supersaturated at the moment the sample first precipitated. (b) Bjerrum curve for chlorpromazine. As soon as the saturation level is reached, the sample precipitates, and points follow the precipitation theoretical curve. The precipitation point also lies on the precipitation theoretical curve, indicating no supersaturation. *Source:* Adapted from Reference 95 with permission.

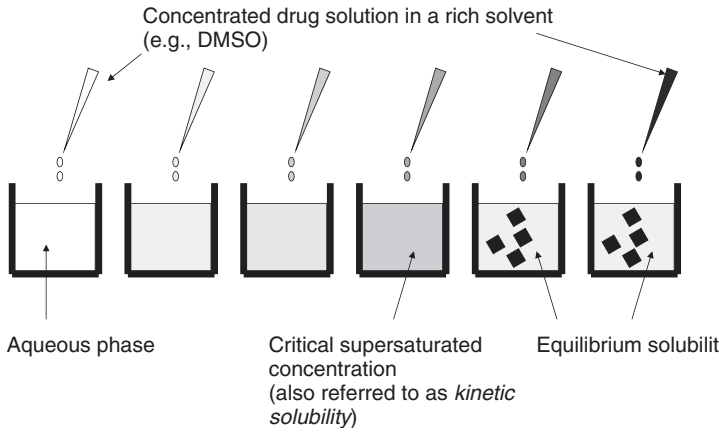

Figure 7.19 The serial dilution method.

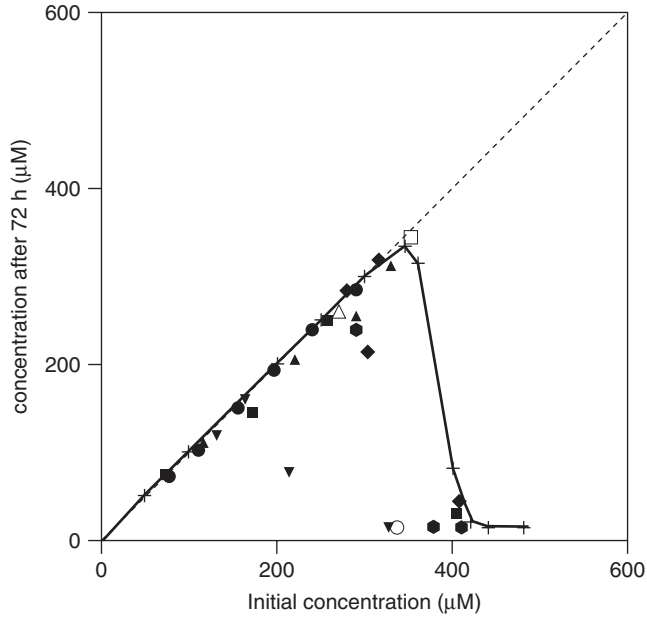

Figure 7.20 Result of the serial dilution method. Bicalutamide was used as a model drug. The solubility of crystalline material is 14.5 μM. The different symbols indicate that experiments have been performed at different occasions. The solid line with crosses represents calculated results for the bulk concentration after 72 h incubation versus initial concentration for different supersaturation ratio. In the calculations, $\lambda = 6.5$ μm and a crystal-water interfacial tension $\gamma_{SL} = 22.1$ mN/m were used together with experimental data for other parameters in the theory. *Source:* Adapted from Reference 96 with permission.

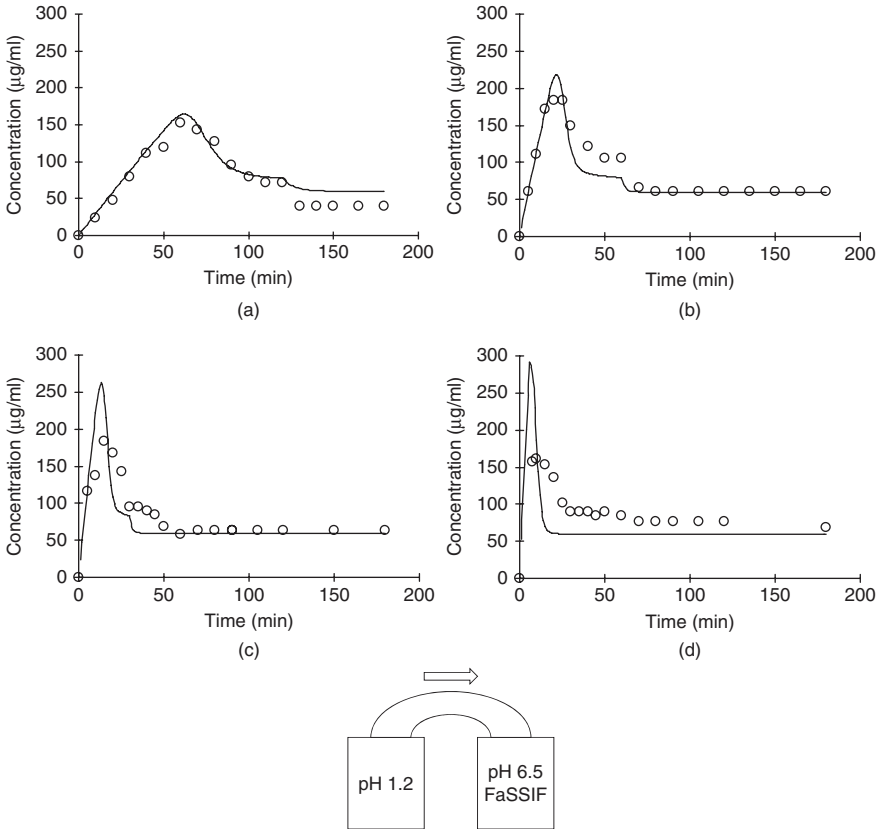

Figure 7.21 Two-chamber transfer method. (a) 0.5 ml/min, (b) 2 ml/min, (c) 4 ml/min, and (d) 9 ml/min.

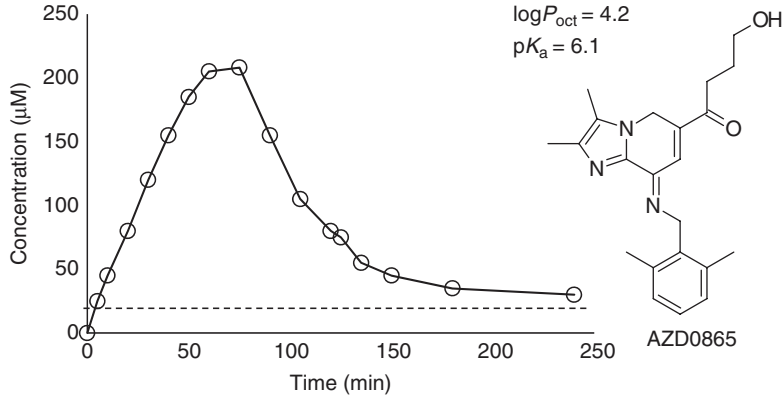

Figure 7.22 Mean (±SD) concentration of AZD0865 dissolved in FaSSIF over time from supersaturated solution using the two-chamber transfer method ($n = 3$). Dotted line represents the equilibrium solubility in FaSSIF. *Source:* Replotted from Reference 97.

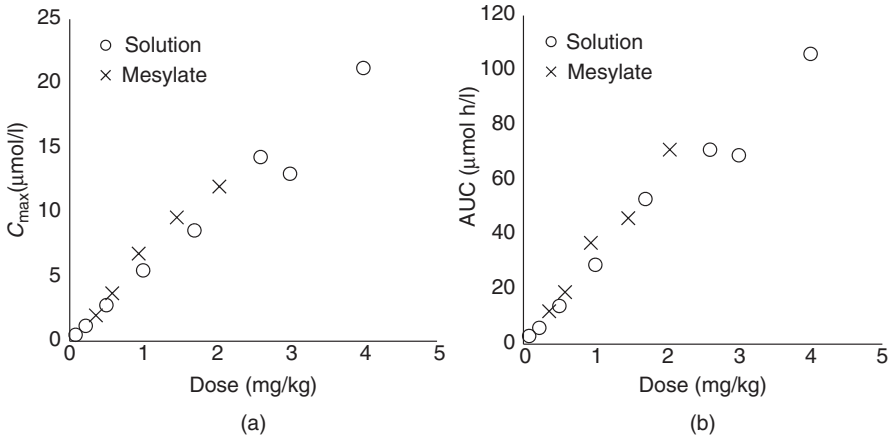

Figure 7.23 (a) C_{max} and (b) AUC of AZD0865 in humans at different doses administered as solution or mesylate salt (tablet). *Source:* Replotted from Reference 97.

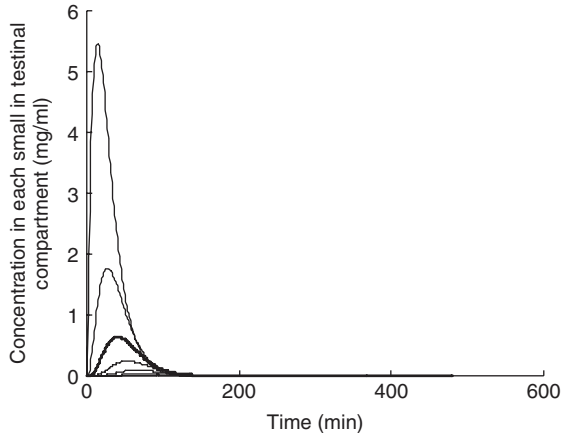

Figure 7.24 Simulated AZ0865 concentration in the small intestine after solution administration. The S1I7C3 model was used for simulation. Dose = 280 mg (4 mg/kg), $P_{eff} = 3.2 \times 10^{-4}$ cm/s, gastric $T_{1/2} = 10$ min, gastric $V_{GI} = 30$ ml, small intestinal $V_{GI} = 130$ ml, and dosing volume = 250 ml. The lines in the figure correspond to each small intestinal compartment (from left to right, compartments 1–7, proximal to distal, respectively.)

7.9 EPITHELIAL MEMBRANE PERMEABILITY

The accuracy of epithelial membrane permeability data (P_{ep}) is critically important for biopharmaceutical modeling of drugs with low to medium lipophilicity.[14]

[14]But it is not critically important for compounds with high lipophilicity (log $D_{oct,pH6.5}$ > circa 2) because the UWL resistance dominates P_{eff}.

To ensure the reliability of P_{ep} data, it is preferable to compare P_{ep} values obtained from two or three different methods.

7.9.1 Back-Estimation from Fa%

When Fa% of a drug administered as a solution is less than 75%[15] (i.e., low permeability), P_{ep} values can be back-estimated from the Fa% as

$$P_{ep} = \frac{R_{GI}}{2DF \cdot PE \cdot VE \cdot f_{mono}} \frac{1}{T_{si}} \cdot \ln(1 - Fa)$$

This method is practically useful in drug discovery, as Fa% in rats is usually routinely measured. A drug with low permeability tends to be less liable to the gut wall metabolism (i.e., Fg $\approx$ 1) and Fh can be calculated from i.v. data. Therefore, the equation $F = FaFgFh$ can be used to calculate Fa from F. The UWL effect and colonic absorption are negligible for drugs with low permeability (Section 11.8.5.2). The Acc of a drug with low permeability is circa 1 (Section 4.6). Data obtained from dogs should not be used for this method as the paracellular pathway in dogs is larger than that in humans. This method cannot be used for Fa% $>$ 75% cases, as ln(1 $-$ Fa) becomes sensitive to a small error in Fa%.

Example P_{ep} of a drug can be estimated from Fa% in rats after solution administration (without precipitation in the GI tract). For example, when Fa% = 50%,

$$P_{ep} = \frac{0.2}{2 \times 1.7 \times 1 \times 5 \times 1} \frac{1}{2 \times 60 \times 60} \cdot \ln(1 - 0.5) = 1.1 \times 10^{-6} \text{cm/s}$$

And then, P_{eff} and Fa% in humans can be estimated by assuming that P_{ep} is identical in both species (in this case, f_{mono} of this drug is assumed to be 1 in both species).

$$\begin{aligned} P_{eff,human} &= PE \cdot VE \cdot f_{mono} \cdot P_{ep} = 3 \times 10 \times 1 \times 1.1 \times 10^{-6} \text{ cm/s} \\ &= 0.33 \times 10^{-4} \text{ cm/s} \\ Fa_{human} &= 1 - \exp\left(-\frac{2DF}{R_{GI}} P_{eff} T_{si}\right) \\ &= 1 - \exp\left(-\frac{2 \times 1.7}{1.5} 0.33 \times 10^{-4} \times 3.5 \times 60 \times 60\right) = 61\% \end{aligned}$$

7.9.2 *In Situ* Single-Pass Intestinal Perfusion

The Loc-I-Gut system has been used to measure the effective permeability values in humans [99]. This permeability value is considered as the authentic P_{eff} value

[15] Without precipitation in the GI tract.

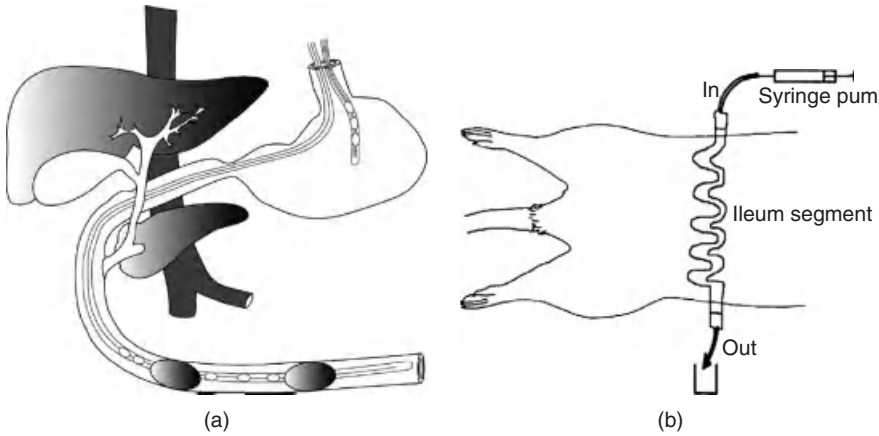

Figure 7.25 (a) Luc-I-Gut and (b) rat *in situ* perfusion methods. Loc-I-Gut is a perfusion technique for the proximal region of the human jejunum. The multichannel tube is 175 cm long and is made of polyvinyl chloride, with an external diameter of 5.3 mm. It contains six channels and is provided distally with two 40-mm-long, elongated latex balloons, placed 10 cm apart and each separately connected to one of the smaller channels. The two wider channels in the center of the tube are for infusion and aspiration of the perfusate. The two remaining peripheral smaller channels are used for administration of marker substances and/or for drainage. A tungsten weight is attached to the distal end of the tube to facilitate passage of the tube into the jejunum. The balloons are filled with air when the proximal balloon has passed the ligament of Treitz. *Source:* Adapted from References 99 and 100 with permission.

in the literature. Figure 7.25a shows the Loc-I-Gut system. Two balloons are inflated in the human intestine and drug solution is perfused. As the human subject is maintained conscious during the experiment, the GI mobility is kept intact. However, this experiment is expensive and not suitable for drug discovery and development.

Rat single-pass intestinal perfusion (SPIP) has been widely used to investigate the intestinal membrane permeability in drug discovery (Fig. 7.25b) [100]. The advantage of this method is that the physiological characteristics of the small intestine, such as paracellular pathway and carrier-mediated transport, are maintained intact (except the GI mobility). The disadvantages of this method are (i) the variation in data could be large when not performed carefully and (ii) the experiment is labor intensive. This method is not suitable for drugs with high lipophilicity, as the UWL of an anesthetized intestine is significantly larger than that of a nonanesthetized intestine.

P_{eff} can be calculated by the well-stirred model [101] as

$$P_{\text{eff}} = \frac{Q_{\text{in}}\left(\frac{C_{\text{in}}}{C_{\text{out}}} - 1\right)}{2\pi R_{\text{GI}} L} \tag{7.5}$$

or by the parallel tube model (for open or semiopen SPIP models in humans) as

$$P_{\text{eff}} = \frac{-Q_{\text{in}} \ln\left(C_{\text{out}}/C_{\text{in}}\right)}{2\pi R_{\text{GI}} L} \tag{7.6}$$

In both the models, the tube shape does not affect the P_{eff} value of a drug. The transit time of a drug from the inlet to the outlet is determined by V_{GI} and the infusion rate (Q_{in}) as $V_{\text{GI}}/Q_{\text{in}}$. A decrease in the V_{GI} of the tube fastens the transit of a solution, whereas it increases k_{perm} (cf. $\text{CL}_{\text{perm}}/V_{\text{GI}}$), canceling out to give a same P_{eff}).

7.9.3 Cultured Cell Lines (Caco-2, MDCK, etc.)

The Caco-2 cell model is most often used as an *in vitro* cell model [102–104]. The Caco-2 cells originated from human colon cancer and represent many common features with the small intestine. When cultured on an adhesive filter support, the Caco-2 cells form a planner membrane with a tight junction. Many transporters such as P-gp, BCRP, and PEP-T1 are expressed in the apical membrane. However, the expression level of these transporters could have significant laboratory to laboratory variations [105].

The MDCK cell model is also often used in drug discovery and development. The MDCK cells originated from the dog kidney and represent some common features with the small intestine. However, transporter expression in the MDCK cells is very different from that in the human small intestine. As for the passive diffusion, Caco-2 and MDCK give similar values (Fig. 7.26) [106]. However, these cells give different values for PEP-T1 transport [107]. The MDCK cells transfected with the P-gp gene (MDCK-MDR1) are also often used in drug discovery [108].

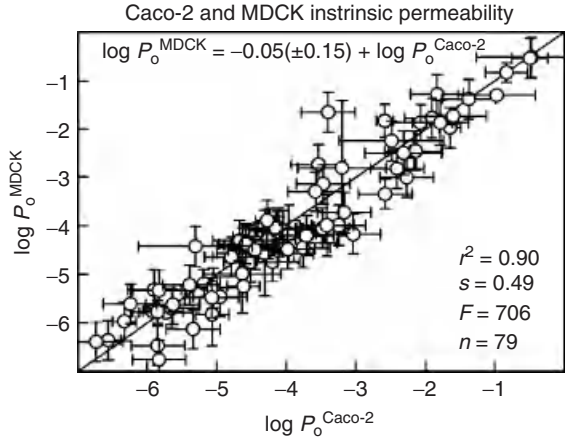

Figure 7.26 Correlation between $P_{\text{trans},0}$ of Caco-2 and MDCK cells. *Source:* Adapted from Reference 106 with permission.

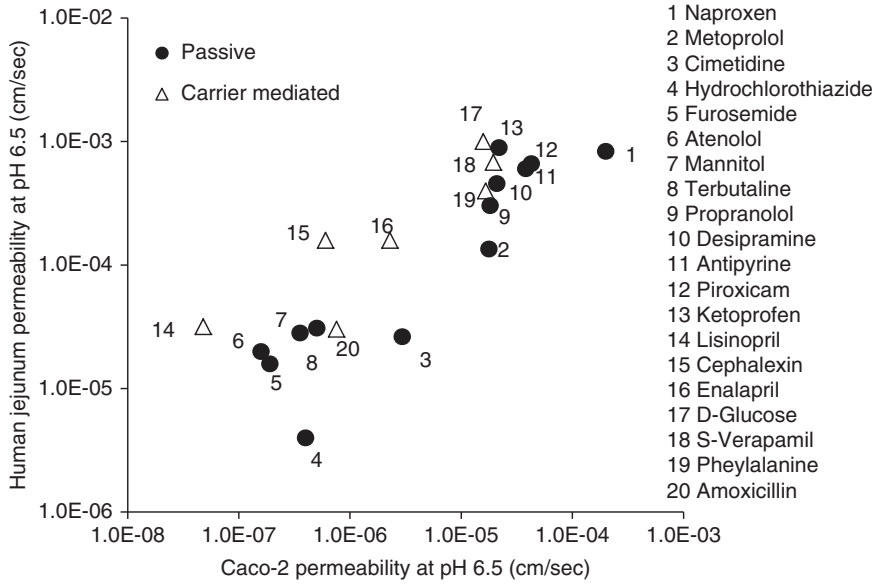

Figure 7.27 Correlation between human jejunum (*in vivo* perfusion) and Caco-2 monolayers (*in vitro*) permeability data for 20 compounds. *Source:* Adapted from Reference 99 with permission.

Figure 7.27 shows the correlation between P_{eff} and P_{app} [109]. This type of empirical relationship has been widely used for biopharmaceutical modeling. However, there are a few cautions for this empirical correlation: (i) this relationship is validated for compounds with low to moderate lipophilicity but not for drugs with high lipophilicity, (ii) the effect of bile-micelle binding is not taken into account, and (iii) the error is greater than 0.5 log unit.

7.9.4 PAMPA

PAMPA was first introduced in 1998 [110]. Since then, PAMPA has rapidly gained wide popularity in drug discovery [111–114]. The term *PAMPA* is now used as the general name for a plate-based (HTS enabled) filter-supported (filter immobilized) [115, 116] artificial membrane. Typically, an organic solvent containing phospholipids is impregnated into the filter to construct a PAMPA membrane (Fig. 7.28). PAMPA is a refined descendant of log P_{oct} and is an improved surrogate assay for passive transcellular permeation. PAMPA was found to show a good correlation with P_{eff} and Fa% (Section 8.4.4).

PAMPA membranes typically consist of phospholipids dissolved in an organic solvent. A proposed membrane structure is shown in Figure 7.29. Phospholipids facilitate the permeability of moderately hydrophilic molecules by ionic or hydrogen bonding interactions (phospholipids are hydrogen bond acceptors). This enables appropriate assessment of permeability for moderately lipophilic

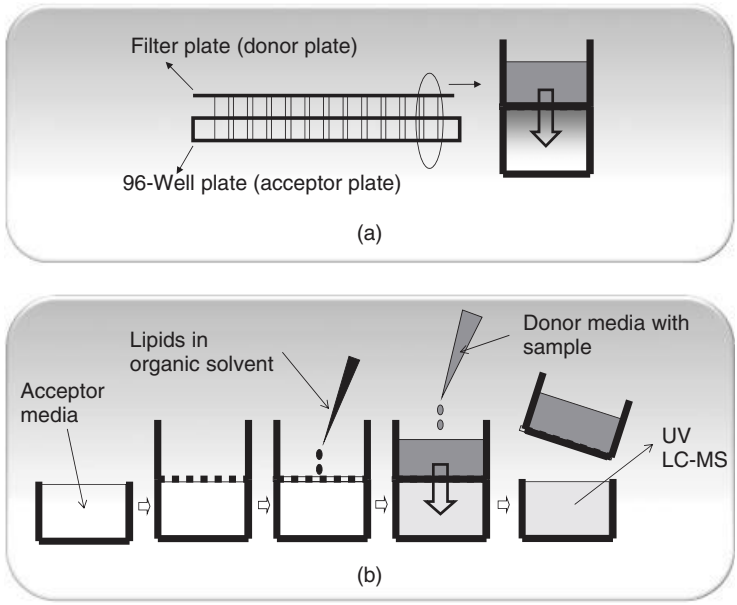

Figure 7.28 Experimental procedure of PAMPA. (a) 96-Well configuration and (b) Experimental procedure (top to bottom permeation).

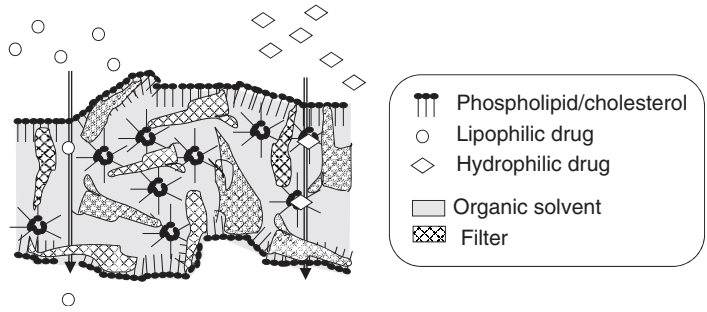

Figure 7.29 Proposed structure of PAMPA membrane.

compounds [117]. Recently, it was shown that anionic phospholipid(s) increases the permeation of basic compounds by ion pair mechanism [118–120]. In many PAMPA variations (and other artificial membrane tools), anionic phospholipid(s) is added to the membrane to increase the predictability for *in vivo* absorption. However, even though the phospholipids may add some similarity to the biological membrane, the organic solvent remaining in the membrane could have a large impact on the permeability. The solubility diffusion theory (Section 4.8.2.1) would support the use of an alkane or alkylidene as an organic solvent in PAMPA [121].

TABLE 7.3 Variations of PAMPA

Name	Composition	References
Original	10% Egg lecithin/*n*-dodecane	110
Double sink (DS)	20% Phospholipid mixture/*n*-dodecane	132
n-Hexadecane (HM)	100% *n*-Hexadecane	112
Biomimetic (BM)	0.8% PC, 0.8% PE, 0.2% PS, 0.2% PI, 1% CHO/1,7-octadiene	111
Lipid/oil/lipid trilayer membrane	Neat DOPC	131
Immobilized phospholipids vesicles	Neat phospholipids vesicles	133
Lipid/cholesterol/octanol mixture	1.7% Egg PC, 2.1% CHO/octanol	129
Three lipid-component model	2.6% PS18:1, 0.9% PC18:1, 1.5% CHO/*n*-dodecane	119
Blood–brain barrier (BBB)	2% Porcine brain extract/*n*-dodecane	113
Skin	70% silicone-30% IPM	134

Composition of PAMPA membranes reported in the literature varies from a pure organic solvent to a pure phospholipid. At the first international conference of PAMPA in 2002 (http://www.pampa2002.com/), it was agreed that these variations would be notated as initials or as a short adjective on the head of PAMPA, for example, BM-PAMPA for the biomimetic PAMPA. The variations of PAMPA are summarized in Table 7.3 [35, 94, 110–114, 122–131].

PAMPA is suitable for use at the early stages of drug discovery. PAMPA membrane is stable to high levels of water-miscible organic solvents (e.g., up to 10–30%, AcCN, EtOH, or DMSO) [135]. Unlike cell monolayer systems, PAMPA does not require any preincubation. A simple UV detection method can be used for quantification of a drug because there is no interference from biological contaminants.

Other artificial membrane assays have also been extensively investigated in the last two decades, such as surface plasmon liposome binding assay [136, 137], immobilized artificial membrane column HPLC [138–144], immobilized liposome chromatography [145–148], and solid-supported lipid membrane [149, 150].

7.9.5 Estimation of $P_{trans,0}$ from Experimental Apparent Membrane Permeability

To use the *in vitro* P_{app} value in a mechanistic model, it must be first converted to $P_{trans,0}$.P_{trans0} can be estimated from P_{app} as

$$P_{trans,0} = \frac{1}{f_0}\left(\frac{1}{\frac{1}{P_{app}} - \frac{h_{UWLvitro}}{D_{mono}}} - P_{para,vitro}\right)$$

where $h_{UWLvitro}$ is the UWL thickness in an *in vitro* permeability assay. It is preferable to use more than two P_{app} values at different pH points. This calculation becomes unstable when a P_{app} value is close to the UWL permeability (circa $20–50 \times 10^{-6}$ cm/s). $P_{para,vitro}$ is the paracellular permeability in the *in vitro* cellular system. To calculate $P_{para,vitro}$, the mesh size and electric potential of the paracellular pathway must be characterized at each laboratory, as these values are known to have large laboratory to laboratory variations [151]. These values can be calculated using the permeability values of model paracellular permeants such as mannitol, urea, atenolol, and nadolol. $h_{UWLvitro}$ can be estimated by various methods (Section 7.9.8.1). $P_{trans,0}$ is then converted to *in vivo* P_{eff}, considering the pH, P_{para}, P_{UWL}, the unbound fraction, the surface area expansion by the fold and villi structures, etc. (Chapter 4). A simple empirical correlation such as Figure 7.27 cannot consider these factors. It would be noteworthy that for structure–permeability relationship analysis, the use of $P_{trans,0}$ is more straightforward than using P_{app}, as a linear free energy relationship can be obtained for $P_{trans,0}$ [125].

7.9.6 Estimation of $P_{trans,0}$ from Experimental log P_{oct}

The correlation between $P_{trans,0}$ and P_{oct} is discussed in Section 4.8.2.3. It is highly recommended to use experimental log P_{oct} value rather than the *in silico* prediction.

7.9.7 Mechanistic Investigation

It is of great importance to understand what process is involved in membrane permeation of a drug. By comparing artificial membrane and Caco-2 permeabilities, the contribution of transporters can be identified (Fig. 7.30) [124].

Comparison of permeabilities in apical-to-basal (A to B) and B to A directions is often used to identify the contribution of transporters. An iso-pH condition (e.g., 7.4/7.4) must be used in this experiment [152]. An inhibition study is often used to identify the contribution of a transporter. A high inhibitor concentration (>1 mM) is often used. In this case, the dissolved inhibitor can change the pH. Therefore, pH should be readjusted after dissolving the inhibitor.

The Michaelis–Menten equation can be used to analyze the concentration dependency of permeation flux (Fig. 7.31). Using the Michaelis–Menten equation, the saturable and nonsaturable components can be separated. The nonsaturable component is usually regarded to undergo passive diffusion because it is nonsaturable and usually identical to the permeability under inhibition and/or in the mock cells.

7.9.8 Limitation of Membrane Permeation Assays

It is important to understand the limitations of each method. Owing to the following reasons, an *in vitro* method may have only a little value for drugs with high lipophilicity or could even give an erroneous low P_{ep} value.

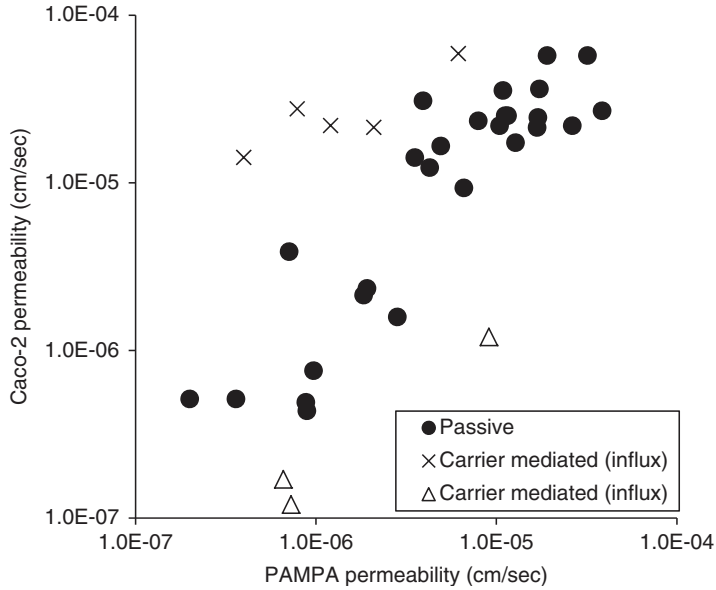

Figure 7.30 Comparison of PAMPA and Caco-2 to study the participation of carrier-mediated transport. •, passive diffusion substrates; ▲, efflux transporter substrates; and ♦, influx transporter substrates. *Source:* Adapted from Reference 124 with permission.

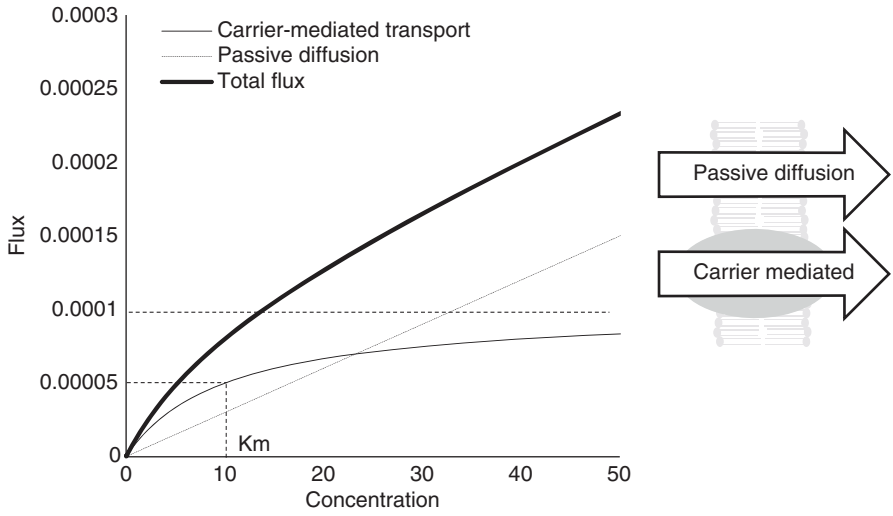

Figure 7.31 Michaelis–Menten equation and passive permeation.

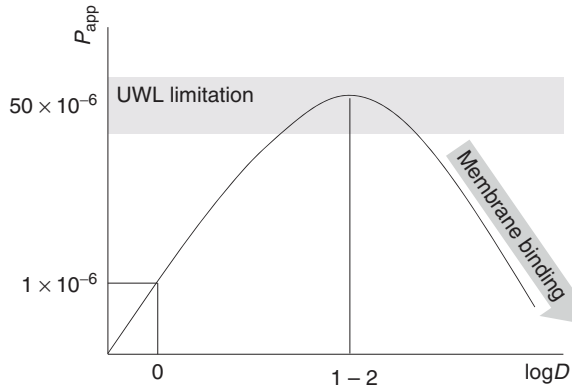

Figure 7.32 Typical lipophilicity–permeability profile.

7.9.8.1 UWL Adjacent to the Membrane. The UWL is only circa 300 μm in the GI tract (Section 6.2.3.3). However, in an *in vitro* permeability assay (planar membrane),[16] the UWL adjacent to the membrane can be up to 1500–4000 μm thick.

When using a planar membrane system, the plate can be shaken to minimize the effects of the UWL. In an *in situ* perfusion study, the flow rate can be increased. A bubbling method can be used to agitate the fluid in the Ussing chamber method. However, an orbital shaker is often not effective, especially for a small-well plate such as the 96-well plate. The agitation effectiveness can be improved by adding beads in the wells. Without strong stirring, the UWL dominates the apparent permeability at $P_{app} >$ ca 30×10^{-6} cm/s. Recently, it has been clearly demonstrated that the quantitative structure–activity relationship was interfered if the effect of the UWL was not removed [20, 125].

The thickness of the UWL in an *in vitro* model ($h_{UWLvitro}$) can be estimated from the pH–permeability profile of a drug, such as ketoprofen. Figure 4.7 shows a typical pH–permeability profile. The merit of using an acidic compound is that the contribution of paracellular pathway can be less significant. Another method to estimate $h_{UWLvitro}$ is to use the P_{app}–lipophilicity profile. Figure 7.32 shows the typical relationship between log D_{oct} and P_{app}. $h_{UWLvitro}$ can be calculated from the P_{app} of compounds in the ceiling region of this profile.

Theoretically, the thickness of the UWL depends on the square or cube root of the flow speed (e.g., the infusion speed (U) for the perfusion model or the rotation speed of the plate) (Section 3.2.4).

$$h_{UWL} = \frac{L}{Sh} \propto Re^{-1/2 \text{ or } 1/3} Sc^{-1/3} = \left(\frac{UL}{\nu}\right)^{-1/2 \text{ or } 1/3} \left(\frac{\nu}{D}\right)^{-1/3} \tag{7.7}$$

[16]The thickness of the UWL in the suspended cells or liposomes would be the same as the radius of the cells (Section 3.2.4.5).

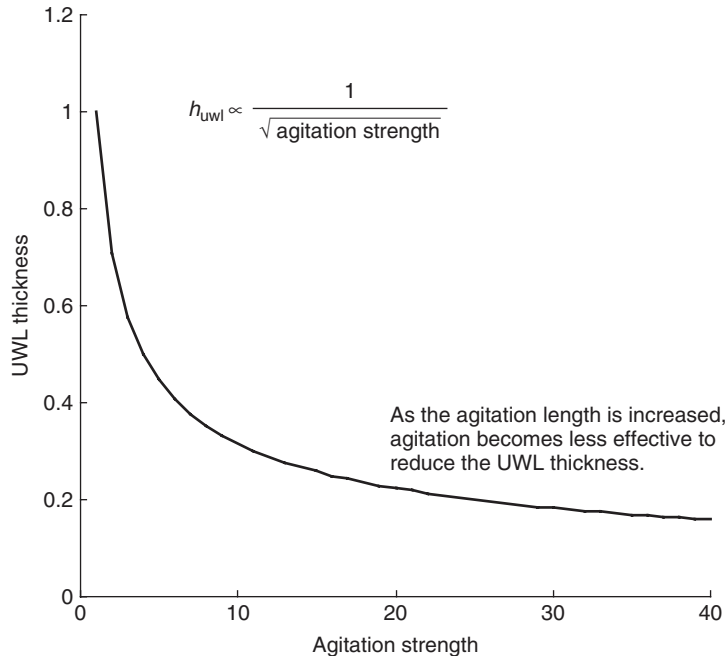

Figure 7.33 Agitation strength versus unstirred water layer thickness.

This equation suggests that, as the agitation strength becomes higher, the UWL thickness becomes insensitive to the increase in the agitation strength (Fig. 7.33) [153]. Therefore, insensitiveness of apparent permeability to the agitation increment cannot be the proof for the permeability being dominated by P_{ep}. Even when a strong agitation is used, the UWL still exists and can become a permeation barrier for drugs with high lipophilicity.

7.9.8.2 Membrane Binding. Membrane binding can also retard the permeability of lipophilic drugs, resulting in artifactual low permeability [154, 155]. As a rule of thumb, when log D_{oct} (at assay pH) is greater than 1.5, the membrane binding could become an issue [155]. This experimental artifact may be mitigated by adding BSA in the acceptor fluid [155–161]. *In vivo*, the blood flow removes the compound from the basolateral side [162].

7.9.8.3 Low Solubility. The solubility of a drug in an assay media should be checked before running the assay. The concentration of a drug in the assay media should be set below the solubility of the drug. When a solubilizing agent is used, the free fraction and activity of a drug would be reduced, resulting in artifactual low permeability (cf., P_{app} is usually calculated based on the total dissolved drug concentration). In addition, the cells could be damaged when a solubilizer is used at high concentration [163, 164]. Generally, only low levels of solubilizing solvents, for example, less than 1% DMSO, can be used to avoid toxicity issues.

7.9.8.4 Differences in Paracellular Pathway. PAMPA does not have aqueous pores and is therefore not suitable for examining the paracellular transport of a drug. Some cell models, for example, Caco-2 and MDCK, have a narrower tight junction compared to the *in vivo* human intestine and may underestimate the paracellular transport. The paracellular permeability of a drug in dogs is significantly larger than that in humans. However, contribution of the paracellular pathway can be corrected using an *in silico* approach (Section 4.8.3).

7.9.8.5 Laboratory to Laboratory Variation. In cell-based assays, significant laboratory to laboratory variations have been observed [105]. Permeability differences can be attributed to a number of factors, e.g., heterogeneity of cell line, passage number, culture conditions, characteristics of the filter membrane, age of monolayers, level of differentiation, and experimental methodologies [165]. Paracellular and carrier-mediated transports tend to show larger laboratory to laboratory variations compared to passive transcellular permeation [105, 151].

7.9.8.6 Experimental Artifacts in Carrier-Mediated Membrane Transport. To obtain K_m and V_{max} values for transporters, P_{app} data at a wide range of concentration is required. It is sometimes difficult to achieve a high concentration. P-gp substrates often have low solubility. Both A to B and B to A permeation data should be obtained with an isotropic pH condition (usually pH 7.4 for both sides) [152]. To obtain K_m accurately, the effect of the UWL should be minimized by efficient stirring [166]. Especially for moderately lipophilic efflux transporter substrates, $P_{app,B-A}$ tends to exceed the UWL permeability (Fig. 4.27). As the unbound drug concentration in the cytosol is lower than that in the donor fluid, the intrinsic K_m value should be obtained by the equations introduced in Section 4.9. The contribution of a carrier-mediated transport *in vivo* is often overestimated by an *in vitro* experiment. This point is discussed in detail in Section 14.4.

7.9.9 Recommendation for P_{ep} and P_{eff} Estimation

Cross-validation of P_{ep} data using multiple methods would increase the reliability of the data. Usually, as the project moves from early discovery to late development, the number of available P_{ep} estimation methods increases. It should be remembered that even though the Caco-2 assay is often refereed to as the golden standard, it has various limitations as discussed above.

7.9.9.1 Hydrophilic Drugs. Hydrophilic drugs ($\log D_{oct,pH6.5} < 0.5$) are usually free from experimental artifacts associated with *in vitro* membrane permeability assays. Thus, Caco-2, MDCK, and other *in vitro* data can be used as a reliable data source. However, the paracellular pathway and transporter expressions of these cell lines could be significantly different from that *in vivo* [167]. Fa% and SPIP data in rats can be used to estimate P_{ep} in humans.

7.9.9.2 Lipophilic Drugs. For a lipophilic drug ($\log D_{oct,pH6.5} > 2$), estimation of P_{ep} from experimental $\log P_{oct}$ would be more reliable than that from *in vitro* permeability assays because an *in vitro* membrane permeation assay could underestimate P_{ep} due to the experimental artifacts. After all, the *in vivo* P_{eff} of these compounds is usually determined by the UWL, and therefore, the accuracy of P_{ep} estimation has little effect on P_{eff} prediction.

7.9.9.3 Drugs with Medium Lipophilicity. The estimation of P_{ep} is most difficult for drugs of $0.5 < \log D_{oct,pH6.5} < 2$. Fortunately, the drugs in this lipophilicity range usually have sufficient solubility and permeability to show good Fa%. However, for appropriate calculation of Fg, P_{ep} should be obtained with sufficient accuracy (Section 4.10).

When not stirred vigorously, because of the very thick UWL *in vitro*, P_{app} becomes significantly smaller than P_{ep}. Drugs with high lipophilicity and MW > 500 also often show moderate passive permeability. When Do < 1, the estimation error of P_{eff} has little effect on Fa%. However, when Do > 1, it would affect Fa% prediction. In the case of dissociable drugs, the pH of the *in vitro* cellular assay can be changed to give a P_{app} value at which the UWL has little effect ($<10 \times 10^{-6}$ cm/s) and then converted to P_{ep} and P_{eff} at a physiological pH.

7.10 *IN VIVO* EXPERIMENTS

In vivo PK data is often used to check the appropriateness of biopharmaceutical modeling (Chapter 15). In drug discovery and development, *in vivo* plasma concentration (C_p)–time profile data is usually available. However, the focus of an *in vivo* PK study in drug discovery tends to be drug disposition and it is often the case that little attention is paid to formulation. As the formulation of a drug has a significant impact on *in vivo* oral absorption, the formulation preparation and characterization for an *in vivo* study are discussed in this section.

7.10.1 P.O

To assess the effect of solubility and the dissolution rate of a drug on *in vivo* oral absorption, the formulation must be carefully prepared before performing *in vivo* experiments. As the reference data, it is preferable to have the PK data from the most stable form. In addition, it is preferable to have the PK data from a solution formulation as the best possible formulation. Precipitation from solution formulation can be tested by an *in vitro* test before the *in vivo* study [168].

In preclinical animal studies, a test compound is often administered as suspensions in vehicles. In this case, it is important to evaluate the crystal form and particle size of a drug in the vehicle. A suspension vehicle is most often composed of an inactive polymer (e.g., methylcellulose) and a small amount of wetting agent (e.g., Tween 80 (<0.1%)). A conventional preparation method to prepare a drug suspension is to use a mortar and pestle. During this preparation

process, an API is subjected to destructive forces by sliding, crushing, and/or compression, which may change the characteristics of the API, such as particle size. In addition, the solid form of an API can change to another form when it is dispersed in an aqueous media (e.g., an anhydrate to a hydrate, a salt to a free form). Therefore, the particle size and solid form of an API should be checked before and after formulation preparation. PXRD, DSC, TG/DTA, PLM, and laser diffraction can be used to characterize the API form and the particle size (Sections 7.4 and 7.5). In addition, the above characteristics might change during storage so that it is preferable to confirm the stability of the formulation during the study period. Preferably, the homogeneity of the suspension should be also confirmed. If a formulation is not homogeneous, the dose amount will vary among individual animals, resulting in larger variations of the PK profiles.

7.10.2 I.V

The PK data after i.v. administration is required to calculate the bioavailability of a drug. In the case of a compound with low solubility, a solubilizer is often used to enable i.v. formulation [169, 170]. However, high concentration of the solubilizer can cause hemolysis. When using a solubilizer, hemolysis should be checked by mixing the formulation with blood. In addition, precipitation at the administered site could also be a problem.

7.10.3 Animal Species

Selection of animal species is important for biopharmaceutical investigations. The difference in physiology between animals and humans should be taken into consideration (Chapter 6).

Dogs are preferentially used to assess the performance of a formulation. Working on gastric-acidity-controlled dogs may reveal the effect of stomach pH on oral absorption [171–173]. A pentagastrin or acidic buffer treatment can be used to consistently lower the stomach pH. A dosing volume of 30–50 ml would be representative for humans (and for dogs with 10 kg body weight). Dogs are also suitable to investigate the food effects [174, 175]. The amount of food should be scaled down for dogs. However, for low permeability drugs, an oral absorption study should not be performed in dogs, as the pore size of the paracellular pathway in dogs is larger than that in humans. For evaluation of the controlled-release formulation, the short GI transit time and the strong mechanical stress in dogs should be carefully considered. The intestinal transit time in dogs can be prolonged to approximate that in humans by coadministration of atropine [176–178]. This dog model was used to evaluate the sustained release and pulsate formulations.

For drugs with low permeability, rats would be more appropriate [179]. A dose volume of 1 ml corresponds to circa 250 ml in humans. It is technically difficult to administer a capsule or a tablet to rats (a special capsule for rats is commercially available if necessary). In rats, the bile is continuously secreted into the duodenum and the bile-micelle concentration is significantly higher than that in humans.

Little is known about the agitation strength in the rat intestine. Owing to these reasons, rats are not suitable to assess the oral absorption of drugs with low solubility.

7.10.4 Analysis

Deconvolution is often used to analyze oral PK data. The blood sampling time schedule should be set to provide sufficient data points in the absorption phase.

The *in vivo* animal PK data is often used to adjust a model parameter before predicting the oral absorption of a drug in humans. However, this model optimization should be performed very carefully. Rather, it should be avoided in many cases because it is difficult to surely identify the parameter truly responsible for the discrepancy between simulated and observed PK profiles. If a significant discrepancy is observed, the reason for the discrepancy should be identified by an independent mechanistic investigation. This point is further discussed in Section 16.2.

REFERENCES

1. Lee, P.H., Ayyampalayam, S.N., Carreira, L.A., Shalaeva, M., Bhattachar, S., Coselmon, R., Poole, S., Gifford, E., Lombardo, F. (2007). In silico prediction of ionization constants of drugs. *Mol. Pharm*., 4, 498–512.
2. Manchester, J., Walkup, G., Rivin, O., You, Z. (2010). Evaluation of pKa estimation methods on 211 druglike compounds. *J. Chem. Inf. Model*., 50, 565–571.
3. Comer, J., Ionization constant and ionization profile, in: B. Testa, H. van de Waterbeemd (Eds.) Comprehensive medicinal chemistry II Volume 5 ADME-Tox approach, Elsevier, Oxford, 2007, pp. 357–397.
4. Box, K., Bevan, C., Comer, J., Hill, A., Allen, R., Reynolds, D. (2003). High-throughput measurement of pKa values in a mixed-buffer linear pH gradient system. *Anal. Chem*., 75, 883–892.
5. Ishihama, Y., Nakamura, M., Miwa, T., Kajima, T., Asakawa, N. (2002). A rapid method for pK(a) determination of drugs using pressure-assisted capillary electrophoresis with photodiode array detection in drug discovery. *J. Pharm. Sci*., 91, 933–942.
6. Poole, S., Patel, S., Dehring, K., Workman, H., Poole, C. (2004). Determination of acid dissociation constants by capillary electrophoresis. *J. Chromatogr., A*, 1037, 445–454.
7. Shalaeva, M., Kenseth, J., Lombardo, F., Bastin, A. (2008). Measurement of dissociation constants (pKa values) of organic compounds by multiplexed capillary electrophoresis using aqueous and cosolvent buffers. *J. Pharm. Sci*., 97, 2581–2606.
8. Jia, Z., Ramstad, T., Zhong, M. (2001). Medium-throughput pKa screening pharmaceuticals by pressure-assisted capillary electrophoresis. *Electrophoresis*, 22, 1112–1118.
9. Wan, H., Holmen, A., Nagard, M., Lindberg, W. (2002). Rapid screening of pKa values of pharmaceuticals by pressure-assisted capillary electrophoresis combined with short-end injection. *J. Chromatogr., A*, 979, 369–377.

10. Wan, H., Holmen, A.G., Wang, Y., Lindberg, W., Englund, M., Nagard, M.B., Thompson, R.A. (2003). High-throughput screening of pKa values of pharmaceuticals by pressure-assisted capillary electrophoresis and mass spectrometry. *Rapid Commun. Mass Spectrom*., 17, 2639–2648.
11. Zhou, C., Jin, Y., Kenseth, J.R., Stella, M., Wehmeyer, K.R., Heineman, W.R. (2005). Rapid pKa estimation using vacuum-assisted multiplexed capillary electrophoresis (VAMCE) with ultraviolet detection. *J. Pharm. Sci*., 94, 576–589.
12. Volgyi, G., Baka, E., Box, K.J., Comer, J.E., Takacs-Novak, K. (2010). Study of pH-dependent solubility of organic bases. Revisit of Henderson-Hasselbalch relationship. *Anal. Chim. Acta*., 673, 40–46.
13. Fiese, E.F. (2003). General pharmaceutics-the new physical pharmacy. *J. Pharm. Sci*., 92, 1331–1342.
14. Balbach, S., Korn, C. (2004). Pharmaceutical evaluation of early development candidates "the 100mg-approach". *Int. J. Pharm*., 275, 1–12.
15. Poulin, P., Theil, F.-P. (2000). A priori prediction of tissue:plasma partition coefficients of drugs to facilitate the use of physiologically-based pharmacokinetic models in drug discovery. *J. Pharm. Sci*., 89, 16–35.
16. Rodgers, T., Rowland, M. (2006). Physiologically based pharmacokinetic modelling 2: predicting the tissue distribution of acids, very weak bases, neutrals and zwitterions. *J. Pharm. Sci*., 95, 1238–1257.
17. Rodgers, T., Rowland, M. (2007). Mechanistic approaches to volume of distribution predictions: understanding the processes. *Pharm. Res*., 24, 918–933.
18. Tomizawa, K., Sugano, K., Yamada, H., Horii, I. (2006). Physicochemical and cell-based approach for early screening of phospholipidosis-inducing potential. *J. Toxicol. Sci*., 31, 315–324.
19. Mannhold, R., Poda, G.I., Ostermann, C., Tetko, I.V. (2009). Calculation of molecular lipophilicity: state-of-the-art and comparison of log P methods on more than 96,000 compounds. *J. Pharm. Sci*., 98, 861–893.
20. Avdeef, A., Bendels, S., Di, L., Faller, B., Kansy, M., Sugano, K., Yamauchi, Y. (2007). Parallel artificial membrane permeability assay (PAMPA)-critical factors for better predictions of absorption. *J. Pharm. Sci*., 96, 2893–2909.
21. Wenlock, M.C., Barton, P., Luker, T. (2011). Lipophilicity of acidic compounds: impact of ion pair partitioning on drug design. *Bioorg. Med. Chem. Lett*., 21, 3550–3556.
22. Pagliara, A., Carrupt, P.A., Caron, G., Gaillard, P., Testa, B. (1997). Lipophilicity profiles of ampholytes. *Chem. Rev*., 97, 3385–3400.
23. Bermejo, M., Avdeef, A., Ruiz, A., Nalda, R., Ruell, J.A., Tsinman, O., Gonzalez, I., Fernandez, C., Sanchez, G., Garrigues, T.M., Merino, V. (2004). PAMPA–a drug absorption model*1: 7. Comparing rat, Caco-2, and PAMPA permeability of fluoroquinolones. *Eur. J. Pharm. Sci*., 21, 429.
24. Nishimura, I., Hirano, A., Yamashita, T., Fukami, T. (2009). Improvement of the high-speed logD assay using an injection marker for the water plug aspiration/injection method. *J. Chromatogr., A*, 1216, 2984–2988.
25. Dohta, Y., Yamashita, T., Horiike, S., Nakamura, T., Fukami, T. (2007). A system for LogD screening of 96-well plates using a water-plug aspiration/injection method combined with high-performance liquid chromatography-mass spectrometry. *Anal. Chem*., 79, 8312–8315.

26. Lombardo, F., Shalaeva, M.Y., Tupper, K.A., Gao, F., Abraham, M.H. (2000). ElogPoct: a tool for lipophilicity determination in drug discovery. *J. Med. Chem*., 43, 2922–2928.
27. Lombardo, F., Shalaeva, M.Y., Tupper, K.A., Gao, F. (2001). ElogD(oct): a tool for lipophilicity determination in drug discovery. 2. Basic and neutral compounds. *J. Med. Chem*., 44, 2490–2497.
28. Yamagami, C., Kawase, K., Iwaki, K. (2002). Hydrophobicity parameters determined by reversed-phase liquid chromatography. XV: optimal conditions for prediction of log P(oct) by using RP-HPLC procedures. *Chem. Pharm. Bull. (Tokyo)*, 50, 1578–1583.
29. Herbert, B.J., Dorsey, J.G. (1995). n-octanol-water partition coefficient estimation by micellar electrokinetic capillary chromatography. *Anal. Chem*., 67, 744–749.
30. Poole, S.K., Patel, S., Dehring, K., Workman, H., Dong, J. (2003). Estimation of octanol-water partition coefficients for neutral and weakly acidic compounds by microemulsion electrokinetic chromatography using dynamically coated capillary columns. *J. Chromatogr., B Analyt. Technol. Biomed. Life Sci*., 793, 265–274.
31. Razak, J.L., Cutak, B.J., Larive, C.K., Lunte, C.E. (2001). Correlation of the capacity factor in vesicular electrokinetic chromatography with the octanol:water partition coefficient for charged and neutral analytes. *Pharm. Res*., 18, 104–111.
32. Poole, S.K., Durham, D., Kibbey, C. (2000). Rapid method for estimating the octanol–water partition coefficient (log P ow) by microemulsion electrokinetic chromatography. *J. Chromatogr., B Biomed. Sci. Appl*., 745, 117–126.
33. Avdeef, A. (1993). pH-metric log P. II: refinement of partition coefficients and ionization constants of multiprotic substances. *J. Pharm. Sci*., 82, 183.
34. Slater, B., McCormack, A., Avdeef, A., Comer, J.E. (1994). pH-metric log P. 4. Comparison of partition coefficients determined by HPLC and potentiometric methods to literature values. *J. Pharm. Sci*., 83, 1280.
35. Faller, B., Grimm, H.P., Loeuillet-Ritzler, F., Arnold, S., Briand, X. (2005). High-throughput lipophilicity measurement with immobilized artificial membranes. *J. Med. Chem*., 48, 2571–2576.
36. Glomme, A., März, J., Dressman, J., Predicting the intestinal solubility of poorly soluble drugs, in: B. Testa, S. Krämer, H. Wunderli-Allenspach, G. Folkers (Eds.) Pharmacokinetic Profiling in Drug Research, Wiley-VCH, Zurich, 2006, pp. 259–280.
37. Wiedmann, T.S., Kamel, L. (2002). Examination of the solubilization of drugs by bile salt micelles. *J. Pharm. Sci*., 91, 1743–1764.
38. Avdeef, A., Box, K.J., Comer, J.E., Hibbert, C., Tam, K.Y. (1998). pH-metric logP 10. Determination of liposomal membrane-water partition coefficients of ionizable drugs. *Pharm. Res*., 15, 209–215.
39. Miyazaki, J., Hideg, K., Marsh, D. (1992). Interfacial ionization and partitioning of membrane-bound local anesthetics. *Biochim. Biophys. Acta*, 1103, 62–68.
40. de Castro, B., Gameiro, P., Guimaraes, C., Lima, J.L., Reis, S. (2001). Partition coefficients of beta-blockers in bile salt/lecithin micelles as a tool to assess the role of mixed micelles in gastrointestinal absorption. *Biophys. Chem*., 90, 31–43.
41. Yamaguchi, T., Ikeda, C., Sekine, Y. (1986). Intestinal absorption of a b-adrenergic blocking agent nadolol. I. Comparison of absorption behavior of nadolol with those of other b-blocking agents in rats. *Chem. Pharm. Bull*., 34, 3362–3369.

42. Yamaguchi, T., Ikeda, C., Sekine, Y. (1986). Intestinal absorption of a b-adrenergic blocking agent nadolol. II. Mechanism of the inhibitory effect on the intestinal absorption of nadolol by sodium cholate in rats. *Chem. Pharm. Bull*., 34, 3836–3843.
43. Yamaguchi, T., Oida, T., Ikeda, C., Sekine, Y. (1986). Intestinal absorption of a b-adrenergic blocking agent nadolol. III. Nuclear magnetic resonance spectroscopic study on nadolol-sodium cholate micellar complex and intestinal absorption of nadolol derivatives in rats. *Chem. Pharm. Bull*., 34, 4259–4264.
44. Giron, D., Testa, B., van de Waterbeemd, H. (Eds.), Artificial membrane technologies to assess transfer and permeation of drugs in drug discovery, in Comprehensive Medicinal Chemistry II Volume 5 ADME-Tox Approach, Elsevier, Oxford, 2007, pp. 509–530.
45. Pudipeddi, M., Serajuddin, A.T.M. (2005). Trends in solubility of polymorphs. *J. Pharm. Sci*., 94, 929–939.
46. Threlfall, T. (2003). Structural and thermodynamic explanations of Ostwald's rule. *Org. Process Res. Dev*., 7, 1017–1027.
47. Hancock, B.C., Parks, M. (2000). What is the true solubility advantage for amorphous pharmaceuticals? *Pharm. Res*., 17, 397–404.
48. Miller, J.M., Collman, B.M., Greene, L.R., Grant, D.J.W., Blackburn, A.C. (2005). Identifying the stable polymorph early in the drug discovery-development process. *Pharm. Dev. Technol*., 10, 291–297.
49. Ruland, W. (1961). X-ray determination of crystallinity and diffuse disorder scattering. *Acta Crystallogr*., 14, 1180–1185.
50. Gardner, C.R., Walsh, C.T., Almarsson, O. (2004). Drugs as materials: valuing physical form in drug discovery. *Nat. Rev. Drug Discov*., 3, 926–934.
51. Morissette, S.L., Almarsson, O., Peterson, M.L., Remenar, J.F., Read, M.J., Lemmo, A.V., Ellis, S., Cima, M.J., Gardner, C.R. (2004). High-throughput crystallization: polymorphs, salts, co-crystals and solvates of pharmaceutical solids. *Adv. Drug Delivery Rev*., 56, 275–300.
52. Kojima, T., Onoue, S., Murase, N., Katoh, F., Mano, T., Matsuda, Y. (2006). Crystalline form information from multiwell plate salt screening by use of raman microscopy. *Pharm. Res*., 23, 806–812.
53. Girolami, G.S. (1994). A simple "back of the envelope" method for estimating the densities and molecular volumes of liquids and solids. *J. Chem. Educ*., 71, 962–964.
54. Cao, X., Leyva, N., Anderson, S.R., Hancock, B.C. (2008). Use of prediction methods to estimate true density of active pharmaceutical ingredients. *Int. J. Pharm*., 355, 231–237.
55. Lipinski, C.A., Lombardo, F., Dominy, B.W., Feeney, P.J. (1997). Experimental and computational approaches to estimate solubility and permeability in drug discovery and development settings. *Adv. Drug Delivery Rev*., 23, 3–25.
56. Dehring, K.A., Workman, H.L., Miller, K.D., Mandagere, A., Poole, S.K. (2004). Automated robotic liquid handling/laser-based nephelometry system for high throughput measurement of kinetic aqueous solubility. *J. Pharm. Biomed. Anal*., 36, 447–456.
57. Chen, T.-M., Shen, H., Zhu, C. (2002). Evaluation of a method for high throughput solubility determination using a multi-wavelength UV plate reader. *Comb. Chem. High Throughput Screen*., 5, 575–581.

58. Pitt, A. (2005). High-throughput screening to determine aqueous drug solubility. *Pharm. Discov*., 5, 46–49.

59. Bhattachar, S.N., Deschenes, L.A., Wesley, J.A. (2006). Solubility: it's not just for physical chemists. *Drug Discov. Today*, 11, 1012–1018.

60. Vertzoni, M., Dressman, J., Butler, J., Hempenstall, J., Reppas, C. (2005). Simulation of fasting gastric conditions and its importance for the dissolution of lipophilic compounds. *Eur. J. Pharm. Biopharm.,* 60, 413–417.

61. Galia, E., Nicolaides, E., Horter, D., Lobenberg, R., Reppas, C., Dressman, J.B. (1998). Evaluation of various dissolution media for predicting performance of class I and II drugs. *Pharm. Res*., 15, 698–705.

62. Jantratid, E., Janssen, N., Reppas, C., Dressman, J.B. (2008). Dissolution media simulating conditions in the proximal human gastrointestinal tract: an update. *Pharm. Res*., 25, 1663–1676.

63. Sugano, K., Okazaki, A., Sugimoto, S., Tavornvipas, S., Omura, A., Mano, T. (2007). Solubility and dissolution profile assessment in drug discovery. *Drug Metab. Pharmacokinet*., 22, 225–254.

64. Scholz, A., Kostewicz, E., Abrahamsson, B., Dressman, J.B. (2003). Can the USP paddle method be used to represent in-vivo hydrodynamics? *J. Pharm. Pharmacol*., 55, 443–451.

65. Baka, E., Comer, J.E., Takacs-Novak, K. (2008). Study of equilibrium solubility measurement by saturation shake-flask method using hydrochlorothiazide as model compound. *J. Pharm. Biomed. Anal*., 46, 335–341.

66. Volgyi, G., Baka, E., Kovacs, M., Takacsne, N.K. (2011). Good laboratory practice of equilibrium solubility measurement II. Study of pH-dependent solubility of ionizable compounds. *Acta Pharm. Hung*., 81, 87–95.

67. Baka, E. (2011). Good laboratory practice of equilibrium solubility measurement. *Acta Pharm. Hung*., 81, 18–28.

68. Seadeek, C., Ando, H., Bhattachar, S.N., Heimbach, T., Sonnenberg, J.L., Blackburn, A.C. (2007). Automated approach to couple solubility with final pH and crystallinity for pharmaceutical discovery compounds. *J. Pharm. Biomed. Anal*., 43, 1660–1666.

69. Sugano, K., Kato, T., Suzuki, K., Keiko, K., Sujaku, T., Mano, T. (2006). High throughput solubility measurement with automated polarized light microscopy analysis. *J. Pharm. Sci*., 95, 2115–2122.

70. Sugaya, Y., Yoshiba, T., Kajima, T., Ishihama, Y. (2002). Development of solubility screening methods in drug discovery. *Yakugaku Zasshi*, 122, 237–246.

71. Pudipeddi, M., Zannou, E.A., Vasanthavada, M., Dontabhaktuni, A., Royce, A.E., Joshi, Y.M., Serajuddin, A.T.M. (2008). Measurement of surface pH of pharmaceutical solids: a critical evaluation of indicator dye-sorption method and its comparison with slurry pH method. *J. Pharm. Sci*., 97, 1831–1842.

72. Serajuddin, A.T.M., Jarowski, C.I. (1985). Effect of diffusion layer pH and solubility on the dissolution rate of pharmaceutical acids and their sodium salts. II: salicylic acid, theophylline, and benzoic acid. *J. Pharm. Sci*., 74, 148–154.

73. Serajuddin, A.T.M., Jarowski, C.I. (1985). Effect of diffusion layer pH and solubility on the dissolution rate of pharmaceutical bases and their hydrochloride salts. I: phenazopyridine. *J. Pharm. Sci*., 74, 142–147.

74. Van Eerdenbrugh, B., Vermant, J., Martens, J.A., Froyen, L., Van Humbeeck, J., Van den Mooter, G., Augustijns, P. (2010). Solubility increases associated with crystalline drug nanoparticles: methodologies and significance. *Mol. Pharm*., 7, 1858–1870.

75. Llinas, A., Glen, R.C., Goodman, J.M. (2008). Solubility challenge: can you predict solubilities of 32 molecules using a database of 100 reliable measurements? *J. Chem. Inf. Model*., 48, 1289–1303.

76. Avdeef, A., Tsinman, K., Tsinman, O., Sun, N., Voloboy, D. (2009). Miniaturization of powder dissolution measurement and estimation of particle size. *Chem. Biodivers*., 6, 1796–1811.

77. Bai, G., Armenante, P.M. (2008). Velocity distribution and shear rate variability resulting from changes in the impeller location in the USP dissolution testing apparatus II. *Pharm. Res*., 25, 320–336.

78. Bai, G., Armenante, P.M. (2009). Hydrodynamic, mass transfer, and dissolution effects induced by tablet location during dissolution testing. *J. Pharm. Sci*., 98, 1511–1531.

79. Bai, G., Armenante, P.M., Plank, R.V. (2007). Experimental and computational determination of blend time in USP dissolution testing apparatus II. *J. Pharm. Sci*., 96, 3072–3086.

80. Bai, G., Armenante, P.M., Plank, R.V., Gentzler, M., Ford, K., Harmon, P. (2007). Hydrodynamic investigation of USP dissolution test apparatus II. *J. Pharm. Sci*., 96, 2327–2349.

81. Mirza, T., Joshi, Y., Liu, Q., Vivilecchia, R. (2005). Evaluation of dissolution hydrodynamics in the USP, Peakand flat-bottom vessels using different solubility drugs. *Dissolut. Technol*., 12, 11–16.

82. Shiko, G., Gladden, L.F., Sederman, A.J., Connolly, P.C., Butler, J.M. (2011). MRI studies of the hydrodynamics in a USP 4 dissolution testing cell. *J. Pharm. Sci*., 100, 976–991.

83. Kostewicz, E.S., Wunderlich, M., Brauns, U., Becker, R., Bock, T., Dressman, J.B. (2004). Predicting the precipitation of poorly soluble weak bases upon entry in the small intestine. *J. Pharm. Pharmacol*., 56, 43–51.

84. Carino, S.R., Sperry, D.C., Hawley, M. (2010). Relative bioavailability of three different solid forms of PNU-141659 as determined with the artificial stomach-duodenum model. *J. Pharm. Sci*., 99, 3923–3930.

85. Carino, S.R., Sperry, D.C., Hawley, M. (2005). Relative bioavailability estimation of carbamazepine crystal forms using an artificial stomach-duodenum model. *J. Pharm. Sci*., 95, 116–125.

86. Gu, C.-H., Rao, D., Gandhi, R.B., Hilden, J., Raghavan, K. (2005). Using a novel multicompartment dissolution system to predict the effect of gastric pH on the oral absorption of weak bases with poor intrinsic solubility. *J. Pharm. Sci*., 94, 199–208.

87. Sugawara, M., Kadomura, S., He, X., Takekuma, Y., Kohri, N., Miyazaki, K. (2005). The use of an dissolution and absorption system to evaluate oral absorption of two weak bases in pH-independent controlled-release formulations. *Eur. J. Pharm. Sci*., 26, 1–8.

88. Kataoka, M., Masaoka, Y., Sakuma, S., Yamashita, S. (2006). Effect of food intake on the oral absorption of poorly water-soluble drugs: assessment of drug dissolution and permeation assay system. *J. Pharm. Sci*., 95, 2051–2061.

89. Kataoka, M., Masaoka, Y., Yamazaki, Y., Sakane, T., Sezaki, H., Yamashita, S. (2003). system to evaluate oral absorption of poorly water-soluble drugs: simultaneous analysis on dissolution and permeation of drugs. *Pharm. Res*., 20, 1674–1680.
90. Buch, P., Langguth, P., Kataoka, M., Yamashita, S. (2009). IVIVC in oral absorption for fenofibrate immediate release tablets using a dissolution/permeation system. *J. Pharm. Sci*., 98, 2001–2009.
91. Kataoka, M., Sugano, K., da Costa Mathews, C., Wong, J.W., Jones, K.L., Masaoka, Y., Sakuma, S., Yamashita, S. (2011). Application of dissolution/permeation system for evaluation of formulation effect on oral absorption of poorly water-soluble drugs in drug development. *Pharm. Res*. DOI: 10.1007/s11095-011-0623-2.
92. Tavornvipas, S., Sugimoto, S., Sugano, K., Hashimoto, N., Mano, T., Yamashita, S. (2007). Application of dissolution-permeation system PAMPA system for predicttion of oral drug absorption of nanoparticle. *J. Pharm. Sci. Tech. Jpn*., 67, 381.
93. Takada, K., Masaoka, Y., Kataoka, M., Sakuma, S., Takano, R., Hayashi, Y., Asoh, Y., Yamashita, S. (2005). assessment of oral absorption of poorly-soluble drugs: use of artificial lipid membrane in dissolution/permeation system. *Drug Metab. Rev*., 288.
94. Sugano, K., Sakai, K., Mucopolysaccharide-layered lipid membrane, membrane permeability-measuring filter/apparatus/kit, membrane permeability evaluation method, and test substance-screening method, in, JP, 2005, p. 13.
95. Box, K.J., Volgyi, G., Baka, E., Stuart, M., Takacs-Novak, K., Comer, J.E.A. (2006). Equilibrium versus kinetic measurements of aqueous solubility, and the ability of compounds to supersaturate in solution-a validation study. *J. Pharm. Sci*., 95, 1298–1307.
96. Lindfors, L., Forssen, S., Westergren, J., Olsson, U. (2008). Nucleation and crystal growth in supersaturated solutions of a model drug. *J. Colloid Interface Sci*., 325, 404–413.
97. Carlert, S., Palsson, A., Hanisch, G., von Corswant, C., Nilsson, C., Lindfors, L., Lennernas, H., Abrahamsson, B. (2010). Predicting intestinal precipitation–a case example for a basic BCS class II drug. *Pharm. Res*., 27, 2119–2130.
98. Gu, C.H., Gandhi, R.B., Tay, L.K., Zhou, S., Raghavan, K. (2004). Importance of using physiologically relevant volume of dissolution medium to correlate the oral exposure of formulations of BMS-480188 mesylate. *Int. J. Pharm*., 269, 195–202.
99. Lennernaes, H. (2007). Animal data: the contributions of the Ussing Chamber and perfusion systems to predicting human oral drug delivery. *Adv. Drug Delivery Rev*., 59, 1103–1120.
100. Salphati, L., Childers, K., Pan, L., Tsutsui, K., Takahashi, L. (2001). Evaluation of a single-pass intestinal-perfusion method in rat for the prediction of absorption in man. *J. Pharm. Pharmacol*., 53, 1007–1013.
101. Lennernaes, H. (2007). Intestinal permeability and its relevance for absorption and elimination. *Xenobiotica*, 37, 1015–1051.
102. Hidalgo, I.J., Raub, T.J., Borchardt, R.T. (1989). Characterization of the human colon carcinoma cell line (Caco-2) as a model system for intestinal epithelial permeability. *Gastroenterology*, 96, 736–749.
103. Artursson, P., Karlsson, J. (1991). Correlation between oral absorption in humans and apparent drug permeability coefficients in human intestinal epithelial Caco2 cells. *Biochem. Biophys. Res. Commun*., 175, 880–885.

104. Artursson, P., Matsson, P., Cell culture absorption models-state of the art, in: B. Testa, S. Krämer, H. Wunderli-Allenspach, G. Folkers (Eds.) Pharmacokinetic Profiling Drug Research, Wiley-VCH, Zurich, 2006, pp. 71–78.

105. Hayeshi, R., Hilgendorf, C., Artursson, P., Augustijns, P., Brodin, B., Dehertogh, P., Fisher, K., Fossati, L., Hovenkamp, E., Korjamo, T., Masungi, C., Maubon, N., Mols, R., Mullertz, A., Monkkonen, J., O'Driscoll, C., Oppers-Tiemissen, H.M., Ragnarsson, E.G., Rooseboom, M., Ungell, A.L. (2008). Comparison of drug transporter gene expression and functionality in Caco-2 cells from 10 different laboratories. *Eur. J. Pharm. Sci*., 35, 383–396.

106. Avdeef, A., Tam, K.Y. (2010). How well can the Caco-2/Madin-darby canine kidney models predict effective human jejunal permeability? *J. Med. Chem*., 53, 3566–3584.

107. Putnam, W.S., Pan, L., Tsutsui, K., Takahashi, L., Benet, L.Z. (2002). Comparison of bidirectional cephalexin transport across MDCK and caco-2 cell monolayers: interactions with peptide transporters. *Pharm. Res*., 19, 27–33.

108. Thiel-Demby, V.E., Humphreys, J.E., St. John Williams, L.A., Ellens, H.M., Shah, N., Ayrton, A.D., Polli, J.W. (2009). Biopharmaceutics classification system: validation and learnings of an permeability assay. *Mol. Pharm*., 6, 11–18.

109. Lennernäs, H. (2007). Animal data: the contributions of the Ussing Chamber and perfusion systems to predicting human oral drug delivery. *Adv. Drug Delivery Rev*., 59, 1103–1120.

110. Kansy, M., Senner, F., Gubernator, K. (1998). Physicochemical high throughput screening: parallel artificial membrane permeation assay in the description of passive absorption processes. *J. Med. Chem*., 41, 1007–1010.

111. Sugano, K., Hamada, H., Machida, M., Ushio, H. (2001). High throuput prediction of oral absorption: Improvement of the composition of the lipid solution used in parallel artificial membrane permeation assay. *J. Biomol. Screen*., 6, 189–196.

112. Wohnsland, F., Faller, B. (2001). High-throughput permeability pH profile and high-throughput alkane/water log P with artificial membranes. *J. Med. Chem*., 44, 923–930.

113. Di, L., Kerns, E.H., Fan, K., McConnell, O.J., Carter, G.T. (2003). High throughput artificial membrane permeability assay for blood-brain barrier. *Eur. J. Med. Chem*., 38, 223–232.

114. Avdeef, A., Strafford, M., Block, E., Balogh, M.P., Chambliss, W., Khan, I. (2001). Drug absorption model: filter-immobilized artificial membranes; 2. Studies of the permeability properties of lactones in Piper methysticum Forst. *Eur. J. Pharm. Sci*., 14, 271–280.

115. Tanaka, M., Fukuda, H., Nagai, T. (1978). Permeation of a drug through a model membrane consisting of millipore filter with oil. *Chem. Pharm. Bull*., 26, 9–13.

116. Camenisch, G., Folkers, G., van de Waterbeemd, H. (1997). Comparison of passive drug transport through Caco-2 cells and artificial membranes. *Int. J. Pharm*., 147, 61–70.

117. Avdeef, A., Absorption and Drug Development, Wiley-Interscience, NJ, Hoboken, 2003.

118. Sugano, K., Nabuchi, Y., Machida, M., Asoh, Y. (2004). Permeation characteristics of a hydrophilic basic compound across a bio-mimetic artificial membrane. *Int. J. Pharm*., 275, 271–278.

119. Seo, P.R., Teksin, Z.S., Kao, J.P.Y., Polli, J.E. (2006). Lipid composition effect on permeability across PAMPA. *Eur. J. Pharm. Sci*., 29, 259–268.
120. Teksin, Z.S., Hom, K., Balakrishnan, A., Polli, J.E. (2006). Ion pair-mediated transport of metoprolol across a three lipid-component PAMPA system. *J. Controlled Release*, 116, 50–57.
121. Xiang, T., Xu, Y., Anderson, B.D. (1998). The barrier domain for solute permeation varies with lipid bilayer phase structure. *J. Membr. Biol*., 165, 77–90.
122. Kansy, M., Avdeef, A., Fischer, H. (2004). Advances in screening for membrane permeability: high-resolution PAMPA for medicinal chemists. *Drug Discove. Today: Technol*., 1, 349–355.
123. Ano, R., Kimura, Y., Shima, M., Matsuno, R., Ueno, T., Akamatsu, M. (2004). Relationships between structure and high-throughput screening permeability of peptide derivatives and related compounds with artificial membranes: application to prediction of Caco-2 cell permeability. *Bioorg. Med. Chem*., 12, 257.
124. Fujikawa, M., Ano, R., Nakao, K., Shimizu, R., Akamatsu, M. (2005). Relationships between structure and high-throughput screening permeability of diverse drugs with artificial membranes: application to prediction of Caco-2 cell permeability. *Bioorg. Med. Chem*., 13, 4721–4732.
125. Fujikawa, M., Nakao, K., Shimizu, R., Akamatsu, M. (2007). QSAR study on permeability of hydrophobic compounds with artificial membranes. *Bioorg. Med. Chem*., 15, 3756–3767.
126. Flaten, G.E., Bunjes, H., Luthman, K., Brandl, M. (2006). Drug permeability across a phospholipid vesicle-based barrier: 2. Characterization of barrier structure, storage stability and stability towards pH changes. *Eur. J. Pharm. Sci*., 28, 336–343.
127. Flaten, G.E., Dhanikula, A.B., Luthman, K., Brandl, M. (2006). Drug permeability across a phospholipid vesicle based barrier: a novel approach for studying passive diffusion. *Eur. J. Pharm. Sci*., 27, 80–90.
128. Flaten, G.E., Skar, M., Luthman, K., Brandl, M. (2007). Drug permeability across a phospholipid vesicle based barrier: 3. Characterization of drug-membrane interactions and the effect of agitation on the barrier integrity and on the permeability. *Eur. J. Pharm. Sci*., 30, 324–332.
129. Corti, G., Maestrelli, F., Cirri, M., Furlanetto, S., Mura, P. (2006). Development and evaluation of an method for prediction of human drug absorption I. Assessment of artificial membrane composition. *Eur. J. Pharm. Sci*., 27, 346–353.
130. Corti, G., Maestrelli, F., Cirri, M., Zerrouk, N., Mura, P. (2006). Development and evaluation of an method for prediction of human drug absorption. *Eur. J. Pharm. Sci*., 27, 354–362.
131. Chen, X., Murawski, A., Patel, K., Crespi, C.L., Balimane, P.V. (2008). A novel design of artificial membrane for improving the parallel artificial membrane permeability assay model. *Pharm. Res*., 25, 1511–1520.
132. Avdeef, A. (2007). Solubility of sparingly-soluble ionizable drugs. *Adv. Drug Delivery Rev*., 59, 568–590.
133. Flaten, G.E., Bunjes, H., Luthman, K., Brandl, M. (2006). Drug permeability across a phospholipid vesicle-based barrier. *Eur. J. Pharm. Sci*., 28, 336–343.
134. Ottaviani, G., Martel, S., Carrupt, P.-A. (2006). Parallel artificial membrane permeability assay: a new membrane for the fast prediction of passive uman skin permeability. *J. Med. Chem*., 49, 3948–3954.

135. Sugano, K., Hamada, H., Machida, M., Ushio, H., Saitoh, K., Terada, K. (2001). Optimized conditions of bio-mimetic artificial membrane permeation assay. *Int. J. Pharm*., 228, 181–188.

136. Danelian, E., Karlen, A., Karlsson, R., Winiwarter, S., Hansson, A., Lofas, S., Lennernas, H., Hamalainen, M.D. (2000). SPR biosensor studies of the direct interaction between 27 drugs and a liposome surface: correlation with fraction absorbed in humans. *J. Med. Chem*., 43, 2083–2086.

137. Frostell-Karlsson, A., Widegren, H., Green, C.E., Hamalainen, M.D., Westerlund, L., Karlsson, R., Fenner, K., van de Waterbeemd, H. (2005). Biosensor analysis of the interaction between drug compounds and liposomes of different properties; a two-dimensional characterization tool for estimation of membrane absorption. *J. Pharm. Sci*., 94, 25–37.

138. Cheng, Y.Y., Song, J.C., Hanlan, L., Pidgeon, C. (1997). Immobilized Artificial Membranes—screens for drug membrane interactions. *Adv. Drug Delivery Rev*., 23, 229–256.

139. Liu, H., Ong, S., Glunz, L., Pidgeon, C. (1995). Predicting drug-membrane interactions by HPLC: structural requirements of chromatographic surfaces. *Anal. Chem*., 67, 3550–3557.

140. Ong, S., Liu, H., Pidgeon, C. (1996). Immobilized-artificial-membrane chromatography: measurements of membrane partition coefficient and predicting drug membrane permeability. *J. Chromatogr., A*, 728, 113–128.

141. Ong, S., Liu, H., Qiu, X., Bhat, G., Pidgeon, C. (1995). Membrane partition coefficients chromatographically measured using immobilized artificial membrane surfaces. *Anal. Chem*., 67, 755–762.

142. Ong, S., Pidgeon, C. (1995). Thermodynamics of solute partitioning into immobilized artificial membranes. *Anal. Chem*., 67, 2119–2128.

143. Pidgeon, C., Ong, S., Liu, H., Qiu, X., Pidgeon, M., Dantzig, A.H., Munroe, J., Hornback, W.J., Kasher, J.S., Glunz, L., et al. (1995). IAM chromatography: an screen for predicting drug membrane permeability. *J. Med. Chem*., 38, 590–594.

144. Shaowei, O., Hanlan, L., Pidgeon, C. (1996). Immobilized-artificial-membrane chromatography: measurements of membrane partition coefficient and predicting drug membrane permeability. *J. Chromatogr., A*, 728, 113–128.

145. Beigi, F., Gottschalk, I., Lagerquist Hagglund, C., Haneskog, L., Brekkan, E., Zhang, Y., Osterberg, T., Lundahl, P. (1998). Immobilized liposome and biomembrane partitioning chromatography of drugs for prediction of drug transport. *Int. J. Pharm*., 164, 129–137.

146. Beigi, F., Lundahl, P. (1999). Immobilized biomembrane chromatography of highly lipophilic drugs. *J. Chromatogr., A*, 852, 313–317.

147. Beigi, F., Yang, Q., Lundahl, P. (1995). Immobilized-liposome chromatographic analysis of drug partitioning into lipid bilayers. *J. Chromatogr., A*, 704, 315–321.

148. Lundahl, P., Beigi, F. (1997). Immobilized liposome chromatography of drugs for model analysis of drug-membrane interactions. *Adv. Drug Delivery Rev*., 23, 221–227.

149. Loidl-Stahlhofen, A., Eckert, A., Hartmann, T., Schottner, M. (2001). Solid-supported lipid membranes as a tool for determination of membrane affinity: high-throughput screening of a physicochemical parameter. *J. Pharm. Sci*., 90, 599–606.

150. Loidl-Stahlhofen, A., Hartmann, T., Schottner, M., Rohring, C., Brodowsky, H., Schmitt, J., Keldenich, J. (2001). Multilamellar liposomes and solid-supported lipid membranes (TRANSIL): screening of lipid-water partitioning toward a high-throughput scale. *Pharm. Res*., 18, 1782–1788.

151. Avdeef, A. (2010). Leakiness and size exclusion of paracellular channels in cultured epithelial cell monolayers-interlaboratory comparison. *Pharm. Res*., 27, 480–489.

152. Neuhoff, S., Ungell, A.-L., Zamora, I., Artursson, P. (2003). pH-dependent bidirectional transport of weakly basic drugs across Caco-2 monolayers: implications for drug-drug interactions. *Pharm. Res*., 20, 1141–1148.

153. Avdeef, A., Nielsen, P.E., Tsinman, O. (2004). PAMPA–a drug absorption model*1: 11. Matching the unstirred water layer thickness by individual-well stirring in microtitre plates. *Eur. J. Pharm. Sci*., 22, 365.

154. Wils, P., Warnery, A., Phung-Ba, V., Legrain, S., Scherman, D. (1994). High lipophilicity decreases drug transport across intestinal epithelial cells. *J. Pharmacol. Exp. Ther*., 269, 654–658.

155. Krishna, G., Chen, K.-J., Lin, C.-C., Nomeir, A.A. (2001). Permeability of lipophilic compounds in drug discovery using in-vitro human absorption model, Caco-2. *Int. J. Pharm*., 222, 77–89.

156. Neuhoff, S., Artursson, P., Ungell, A.L. (2007). Advantages and disadvantages of using bovine serum albumin and/or Cremophor EL as extracellular additives during transport studies of lipophilic compounds across Caco-2 monolayers. *J. Drug Delivery Sci. Technol*., 17, 259–266.

157. Neuhoff, S., Artursson, P., Zamora, I., Ungell, A.-L. (2006). Impact of extracellular protein binding on passive and active drug transport across Caco-2 cells. *Pharm. Res*., 23, 350–359.

158. Sawada, G.A., Ho, N.F., Williams, L.R., Barsuhn, C.L., Raub, T.J. (1994). Transcellular permeability of chlorpromazine demonstrating the roles of protein binding and membrane partitioning. *Pharm. Res*., 11, 665–673.

159. Yamashita, S., Furubayashi, T., Kataoka, M., Sakane, T., Sezaki, H., Tokuda, H. (2000). Optimized conditions for prediction of intestinal drug permeability using Caco-2 cells. *Eur. J. Pharm. Sci*., 10, 195–204.

160. Aungst, B.J., Nguyen, N.H., Bulgarelli, J.P., Oates-Lenz, K. (2000). The influence of donor and reservoir additives on Caco-2 permeability and secretory transport of HIV protease inhibitors and other lipophilic compounds. *Pharm. Res*., 17, 1175–1180.

161. Liu, T., Chang, L.J., Uss, A., Chu, I., Morrison, R.A., Wang, L., Prelusky, D., Cheng, K.C., Li, C. (2010). The impact of protein on Caco-2 permeability of low mass balance compounds for absorption projection and efflux substrate identification. *J. Pharm. Biomed. Anal*., 51, 1069–1077.

162. Yamashita, S., Tanaka, Y., Endoh, Y., Taki, Y., Sakane, T., Nadai, T., Sezaki, H. (1997). Analysis of drug permeation across Caco-2 monolayer: implication for predicting drug absorption. *Pharm. Res*., 14, 486–491.

163. Saha, P., Kou, J.H. (2000). Effect of solubilizing excipients on permeation of poorly water-soluble compounds across Caco-2 cell monolayers. *Eur. J. Pharm. Biopharm*., 50, 403–411.

164. Takahashi, Y., Kondo, H., Yasuda, T., Watanabe, T., Kobayashi, S., Yokohama, S. (2002). Common solubilizers to estimate the Caco-2 transport of poorly water-soluble drugs. *Int. J. Pharm*., 246, 85–94.

165. Volpe, D.A. (2008). Variability in Caco-2 and MDCK cell-based intestinal permeability assays. *J. Pharm. Sci*., 97, 712–725.

166. Naruhashi, K., Tamai, I., Li, Q., Sai, Y., Tsuji, A. (2003). Experimental demonstration of the unstirred water layer effect on drug transport in caco-2 cells. *J. Pharm. Sci*., 92, 1502–1508.

167. Putnam, W.S., Ramanathan, S., Pan, L., Takahashi, L.H., Benet, L.Z. (2002). Functional characterization of monocarboxylic acid, large neutral amino acid, bile acid and peptide transporters, and P-glycoprotein in MDCK and Caco-2 cells. *J. Pharm. Sci*., 91, 2622–2635.

168. Takano, R., Furumoto, K., Shiraki, K., Takata, N., Hayashi, Y., Aso, Y., Yamashita, S. (2008). Rate-limiting steps of oral absorption for poorly water-soluble drugs in dogs; prediction from a miniscale dissolution test and a physiologically-based computer simulation. *Pharm. Res*., 25, 2334–2344.

169. Lee, Y.C., Zocharski, P.D., Samas, B. (2003). An intravenous formulation decision tree for discovery compound formulation development. *Int. J. Pharm*., 253, 111–119.

170. Bittner, B., Mountfield, R.J. (2002). Intravenous administration of poorly soluble new drug entities in early drug discovery: the potential impact of formulation on pharmacokinetic parameters. *Curr. Opin. Drug Discov. Devel*., 5, 59–71.

171. Akimoto, M., Nagahata, N., Furuya, A., Fukushima, K., Higuchi, S., Suwa, T. (2000). Gastric pH profiles of beagle dogs and their use as an alternative to human testing. *Eur. J. Pharm. Biopharm*., 49, 99–102.

172. Sagawa, K., Li, F., Liese, R., Sutton, S.C. (2009). Fed and fasted gastric pH and gastric residence time in conscious beagle dogs. *J. Pharm. Sci*., 98, 2494–2500.

173. Polentarutti, B., Albery, T., Dressman, J., Abrahamsson, B. (2010). Modification of gastric pH in the fasted dog. *J. Pharm. Pharmacol*., 62, 462–469.

174. Lentz, K.A. (2008). Current methods for predicting human food effect. *AAPS J*., 10, 282–288.

175. Lentz, K.A., Quitko, M., Morgan, D.G., Grace, J.E. Jr., Gleason, C., Marathe, P.H. (2007). Development and validation of a preclinical food effect model. *J. Pharm. Sci*., 96, 459–472.

176. Sagara, K., Kawata, M., Mizuta, H., Shibata, M. (1994). Utility of gastrointestinal physiology regulated-dogs: bioavailability study of a commercial sustained-release dosage form of theophylline. *Biol. Pharm. Bull*., 17, 931–934.

177. Sagara, K., Nagamatsu, Y., Yamada, I., Kawata, M., Mizuta, H., Ogawa, K. (1992). Bioavailability study of commercial sustained-release preparations of diclofenac sodium in gastrointestinal physiology regulated-dogs. *Chem. Pharm. Bull. (Tokyo)*, 40, 3303–3306.

178. Sagara, K., Yamada, I., Matsuura, Y., Kawata, M., Shibata, M. (1996). Gastrointestinal physiology-regulated dogs for bioavailability evaluation of an oral controlled-release dosage form composed of pulsatile release granules. *Biol. Pharm. Bull*., 19, 1184–1188.

179. Cao, X., Gibbs, S.T., Fang, L., Miller, H.A., Landowski, C.P., Shin, H.C., Lennernas, H., Zhong, Y., Amidon, G.L., Yu, L.X., Sun, D. (2006). Why is it challenging to predict intestinal drug absorption and oral bioavailability in human using rat model. *Pharm. Res*., 23, 1675–1686.

CHAPTER 8

VALIDATION OF MECHANISTIC MODELS

> "The aim of science is not to open the door to infinite wisdom, but to set a limit to infinite error."
>
> —Bertolt Brecht

Biopharmaceutical modeling is not perfect. Therefore, it is important to understand its limitations. For example, some of the physiological data has large uncertainty. The solubilities of a drug in artificial GI fluids can be different from those in *in vivo* GI fluids. There are many other factors that should be improved in the future (Chapter 16). Therefore, it is important to know the limitations of current biopharmaceutical modeling before applying it to practical uses in drug discovery and development.

In this section, the GUT framework is used as an example.[1] All the equations in the GUT framework have been published and available for everyone. The drug and physiological data used in this section are all published ones. In addition, to increase the transparency of validation processes, the simplest equation is used as long as it is sufficient. This policy is also in accordance with Occam's razor principle.

In this section, we focus on the validation of *in vivo* results. The reliability of each primary equation has already been discussed in Section 2.5, therefore

[1]For commercial programs employing the other model equations, please ask the vendors for the thorough validation results.

Biopharmaceutics Modeling and Simulations: Theory, Practice, Methods, and Applications, First Edition. Kiyohiko Sugano.

it is not repeated in this section. Usually, the mechanistic equation of each primary process has been validated by comparison with well-controlled *in vitro* experiments. For example, the Henderson–Hasselbalch (HH) equation was validated with experimental pH–solubility profiles [1]. Generally speaking, physical equations such as the HH equation were well validated for a wide range of physical conditions, covering the physiological conditions in the GI tract (e.g., from pH 1 to 9).

8.1 CONCERNS RELATED TO MODEL VALIDATION USING *IN VIVO* DATA

The current status of biopharmaceutical modeling is that a perfect a priori prediction of Fa% (e.g., <30% error from *in vitro* data) is in principle unattainable because of (i) differences between *in vivo* and *in vitro* drug data (e.g., real intestinal fluid vs FaSSIF, *in vivo* intestinal membrane vs Caco-2), (ii) uncertainty of GI physiological data (e.g., fluid volume, fluid dynamics, transporter expression level), and (iii) imperfect theoretical equations (e.g., nucleation theory, first-pass metabolisms). In contrast, there were many publications seemingly suggesting perfect predictions. However, it is misleading to take these publications as validation of biopharmaceutical modeling. We discuss this point in depth in Chapter 16.

In many of the publications suggesting perfect predictions, the plasma concentration (C_p)–time profiles of one or a few drugs were selected as the target of simulation. However, the use of C_p–time profiles for the validation of biopharmaceutical modeling has some issues. As an *in vivo* PK model is additionally required, the simulation processes for a C_p–time profile have become more complicated than those for Fa%, making it difficult to validate the simulation processes. It could distract us from the essential points of oral absorption and focus too much on nonessential points (such as the subtle nuance in the shape of a C_p–time profile). When this type of "all in all" validation is employed, it is often difficult to be aware of the pitfalls in the simulation processes. In addition, the estimation of Fg and Fh has large uncertainty even when starting with *in vivo* CL data. In many cases of drugs with low solubility, i.v. PK data is not available.

8.2 STRATEGY FOR TRANSPARENT AND ROBUST VALIDATION OF BIOPHARMACEUTICAL MODELING

To avoid the above-mentioned concerns, for the validation of the GUT framework, we use the following principles:

- The simplest model equation required for each category of drugs (Occam's razor principle)

- To keep transparency, the simplest model should be used for validation. The use of unnecessary complex model decreases the transparency of validation process. Considering the variation of *in vivo* data used for validation, it would be impossible to prove the subtle advantage of a complex model. Parameter fitting is not performed unless the physiological parameter is not available in the literature. When parameter fitting is inevitable, the parameter is optimized with more than four Fa% data.
- Fa% data (but neither BA% nor C_p–time data)

  Fa% data were used for validation to avoid interference from the first-pass metabolisms and other uncertainties. For drugs with low solubility, the method explained in Section 5.5 was used to calculate Fa% from *in vivo* data.
- A large number of *in vivo* Fa% data for structurally and physicochemically diverse drugs (Table 8.1)

  Hundreds of Fa% data were used to increase the robustness of validation. This type of validation became possible, as Fa% data has been accumulated in the literature. Especially, the Fa% data of drugs with low solubility became available by introducing several calculation criteria as discussed in Section 5.5.
- Cross-validation with different data set

  The GUT framework is validated by several different experimental observations, such as *in vivo*/*in situ*/*in vitro* studies in humans/dogs/rats. This increases the robustness of the validation.
- Step-by-step validation

  A step-wise validation is pursued. The models are validated from the simplest one to the more complicated one, that is, (i) permeability-limited cases (Section 8.4), (ii) dissolution-rate and solubility-permeability-limited cases without the stomach effect (Section 8.5), and (iii) cases with the stomach effect (Section 8.6).

Validation of other specific processes such as colonic absorption and carrier-mediated absorption are discussed in the later sections.

8.3 PREDICTION STEPS

Before moving on to the validation processes, the prediction process step (PPS) is introduced to roughly categorize the available input data [2].

PPS I: Chemical structure only (*in silico* in a narrow sense)

PPS II: PPS I + *in vitro* data

A: Simple *in vitro* data (e.g., solubility, Caco-2)

B: Complex *in vitro* data (e.g., dissolution test, intestinal perfusion)

TABLE 8.1 Fa% Values and Physicochemical Properties of Drugs

Name	MW	log P_{oct}[a]	pK_a[b]	log D, pH 6.5[c]	Fa%	References
AAFC	243	−1.3(±1)[d]	—	−1.3	32	3
Acarbose	645	−6.8	—	−6.8	1	4
Acebutolol	336	2.0	9.5 (B)	−1.0	89.5	4
Acefylline	238	−0.8(±0.52)[d]	3.7 (A)[e]	−3.6	<10	5
Acetaminophen	151	0.3	—	0.3	100	4
Acetylsalicylic acid	180	0.9	3.5 (A)	−2.1	84	3
Acrivastatine	348	—	2.2 (A), 9.6 (B)	−0.1(pH 6.5)	88	3
Acyclovir	225	−1.7	—	−1.7	29	6
Adefovir	273	0.8	2.6 (A)[g]	−3.1	16	4
Adinazolam	351	4.4	5.7 (B)	4.3	100	4
Alfentanil	417	2.4	6.5 (B)	2.1	100	4
Alizapride	315	1.8	9.0 (B)	−0.7	100	4
Allopurinol	136	−1.0	—	−1.0	90	4
Alprazolam	308	2.6	—	2.6	92	4
Alprenolol	249	3.0	9.5 (B)	0.0	93	4
Amantadine	151	2.4	10.5 (B)	−1.6	95	4
Amiloride	229	−0.3	8.7 (B)	−2.5	50	6
Aminopyrine	231	0.9	5.1 (B)	0.8	100	3
Amiodarone	645	7.8	9.1 (B)	5.2	100	4
Amisulpride	369	1.1	9.0 (B)	−1.4	48	4
Amitriptyline	277	4.8	9.5 (B)	1.8	95	4
Amlodipine	408	3.7	9.3 (B)	1.0	95	4
Amoxicillin	365	—	2.6 (A), 7.3 (B)	−1.9(pH 7.4)	93	4
Amphetamine	135	1.8	10.1 (B)	−1.8	90	3
Amphotericin B	923	—	5.7 (A), 10.0 (B)	—	5	4
Ampicillin	349	—	2.6 (A), 7.1 (B)	−1.4(pH 7.0)	57.6	7
Amrinone	187	−0.2(±0.67)[d]	—	−0.2	93	3
Antipyrine	188	0.7	—	0.7	97	4
Ascorbic acid	176	−1.9	4.1 (A)	−4.3	35	3
Atenolol	266	0.2	9.5 (B)	−2.8	50	4
Atomoxetine	255	3.7	9.2 (B)	1.0	100	4
Atovaquone	366	5.1	—	5.1	6	4
Atropine	289	1.9	9.8 (B)	−1.5	98	4
Azithromycin	749	3.9	8.8 (B), 8.1 (B)	0.0	60	4
Azosemide	370	1.3 (±0.8)[d]	3.8 (A)[f]	−1.4	> 10	3
Aztreonam	435	−1.5(±1.6)[d]	−2.6(A)[h]	−10.6	1	4
Balsalazide	357	2.8 (±0.58)[d]	2.7 (A), 4.4 (A)[e]	−3.2	< 10	5
Benazepril	424	—	3.1 (A)	−0.2(pH 7.4)	37	3
Benserazide	257	−1.7	7.1 (B)	−2.4	70	5
Benzylpenicillin	334	1.5	2.5 (A)	−2.5	15–30	3
Betaxolol	307	2.4	9.4 (B)	−0.5	100	4
Biperiden	311	4.1	9.7 (B)[f]	0.9	100	4
Bisoprolol	325	2.2	9.6 (B)	−0.9	95	4
Bornaprine	329	4.5 (±0.63)[d]	9.9 (B)[f]	1.1	100	3
Bretylium tosylate	242	—	(Q)	—	23	3
Bromazepam	315	1.7	—	1.6	84	4
Bromfenac	333	3.4	4.3 (A)	1.2	100	4
Bromocriptine	653	4.2	5.4 (B)	4.2	28	6

(*continued*)

TABLE 8.1 (*Continued*)

Name	MW	log P_{oct} [a]	pK_a [b]	log D, pH 6.5 [c]	Fa%	References
Budesonide	430	1.9	—	1.9	100	4
Buflomedil	307	2.4 (±0.37) [d]	10.0 (B) [f]	−1.1	100	4
Bufuralol	261	3.5	8.9 (B)	1.1	100	4
Bumetanide	364	4.1	4.0 (A)	1.6	90	4
Bupivacaine	288	3.6	8.1 (B)	2.0	90	4
Bupropion	240	3.0	7.9 (B)	1.6	87	6
Busulphan	246	−0.3	—	−0.3	94	4
Caffeine	194	0.1	—	0.1	100	4
Camazepam	371	2.7	—	2.7	100	3
Captopril	217	0.3	3.7 (A)	−2.5	84	4
Carfecillin	454	3.0	2.9 (A)	−0.6	99	3
Carvedilol	406	4.1	8.0 (B)	2.7	65	4
Cefaclor	367	—	1.6 (A), 7.2 (B)	—	90	7
Cefadroxil	363	−0.1	2.6 (A), 7.2 (B)	−4.0	100	4
Cefatrizine	463	—	2.6 (A), 7.0 (B)	—	76	4
Cefazolin	454	−1.5	2.3 (A)	−5.7	6	8
Cefcanel daloxate	478	1.2 (±0.91) [d]	7.0 (B) [e]	0.5	42	4
Cefetamet pivoxil	397	1.8	—	1.8	52	4
Cefixime	453	−0.3(±0.45) [d]	2.1 (A), 3.7 (A)	−4.7	30	4
Cefotiam	525	—	4.6 (A), 7.0 (B)	—	3.1	7
Cefpodoxime pivoxil	427	0.2	—	0.2	50	5
Ceftibuten	446	−1.0	2.2 (A), 3.7 (A)	−5.3	70.5	7
Ceftizoxime	383	0.0 (±0.45) [d]	3.0 (A)	−3.6	72	3
Ceftriaxone	554	−1.7	3.2 (A), 4.3 (A)	−7.2	1	4
Cefuroxime	424	−0.8	2.1 (A)	−5.2	5	6
Cephalexin	347	—	2.6 (A), 7.1 (B)	−1.0(pH 6.5)	90	7
Cephaloridine	415	—	(A), (Q)	−1.52	< 5	44
Cephalothin	398	0	2.4 (A)	−4.1	< 5	9
Cephradine	349	—	2.6 (A), 7.3 (B)	−1.6(pH 7.4)	94	7
Cerivastatin	459	3.4	4.9 (A)	1.8	100	4
Ceronapril	440	—	1.9 (A), 4.2 (A), 1018.0 (B)	—	76	10
Cetirizine	389	—	2.9 (A), 8.0 (B)	1.5 (pH 6.5)	> 80	11
Chlorambucil	304	3.4	5.8 (A)	2.6	100	4
Chloramphenicol	322	1.1	—	1.1	90	4
Chlordiazepoxide	299	1.7	—	1.7	100	4
Chloroquine	319	4.7	10.4 (B), 8.4 (B)	−1.2	100	4
Chlorothiazide	295	−0.2	—	−0.2	56	12
Chlorpheniramine	202	3.4	9.3 (B)	0.6	94	4
Chlorpromazine	319	5.3	9.2 (B)	2.6	100	4
Chlorpropamide	319	5.3	9.2 (B)	2.6	100	4
Chlortetracycline	479	—	—	−0.9(pH 7.5)	60	5
Chlorthalidone	338	1.3	—	1.3	82	4
Cibenzoline	262	3.4 (±0.6) [d]	9.4 (B) [f]	0.6	100	4
Cicaprost	374	2.9 (±0.63) [d]	3.4 (A) [f]	−0.2	100	3
Cidofovir	279	−3.9	2.6 (A) [g]	−7.8	3	6
Cilazapril	435	—	3.3 (A), 6.5 (B)	−0.2(pH 7.4)	90	13, 14
Cilazaprilate	389	—	(A), (A), (B)	−2.2(pH 7.4)	19	13, 14
Cilomilast	343	3.5 (±0.62)*d*	4.6 (A)	1.6	100	4

TABLE 8.1 (*Continued*)

Name	MW	log P_{oct} [a]	pK_a [b]	log D, pH 6.5 [c]	Fa%	References
Cimetidine	252	0.4	7.1 (B)	−0.2	68	4
Ciprofloxacin	331	—	8.6 (B), 6.2 (A)	−1.1(pH 7.4)	63	4
Cisapride	465	3.3	7.8 (B)	2.0	100	3
Citalopram	324	3.9	9.6 (B)	0.8	100	4
Clarithromycin	747	3.2	8.5 (B)	1.2	89	4
Clavulanic acid	199	−1.4(±0.67)[d]	2.7 (A)	−5.2	75	4
Clinafloxacin	366	—	5.3 (A), 9.0 (B)	−0.4(pH 7.0)	100	4
Clindamycin	424	1.6	7.5 (B)	0.6	100	4
Clofibrate	242	3.7	—	3.7	97	3
Clonazepam	315	3.0	—	3.0	98	4
Clonidine	229	1.6	8.1 (B)	0.0	95	3
Cloxacillin	435	3.0	2.8 (A)	−0.7	49	6
Clozapine	327	3.2	7.9 (B)	1.8	55	4
Codeine	299	1.1	8.2 (B)	−0.6	95	3
Conivaptan	498	6.3	—	6.3	100	4
Corticosterone	346	2.3	—	2.3	100	3
Cotinine	176	0.1	—	0.1	90	4
Creatinine	113	−2.2	—	−2.2	80	6
Cromolyn sodium	468	2.0	2.2 (A), 2.2 (A)	−6.7	0.5	15
Cyclacillin	341	—	2.7 (A), 7.5 (B)	−2.5(pH 7.4)	95	7
Cyclophosphamide	260	0.8	—	0.8	90	4
Cycloserine	102	−0.9	7.4 (B)	−1.9	73	3
Cyclosporine	1,203	3.5	—	3.5	86	4
Cymarin	548	0.6	—	0.6	47	6
Cyproterone acetate	374	3.8 (±0.47)[d]	—	3.8	100	3
Cytarabine	243	−2.8	—	−2.8	20	6
Dapsone	248	0.9	—	0.9	100	4
Demeclocycline	464	—	—	−0.7(pH 6.6)	66	5
Desferrioxamine	561	−2.2	8.0 (B), 9.1 (B), 9.9 (B)	−6.3	2	4
Desipramine	266	3.8	10.2 (B)	0.1	100	4
Dexamethasone	392	1.1	—	1.1	90	4
Dexloxiglumide	461	4.5	4.5 (A)	2.5	95	4
Diazepam	285	2.9	—	2.9	100	4
Diazoxide	230	1.3	—	1.3	91	4
Diclofenac	295	4.5	4.0 (A)	2.0	100	4
Dicloxacillin	469	3.7	2.8 (A)	0.0	55	6
Didanosine	236	−0.2	—	−0.2	50	4
Digoxin	781	1.3	—	1.3	81	4
Dihydrocodeine	301	1.8 (±0.33)[d]	8.8 (B)	−0.5	89	3
Diltiazem	415	3.2	8.0 (B)	1.7	90	4
Diltiazem	415	3.2	8.0 (B)	1.7	80	6
Diprophylline	254	−1.5	—	−1.5	95	4
Disopyramide	339	2.4	8.4 (B)	0.5	83	4
Distigmine bromide	578	—	—	—	8	3
Disulfiram	296	1.9	—	1.9	97	3
Dofetilide	441	2.1	7.0 (B)	1.5	96	4
Domperidone	426	2.4	7.8 (B)	1.1	93	4
Doxapram	378	3.6	6.7 (B)	3.2	100	4

(*continued*)

TABLE 8.1 (*Continued*)

Name	MW	log P_{oct} [a]	pK_a [b]	log D, pH 6.5 [c]	Fa%	References
Doxifluridine	246	−1.4	—	−1.4	90	4
Doxorubicin	544	1.4	8.3 (B)	−0.4	12	4
Doxycycline	444	—	8.9 (B)	−0.2(pH 7.5)	100	4
Drotaverine	398	4.7 (±0.76)	—	4.7	100	4
Eflornithine	182	—	0.1 (A), 10.4 (B), 6.4 (B)	−3.3(pH 7.4)	55	3
Enalapril	376	—	5.4 (B), 2.9 (A)	−1.8(pH 7.0)	66	6
Enalaprilat	376	—	7.8 (B), 3.2 (A), 1.3 (A)	—	10	15
Encainide	352	4.0	10.2 (B)	0.3	95	4
Entacapone	305	2.0	4.5 (A)	0.0	96	4
Epristeride	400	4.7 (±0.48)[d]	4.8 (A)	3.0	93	4
Eprosartan	424	—	4.1 (A), 5.7 (A), 8.7 (B)	−1.3(pH 7.2)	15	4
Erythritol	122	−2.3	—	−2.3	90	6
Erythromycin	733	2.5	8.8 (B)	0.2	50	4
Ethambutol	204	−0.3	9.2 (B), 6.1 (B)	−3.1	80	6
Ethinylestradiol	296	3.4	—	3.4	100	3
Ethionamide	166	0.5	—	0.5	80	6
Etilefrine	181	0.3	9.0 (B)	−2.2	100	4
Etoposide	589	0.5	—	0.5	52	4
Famciclovir	321	0.6	—	0.6	77	3
Famotidine	337	−0.6	7.1 (B)	−1.3	38	6
Faropenem	312	−1.5	3.5 (A)	−4.5	20	16
Felbamate	238	0.3	—	0.3	90	3
Felodipine	383	4.3	—	4.3	88	4
Fenclofenac	297	4.8	4.4 (A)	2.6	100	3
Fenoterol	303	1.2 (±0.39)[d]	8.5 (B)	−0.8	60	6
Fenspiride	260	2.0 (±0.21)[d]	9.4 (B)[f]	−0.9	100	4
Fexofenadine	502	—	4.3 (A), 9.5 (B)	0.3 (pH 7.0)	34	17
Finasteride	372	4.7	—	4.7	80	4
Flecainide	414	4.6	9.3 (B)	1.8	81	4
Fleroxacin	369	—	5.5 (A), 8.0 (B)	−0.6(pH 7.4)	100	4
Fluconazole	306	0.5	—	0.5	95	4
Flucytosine	129	−1.1	—	−1.1	88	4
Fludarabine	365	−2.8	1.2 (A), 6.1 (A)	−8.6	75	5
Flumazenil	303	1.6	—	1.6	95	4
Flupirtine	304	2.5 (±0.2)[d]	5.3 (B)	2.5	100	4
Fluvastatin	411	4.0	4.3 (A)	1.8	100	4
Folinic acid	473	−1.6	3.1 (A), 4.6 (A)	−6.9	36	4
Foscarnet	126	−2.1	2.6 (A)[g]	−6.0	17	4
Fosfomycin	138	−1.6	2.6 (A)[g]	−5.5	31	4
Fosinopril	563	5.6	3.8 (A)	2.8	36	3
Fosmidomycin	183	−2.2(±1.1)[d]	2.6 (A)[g]	−6.1	30	3
Frovatriptan	243	0.9	9.9 (B)	−2.5	40	4
Furosemide	330	2.6	3.5 (A)	−0.4	61	4
Gabapentin	171	—	3.7 (A), 10.7 (B)	−1.3(pH 7.4)	60	4
Gallopamil	485	4.4 (±0.88)[d]	10.5 (B)	0.4	100	3
Ganciclovir	255	−1.7	—	−1.7	5.6	12
Gatifloxacin	375	—	6.0 (A), 9.2 (B)	−0.9(pH 6.9)	96	4
Genaconazole	331	0.7 (±0.94)[d]	—	0.7	100	4

TABLE 8.1 (*Continued*)

Name	MW	log P_{oct} [a]	pK_a [b]	log D, pH 6.5 [c]	Fa%	References
Gentamicin	477	−3.1	8.6 (B)	−5.2	0	4
Ginkgolide A	408	−0.1(±1.33) [d]	—	−0.1	90	4
Ginkgolide B	424	−0.8(±1.23 [d]	—	−0.8	90	4
Glibenclamide	494	4.4	6.8 (A)	4.2	100	4
Gliclazide	323	2.6	5.8 (A)	1.8	97	3
Glimepiride	490	3.5	6.2 (A)	3.0	100	4
Glipizide	445	2.6	5.1 (A)	1.2	100	4
Glycine	75	—	2.3 (A), 9.6 (B)	—	100	3
Glycopyrrolate	318	—	(Q)	—	10–25	5
Granisetron	312	2.6	9.4 (B)	−0.3	100	4
Guanabenz	230	3.0	8.1 (B)	1.4	75	6
Guanfacine	245	1.7	7.1 (B)	1.0	100	4
Guanoxan	207	0.4 (±0.2) [d]	13.6 (B)	−6.7	50	3
Haloperidol	376	3.6	8.4 (B)	1.7	100	4
HBED	388	—	0.9 (A), 1.6 (A), 8.3 (B)	—	5	6
Hydrochlorothiazide	297	0.0	—	0.0	67	6
Hydrocortisone	362	1.8	—	1.8	91	6
Hydroflumethazide	331	0.5	—	0.5	62	4
Hydroxyurea	76	−1.6	—	−1.6	100	4
Ibuprofen	206	3.5	4.5 (A)	1.4	95	4
Idarubicin	497	1.8	8.0 (B)	0.3	30	5
Idazoxan	204	1.1 (±0.33) [d]	8.8 (B)	−1.2	95	4
Ifosfamide	260	0.8	—	0.8	100	4
Imipenem	299	—	3.2 (A), 10.8 (B)	—	2.5	4
Imipramine	280	4.4	9.5 (B)	1.4	100	6
Indomethacin	358	4.3	4.4 (A)	2.2	100	4
Iothalamate sodium	613	2.2 (±0.95) [d]	1.1 (A)	−3.2	1.9	3
Iotroxic acid	1216	4.5	1.1 (A), 1.7 (A)	−5.6	< 10	5
Isoniazid	137	−0.8	—	−0.8	80	6
Isosorbide-5-mononitrate	236	−0.9	—	−0.9	100	4
Isoxicam	335	2.8	3.9 (A)	0.3	100	4
Isradipine	371	2.9	—	2.9	92	3
Itraconazole	704	5.7	—	5.7	85	4
Kanamycin	484	−6.3	7.2 (B)	−7.1	1	3
Ketanserin	395	3.3	7.5 (B)	2.3	100	4
Ketoprofen	254	3.2	4.0 (A)	0.6	92	4
Ketorolac	255	5.0	3.5 (A)	2.0	100	4
k-Strophanthoside	872	−2.4(±1.11) [d]	—	−2.4	16	3
Labetalol	328	—	9.4 (B)	0.3 (pH 6.5)	95	3
Lactulose	342	−4.3	—	−4.3	0.6	6
Lamivudine	229	−1.4	—	−1.4	100	4
Lamotrigine	256	2.1	5.7 (B)	2.0	100	4
Lansoprazole	369	1.9	—	1.9	100	4
Letrozole	285	2.5	—	2.5	100	4
Levodopa	197	−1.8	2.3 (A)	−6.0	86	3
Levofloxacin	361	—	6.1 (A), 8.1 (B)	−0.3(pH 7.0)	100	4
Levomepromazine	328	4.7	9.2 (B)	2.0	100	18
Levonorgestrel	312	3.8	—	3.8	100	3

(*continued*)

TABLE 8.1 (*Continued*)

Name	MW	log P_{oct}[a]	pK_a[b]	log D, pH 6.5[c]	Fa%	References
Levoprotiline	293	3.4 (±0.37)[d]	9.6 (B)[f]	0.3	100	4
Lincomycin	406	0.6	7.6 (B)	−0.6	28	6
Linezolid	337	0.9	—	0.9	100	4
Lisinopril	405	—	4.0 (A), 4.0 (A), 6.7 (B), 10.1 (B)	—	28	4
Loracarbef	349	—	2.0 (A), 7.3 (B)	—	>86	3
Lorazepam	320	2.5	—	2.5	100	4
Lorcainide	371	4.2	9.4 (B)	1.2	100	4
Lormetazepam	335	2.7	—	2.7	100	4
Lornoxicam	372	2.6	4.7 (A)	0.8	100	3
Losartan	422	2.9	4.3 (A)	0.7	80	4
Lovastatin	423	3.9	—	3.9	31	4
Loxiglumide	460	3.7 (±0.39)[d]	4.5 (A)[f]	1.6	100	4
Mannitol	182	−3.9	—	−3.9	16–80	19
Mebendazole	295	3.1	—	3.1	100	4
Melagatran	429	—	11.5 (B), 2.0 (A)	−1.3(pH 9.7)	15	4
Meloxicam	351	3.4	4.2 (A)	1.1	90	4
Mesna	142	−1.1(±0.74)[d]	−2.6(A)[h]	−10.2	77	3
Metaproterenol	211	0.6 (±0.49)[d]	8.6 (B)	−1.5	44	6
Metformin	129	−0.5	12.4 (B)	−6.4	52	4
Methadone	309	4.2	8.9 (B)	1.8	100	4
Methotrexate	454	−0.1	4.0 (A), 3.3 (A), 5.4 (B)	−2.6	70	4
Methyldopa	211	—	2.2 (A), 9.2 (B)	—	40	4
Methylprednisolone	374	2.1	—	2.1	82	6
Metoclopramide	300	2.4	9.2 (B)	−0.3	100	4
Metolazone	365	4.1	—	4.1	64	4
Metoprolol	267	2.0	9.6 (B)	−1.1	98	4
Metronidazole	171	0.0	—	0.0	100	4
Mibefradil	495	5.4 (±0.56)[d]	5.5 (B)	5.4	69	3
Midazolam	325	3.2	6.2 (B)	3.1	90	4
Mifobate	358	1.2 (±0.6)[d]	—	1.2	82	3
Miglitol	207	−2.7	—	−2.7	59	4
Milrinone	211	0.4	—	0.4	100	4
Minocycline	457	—	9.5 (B)	0.0 (pH 7.5)	100	4
Minoxidil	209	0.6	—	0.6	98	3
Mirtazapine	265	3.0	7.1 (B)	2.3	80	4
Moclobemide	268	1.5	6.2 (B)	1.3	98	4
Montelukast	585	2.9	6.5 (A)	2.6	80	4
Morphine	285	0.9	8.2 (B)	−0.8	85	3
Moxifloxacin	401	—	6.4 (A), 9.5 (B)	−0.6(pH 7.0)	90	4
Moxonidine	242	0.9	7.4 (B)	0.0	99	4
Nadolol	309	0.9	9.7 (B)	−2.3	35	6
Naloxone	327	2.2	7.9 (B)	0.8	91	3
Naltrexone	341	0.7	8.1 (B)	−0.9	96	6
Naproxen	230	3.3	4.2 (A)	1.0	99	6
Naratriptan	335	2.0	9.7 (B)	−1.3	80	4

TABLE 8.1 (*Continued*)

Name	MW	log P_{oct}[a]	pK_a[b]	log D, pH 6.5[c]	Fa%	References
Nateglinide	317	3.9	3.1 (A)	0.5	90	4
Nedocromil	371	2.2	2.8 (A), 3.5 (A)	−4.5	< 10	5
Nefazodone	469	4.7	6.8 (B)	4.2	100	4
Neomycin	614	−7.8	9.3 (B), 8.8 (B), 8.2 (B), 7.6 (B)	−12.9	1	3
Neostigmine	223	—	(Q)	—	5	4
Netivudine	282	−1.1(±0.28)[d]	—	−1.1	28	3
Nevirapine	266	2.5	—	2.5	100	4
Nicardipine	479	3.8	7.1 (B)	3.1	95	4
Nicotine	162	1.3	8.1 (B)	−0.3	100	4
Nicotinic acid	123	0.2	2.2 (A)	−4.1	88	3
Nifedipine	346	3.2	—	3.2	100	4
Nimodipine	418	2.7	—	2.7	90	4
Nisoldipine	388	3.1	—	3.1	90	4
Nitrazepam	281	2.4	—	2.4	78	4
Nitrendipine	360	3.6	—	3.6	88	3
Nizatidine	331	1.1	6.8 (B)	0.7	100	4
Nomifensine	238	3.4 (±0.4)[d]	8.5 (B)[f]	1.4	100	4
Nordiazepam	270	3.2	—	3.2	99	3
Norfloxacin	319	—	8.5 (B), 6.2 (A)	−1.0(pH 7.4)	34	6
Nortriptyline	263	4.4	10.1 (B)	0.8	100	4
Ofloxacin	361	—	5.7 (A), 7.9 (B)	−0.44(pH 7.4)	100	4
Olsalazine	302	2.3	2.5 (A), 2.5 (A)	−5.7	2	6
Omeprazole	345	1.8	—	1.8	95	4
Ondansetron	293	2.4	7.4 (B)	1.4	100	4
Oseltamivir	312	1.2	7.8 (B)	−0.1	80	4
Ouabain	584	−1.2	—	−1.2	1.4	3
Oxacillin	401	2.4	2.8 (A)	−1.3	33	6
Oxatomide	427	3.2	7.2 (B)	2.4	100	3
Oxazepam	286	2.8	—	2.8	92.8	4
Oxiracetam	158	−2.2(±0.42)[d]	—	−2.2	75	4
Oxprenolol	265	2.5	9.6 (B)	−0.6	95	3
Oxyfedrine	313	2.5 (±0.23)[d]	8.2 (B)[f]	0.8	85	3
Oxytetracycline	460	—	9.1 (B)	—	60	6
Pafenolol	337	1.8	9.4 (B)	−1.1	> 29	3
Pantoprazole	383	1.3	—	1.3	100	4
Papaverine	339	3.0	6.4 (B)	2.7	100	4
Paricalcitol	416	4.6	—	4.6	86.1	4
Paromomycin	615	−7.4	8.9 (A), 8.2 (B), 7.6 (B), 7.1 (B)	−9.9	3	20
Pefloxacin	333	—	6.2 (A), 7.9 (B)	0.18 (pH 7.4)	95	4
Penciclovir	253	−1.1	—	−1.1	10	4
Phencyclidine	243	4.7	8.3 (B)	2.9	95	4

(*continued*)

TABLE 8.1 (*Continued*)

Name	MW	log P_{oct} [a]	pK_a [b]	log D, pH 6.5 [c]	Fa%	References
Phenethicillin	402	2.2	2.8 (A)	−1.5	78	21
Phenglutarimide	288	2.1 (±0.32) [d]	10.0 (B) [f]	−1.4	100	3
Phenobarbital	232	1.5	—	1.5	100	4
Phenoxymethylpenicillin	350	2.1	2.8 (A)	−1.6	38	4
Phenytoin	252	2.5	—	2.5	90	4
Pindolol	248	1.8	9.5 (B)	−1.2	100	4
Pirbuterol	240	0.2 (±0.36) [d]	10.3 (B)	−3.7	60	3
Pirmenol	338	3.3	10.2 (B)	−0.4	95	4
Piroxicam	331	2.0	5.1 (A)	0.5	100	3
Piroximone	217	0.5 (±0.25) [d]	—	0.5	81	3
Practolol	266	0.8	9.5 (B)	−2.2	100	4
Pralidoxime	137	—	(Q)	—	< 30	5
Pravastatin	424	2.2	4.6 (A)	0.3	34	4
Praziquantel	312	2.4	—	2.4	100	3
Prazosin	383	1.4	7.1 (B)	0.7	86	4
Prednisolone	358	1.7	—	1.7	99	4
Prednisone	358	1.7	—	1.7	95	4
Probenecid	285	2.9	3.4 (A)	−0.2	100	4
Procainamide	235	1.2	9.2 (B)	−1.5	85	4
Procyclidine	287	4.2	10.2 (B) [f]	0.5	100	4
Progesterone	314	3.6	—	3.6	100	3
Propiverine	367	5.0	8.6 (B)	3.0	84	3
Propranolol	259	2.9	9.5 (B)	−0.1	99	4
Propylthiouracil	170	0.4	—	0.4	90	4
Proxyphylline	238	−0.1	6.4 (B)	−0.4	100	22
Pyridostigmine	181	—	(Q)	—	10	4
Quinapril	438	—	2.8 (A), 5.4 (B)	−0.5(pH 7.4)	61	4
Quinidine	324	2.9	8.6 (B)	0.8	100	4
Quinine	324	2.9	8.6 (B)	0.8	80	4
Rabeprazole	359	2.3	—	2.3	90	4
Raffinose	504	−5.5(±1.02) [d]	—	−5.5	0.3	6
Ramipril	416	—	3.1 (A), 5.6 (B)	0.1 (pH 7.0)	60	10
Ranitidine	314	−0.1	8.4 (B)	−2.0	50	6
Reboxetine	313	3.1	8.3 (B)	1.3	100	4
Recainam	263	2.4 (±0.37) [d]	10.0 (B) [e]	−1.1	80	4
Remoxipride	370	2.9	8.9 (B)	0.5	100	4
Repaglinide	452	—	4.0 (A), 6.2 (B)	3.7 (pH 6.5)	95	4
Reproterol	389	0.4	8.2 (B) [e]	−1.3	60	3
Ribavirin	244	−2.2	—	−2.2	33−> 52	3
Rifabutin	846	4.6	6.9 (B)	4.0	53	4
Rifampin	822	2.7	7.9 (B)	1.3	100	4
Rimiterol	223	0.9 (±0.47) [d]	8.7 (B)	−1.4	48	3
Risedronate	283	−3.6	2.6 (A) [g]	−7.5	0.63	4
Risperidone	410	2.8	8.2 (B)	1.1	100	4
Ritonavir	693	4.3	—	4.3	70	4
Roquinimex	308	2.3 (±0.67) [d]	4.3 (A) [e]	0.1	100	4
Rosiglitazone	357	—	6.1 (B), 6.8 (A)	2.6 (pH 7.4)	100	4
Rosuvastatin	481	2.5	4.6 (A)	0.6	50	4

TABLE 8.1 (*Continued*)

Name	MW	log P_{oct} [a]	pK_a [b]	log D, pH 6.5 [c]	Fa%	References
Saccharin	183	0.9	4.0 (A)	−1.6	88	3
salbutamol	239	1.4	9.3 (B)	−1.4	100	4
Salicylicacid	138	2.4	2.9 (A)	−1.2	100	3
Saquinavir	671	4.1	7.0 (B)	3.5	80	4
Scopolamine	303	0.8	7.7 (B)	−0.4	95	4
Selegiline	187	2.7	6.9 (B)	2.2	100	4
Sematilide	313	—	9.5 (B)	−1.0(pH 7.4)	65	4
Sildenafil	474	1.9	6.8 (B)	1.4	92	4
Sitafloxacin	410	—	5.7 (A), 9.2 (B)	−0.6(pH 7.0)	95	4
Sitagliptin	407	1.5	—	1.5	95	4
Solifenacin	480	3.2	8.5 (B)	1.2	100	4
Sorivudine	349	−1.0(±0.39) [d]	—	−1.0	82	3
Sotalol	272	−0.5	8.3 (B)	−2.3	95	4
Sparfloxacin	392	—	6.3 (A), 8.8 (B)	−0.1(pH 6.8)	100	4
Spironolactone	416	3.3	—	3.3	73	3
Stavudine	224	−0.8	—	−0.8	100	3
Streptomycin	581	−6.4	10.0 (B)	−9.9	1	3
Sudoxicam	337	1.6	5.3 (A)	0.4	100	3
Sufentanil	386	2.8	8.0 (B)	1.3	90	4
Sulfadiazine	250	−0.1	6.4 (A)	−0.5	85	4
Sulfamethoxazole	270	0.9	—	0.9	100	4
Sulfasalazine	398	3.6	2.4 (A)	−0.6	13	6
Sulfinpyrazone	404	3.6	3.3 (A)	0.3	93	4
Sulfisoxazole	267	1.0	5.0 (A)	−0.5	100	4
Sulindac	356	3.6	4.1 (A)	1.2	90	6
Sulpiride	341	0.6	9.0 (B)	−1.9	44	4
Sultopride	354	1.1	9.1 (B)	−1.5	89	3
Sumatriptan	295	1.3	9.6 (B)	−1.8	57	4
Suprofen	260	2.4	3.9 (A)	−0.2	92	4
Suramin	1,296	−0.9(±2.74) [d]	−2.6(A) [h]	< −10.0	0	4
Tacrolimus	803	3.3	—	3.3	15	4
Talinolol	363	3.1	9.4 (B)	0.2	65	4
Tamsulosin	408	2.3	8.4 (B)	0.4	100	4
Tegaserod	301	2.6	11.5 (B) [e]	−2.4	50	4
Telmisartan	514	3.2	4.1 (A)	0.8	90	4
Tenidap	321	4.0	3.1 (A)	0.5	89	3
Tenoxicam	337	1.9	5.5 (A)	0.9	100	4
Terazosin	387	2.3	7.0 (B)	1.6	90	4
Terbutaline	225	−0.1	8.7 (B)	−2.3	62	4
Terodiline	281	5.1 (±0.26) [d]	9.3 (B)	2.3	100	4
Tesaglitazar	408	3.1 (±0.46) [d]	3.6 (A) [f]	0.2	100	4
Testosterone	288	3.0	—	3.0	100	3
Tetracycline	444	—	9.6 (B)	−1.4(pH 7.5)	78	6
Theophylline	180	0.0	—	0.0	100	4
Thiacetazone	236	1.5	5.8 (B)	1.4	> 20	3
Tiacrilast	262	1.3 (±0.36) [d]	4.4 (A) [f]	−0.8	99	23
Tiagabine	375	—	3.3 (A), 9.4 (B)	1.6 (pH 7.0)	95	4
Tilidine	273	3.2 (±0.38) [d]	8.3 (B)	1.4	100	4

(*continued*)

TABLE 8.1 (*Continued*)

Name	MW	log P_{oct} [a]	pK_a [b]	log D, pH 6.5 [c]	Fa%	References
Timolol	316	2.1	—	2.1	95	4
Tinidazole	247	0.7	—	0.7	100	4
Tizanidine	253	1.4	7.4 (B)	0.4	100	4
Tocainide	192	1.1	7.8 (B)	−0.2	100	4
Tolbutamide	270	2.2	5.2 (A)	0.8	85	4
Tolmesoxide	214	1.2 (±0.48) [d]	—	1.2	100	3
Tolterodine	325	5.6	9.9 (B)	2.2	> 77	4
Topiramate	339	0.6	—	0.6	86	3
Toremifene	405	6.8	8.0 (B)	5.3	100	3
Torsemide	348	2.3	—	2.2	96	4
Tramadol	263	2.7	9.5 (B)	−0.3	90	4
Tranexamic acid	157	—	4.5 (A), 10.7 (B)	—	55	6
Trapidil	205	1.4	—	1.4	97	3
Trazodone	372	3.5	6.8 (B)	3.0	100	4
Triazolam	342	5.5	—	5.5	85	4
Trimethoprim	290	0.8	7.1 (B)	0.2	97	4
Trovafloxacin	416	—	5.9 (A), 8.1 (B)	0.3 (pH 6.5)	95	4
Urapidil	387	1.6	7.1 (B)	0.9	100	4
Valproic Acid	144	2.6	4.8 (A)	0.9	100	4
Valsartan	435	3.9	3.6 (A), 4.7 (A)	−0.8	55	4
Vancomycin	1447	−3.1	8.6 (B), 7.5 (B), 2.7 (A)	−6.3	5	4
Vardenafil	488	3.4	6.7 (B)	3.0	90	4
Venlafaxine	277	3.6	9.4 (B)	0.7	97	4
Verapamil	455	4.2	9.1 (B)	1.6	100	4
Vigabatrin	129	—	4.7 (A), 8.6 (B)	—	58	3
Viloxazine	237	1.8	8.1 (B)	0.2	98	3
Warfarin	308	3.1	4.8 (A)	1.4	98	4
Xamoterol	339	0.0	7.9 (B) [e]	−1.4	5	4
Ximoprofen	261	2.7 (±0.41) [d]	4.4 (A) [f]	0.6	98	3
Xipamide	355	2.8	4.6 (A)	0.9	97	24
Zalcitabine	211	−1.3	—	−1.3	100	4
Zaleplon	305	0.9	—	0.9	100	4
Zanamivir	332	—	13.0 (B), 2.4 (A)	—	11	4
Zidovudine	267	−0.1	—	−0.1	100	6
Ziprasidone	412	3.8 (±0.65) [d]	6.5 (B)	3.5	90	4
Zofenopril	430	4.4	3.5 (A)	1.4	96	10
Zolmitriptan	287	1.6	9.5 (B)	−1.4	92	4
Zolpidem	307	1.2	6.2 (B)	1.0	100	4
Zopiclone	388	1.5	6.8 (B)	1.0	100	4

[a] Experimental value unless otherwise noted.
[b] Experimental value unless otherwise noted. (A) acid, (B) base, and (Q) quaternary ammonium.
[c] Calculated from log P_{oct} and pK_a. For zwitter ions, experimental values at a pH.
[d] Calculated by *A* log *P*s (http://www.vcclab.org/lab/alogps/start.html). *A* log *P*s is the consensus-based estimation.
[e] Calculated by SPARC (http://archemcalc.com/sparc/).
[f] Calculated by ACD.
[g] Assumed to be same as *n*-butylphosphonate.
[h] Assumed to be same as mesylate.

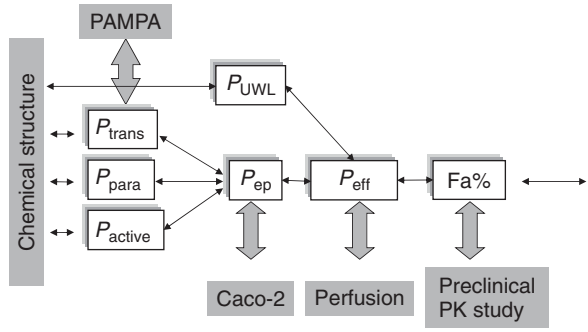

Figure 8.1 Prediction process steps for intestinal membrane permeability.

PPS III: PPS II + *in vivo* animal data
PPS IV: PPS III + human data

Overall prediction error becomes larger as the prediction step becomes longer. Predictability largely depends on the quality of the available data and the compound characteristics. PPS I has the maximum prediction error, whereas PPS IV has the minimum error. PPS I and IIA predictions are mainly used in the drug discovery stages, whereas PPS IIB and III are mainly used at the early developmental stages. PPS IV is used in the late developmental stages (after the phase I study) and the product enhancement stages. When considering the validation of a prediction scheme, it is important to be explicitly conscious regarding what type of prediction process is involved (Fig. 8.1).

8.4 VALIDATION FOR PERMEABILITY-LIMITED CASES

8.4.1 Correlation Between Fa% and P_{eff} Data for Humans (Epithelial Membrane Permeability-Limited Cases PL-E)

The first validation step is to check the predictability of human Fa% from human P_{eff}. This corresponds to the PPS IV. The experimental human P_{eff} and Fa% data were used to validate the model equation. As shown in Figure 8.2, the analytical solutions for Fa% calculation are almost identical between the one-compartment model and the S1I7C3 model.

$$\mathrm{Fa} = 1 - \left(1 + \frac{2}{7R_{GI}}\mathrm{DF} \cdot P_{eff} \cdot T_{si}\right)^{-7} \approx 1 - \exp\left(-\frac{2}{R_{GI}}\mathrm{DF} \cdot P_{eff} \cdot T_{si}\right) \quad (8.1)$$

The intestinal transit time (T_{si}) is set to 3.5 h. The intestinal radius (R_{GI}) is set to 1.5 cm. These physiological data were consistent among many reports and thought to be highly reliable (Chapter 6). The contribution of colonic absorption on Fa% was neglected, as Fa% < 80% data determine the validity of the

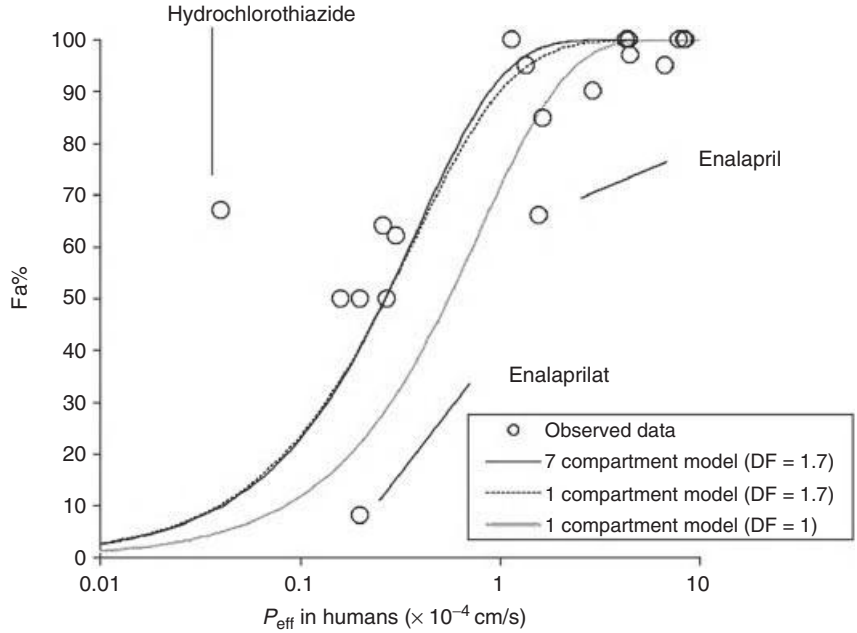

Figure 8.2 P_{eff}—Fa% correlation in humans.

model and in this Fa% region, the drugs have low colonic permeability (c.f. the contribution of colonic absorption on Fa% is <20%). From the standpoint of mechanistic modeling, the degree of flatness (DF) should be independently obtained from the shape of the intestinal tube. However, no reliable data on the intestinal tube shape is available. Therefore, DF had to be obtained by fitting Equation 8.1 to the experimental P_{eff}–Fa% profile. To avoid overlearning, P_{eff} and Fa% data were collected from the literature as much as possible. Theoretically, DF is 1 for a cylindrical tube (hence, $2DF/R_{GI}(= SA_{GI}/V_{GI})$ becomes 1.3 for humans). However, because the small intestine is like a deflated tube, DF should be larger than 1.

The P_{eff} and Fa% data are summarized in Table 8.2. The optimum DF was found to be 1.7 (hence, $2DF/R_{GI}(= SA_{GI}/V_{GI})$ becomes 2.3 for humans). This value is in good agreement with the deflated tube shape. The $2DF/R_{GI}$ model explains well the species differences (similarity) of Fa% between humans and rats (Section 13.5), that is, even though the rat P_{eff} is ca. sixfold smaller than the human P_{eff}, Fa% of a drug in rats and humans becomes similar, because of the smaller R_{GI} values in rats (Fig. 13.4).

Because of the variation in the human P_{eff} values, further refinement of the GI model (e.g., the difference of DF and R_{GI} in each GI region) was impossible by this data set. For comparison, the DF = 1 case ($2DF/R_{GI} = 1.3$) is also shown in Figure 8.2.

TABLE 8.2 Observed P_{eff} and Fa%

				P_{eff}				Fa%			
Compound[a]	MW	pK_a[b,c]	log P_{oct}[b]	Humans[d]	Monkey[l]	Dog[e]	Rat[f]	Human[a]	Monkey[m]	Dog[g]	Rat[h]
Acetaminophen	151	—	0.2	—	−3.8	—	−4.1[k]	100	—	—	—
Amiloride	230	8.65 (B)	−1.03[a]	−3.8	—	—	–	50	—	—	—
Antipyrine	188	—	0.56	−3.3	−3.7	—	−4.2	97	—	—	100
Atenolol	266	9.54 (B)	0.22	−4.7	−4.4	—	−4.8	50	45	100	49
Carbamazepine	236	—	2.45	−3.4	—	—	−4.2	—	100	—	—
Cimetidine	241	6.93 (B)	0.48	−4.6	—	—	−4.3	64	—	98	100
Creatinine	113	—	−1.82[a]	−4.5	—	—	—	80	—	—	—
Desipramine	266	10.16 (B)	3.79	−3.3	—	—	—	100	—	—	—
Fluvastatine	411	4.31 (A)[a]	4.17	−3.6	—	—	—	100	—	100	100[g]
Furosemide	331	3.52 (A)	2.56	-4.8[i]	—	—	−4.5	61	63	54	60
Hydrochlorothiazide	298	—	−0.03	−5.4	—	—	−4.7	67	—	—	65
Ketoprofen	254	3.98 (A)	3.16	−3.1	—	—	−4.0	100	—	—	100
Metoprolol	267	9.56 (B)	1.95	−3.9	—	—	−4.5	95	92	—	—
Midazolam	—	—	—	—	−3.8	—	—	—	—	—	—

(*continued*)

TABLE 8.2 (*Continued*)

Compound[a]	MW	pK_a[b,c]	log P_{oct}[b]	P_{eff}				Fa%			
				Humans[d]	Monkey[l]	Dog[e]	Rat[f]	Human[a]	Monkey[m]	Dog[g]	Rat[h]
Naproxen	230	4.18 (A)	3.24	−3.1	—	—	−3.7[j]	99	—	—	92
Piroxicam	331	5.07 (A)	1.98	−3.2	−3.6	—	−4.1	100	—	—	—
Propranolol	259	9.53 (B)	3.48	−3.5	−4.0	−4.2	−4.3	90	100	100	99
Ranitidine	314	8.31 (B)	1.28	−4.6	—	—	−4.7	50	—	100	63
Terbutaline	225	8.67 (B)	−0.08	−4.5	—	—	−5.3[j]	62	—	78	60
Verapamil	454	9.1 (B)	4.2	−3.2	−4.0	—	—	100	—	—	—

[a] Compound set from Obata et al. [25].
[b] Data from Avdeef, A., 2003 [26] unless otherwise noted.
[c] (A), acid ($pK_a < 6.5$); (B), base ($pK_a > 6.5$).
[d] Data from Lennernas [27].
[e] Data from Lipka et al. [28].
[f] Data from Zakeri-Milani et al. [29].
[g] Data from Chiou et al. [30].
[h] Data from Chiou and Barve [31] unless otherwise noted.
[i] Data from Knutson et al. [32].
[j] Data from Fagerholm et al. [33].
[k] Data from Kalantzi et al. [34]
[l] Data from Takahashi et al. [35].
[m] Data from Chiou et al. [36].

8.4.2 Correlation Between *In Vitro* Permeability and P_{eff} and/or Fa% (PL-E Cases)

Prediction of human P_{eff} and Fa% from *in vitro* permeability data (e.g., Caco-2, MDCK, and rat SPIP) has been extensively investigated (Fig. 8.3).

A simple empirical linear relationship has been widely used to correlate P_{app} to P_{eff} (Fig. 7.27).

$$P_{eff} = aP_{app}^{b} \tag{8.2}$$

where a and b are fitting coefficients. In many reports, P_{app} and Fa were correlated by Equation 8.3, in which the prepermeability coefficient (A) and intestinal transit time (T_{si}) is lumped in the fitting coefficient (A').

$$\text{Fa} = 1 - \exp(-A'P_{app}) \tag{8.3}$$

However, these types of empirical equations cannot handle many characteristics of *in vivo* membrane permeation, such as species difference, bile-micelle effect (food effect), microclimate pH effect, unstirred water layer effect, difference in the paracellular pathways, and particle drifting effect. Mechanistic equations used in the GUT framework can handle these cases (Chapter 4). In addition, the contribution of each process can also be estimated, leading to better understanding of the permeation mechanism of a drug.

8.4.2.1 Caco-2. Figure 8.4 shows the Fa% predictability from Caco-2 data. The paracellular component was corrected using the Renkin's electric field model in the same manner as the GUT framework (Section 4.8.3). Transporter substrates are excluded from the analysis.

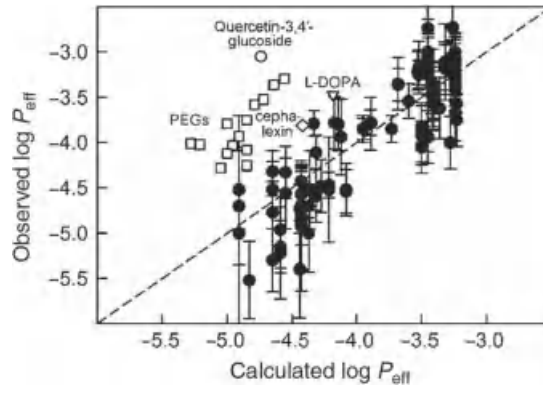

Figure 8.3 P_{eff} prediction from Caco-2 after correction for the paracellular pathway and UWL contribution. Source: Adapted from Reference 37 with permission.

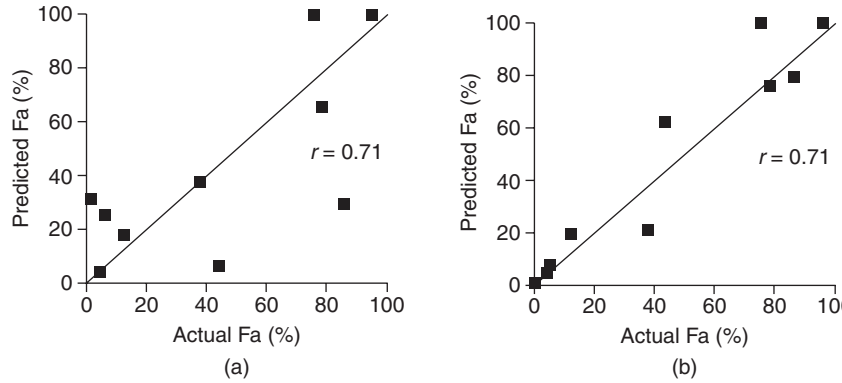

Figure 8.4 Fa% prediction from Caco-2 after correction for the paracellular pathway contribution. (a) Paracellular pathway not corrected, (b) Corrected. *Source:* Adapted from Reference 8 with permission.

The contribution of the paracellular pathway and the UWL were quantified for the drugs whose P_{eff} were reported [37]. Figure 8.5 shows the percentage of drugs categorized by the main permeability determinant. The contribution of the paracellular pathway and the UWL was estimated to be larger than usually thought. For example, for metoprolol ($P_{\text{eff}} = 1.3 \times 10^{-4}$ cm/s) [27], which is a marker compound for high/low boundary permeability, the UWL resistance was estimated to be about 50% of the total permeation resistance, suggesting that the UWL would be the main permeation barrier for BCS (biopharmaceutical classification system) drugs with high permeability. The UWL determines the upper limit of P_{eff} and should be taken into account in the case of lipophilic compounds ($\log D_{\text{oct}} > 0.5–2$). An *in vitro* membrane permeation study, such as Caco-2, can have various UWL thickness values depending on the agitation strength and the size and shape of the apparatus (Section 7.9.8.1). It could coincidentally give an appropriate *in vivo* UWL permeability value, as the excess thickness of UWL *in vitro* ($\approx$1500–3000 μm) could be canceled out by the lack of villi expansion, resulting in similar $P'_{\text{ep}}/P_{\text{UWL}}$ ratio. However, this point should not be misapprehended as the effect of UWL is negligible in the $P_{\text{app}} - P_{\text{eff}}$ extrapolation. The empirical $\log P_{\text{app}} - P_{\text{eff}}$ extrapolation line (Fig. 7.27) was validated only for compounds with low to medium lipophilicity and not for compounds with high lipophilicity.

As discussed earlier, correction for the paracellular pathway improved the predictability for both Fa% and P_{eff} [6, 8, 11, 25, 37–41] (this improvement is more explicitly observed when using PAMPA (Section 8.4.4)). Even though the paracellular pathway was sometimes referred to have only minor contribution, for many blockbuster compounds such as H2 blockers and hydrophilic β-blockers, the contribution of paracellular pathway is estimated to be significant (>50% of total permeability).

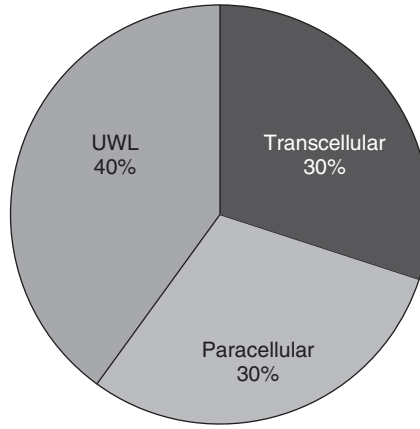

Figure 8.5 Theoretically estimated main P_{eff} determinant of the drugs for which human P_{eff} has been measured. The paracellular markers such as PEGs are excluded from the analysis [37].

From $P_{\text{app}} - P_{\text{eff}}$ correlation, plica–villi expansion coefficient (PE × VE) was back-estimated to be ca. 33 [37]. This is in good agreement with the anatomical value for humans ($3 \times 10 = 30$).

8.4.2.2 PAMPA. As discussed in Section 7.9.4, many versions of PAMPA have been reported in the literature. In this section, the biomimetic PAMPA is used as an example [6, 38, 42, 43]. As clearly shown in Figures 8.6 and 8.7, because a PAMPA membrane does not possess the paracellular pathway, the correction for the paracellular pathway is one of the key factors to improve the predictability of PAMPA (Fig. 8.6).

8.4.2.3 Experimental log P_{oct} and pK_a. Octanol–water partition coefficient (P_{oct}) can be used as a surrogate for $P_{\text{trans,0}}$. Considering the fact that log P_{oct} prediction from the chemical structure has an average error of 1 log unit, the use of experimental value is recommended for biopharmaceutical modeling. Figure 8.8 shows the relationship between log D_{oct} (pH 6.5) and Fa% in humans. When log D_{oct} of a drug is larger than 0, Fa% becomes >50%. In the case of small MW molecules, Fa% tends to be higher than expected from that obtained using log D_{oct}, especially in the case of cationic drugs. This is due to the contribution of the paracellular pathway (Fig. 4.15).

Figure 8.9 shows the predictions of Fa% and P_{eff} from the experimental log P_{oct} data [44]. In addition to human P_{eff}, species differences in P_{eff} are also well predicted by the GUT framework (Sections 6.1 and 13.5.1).

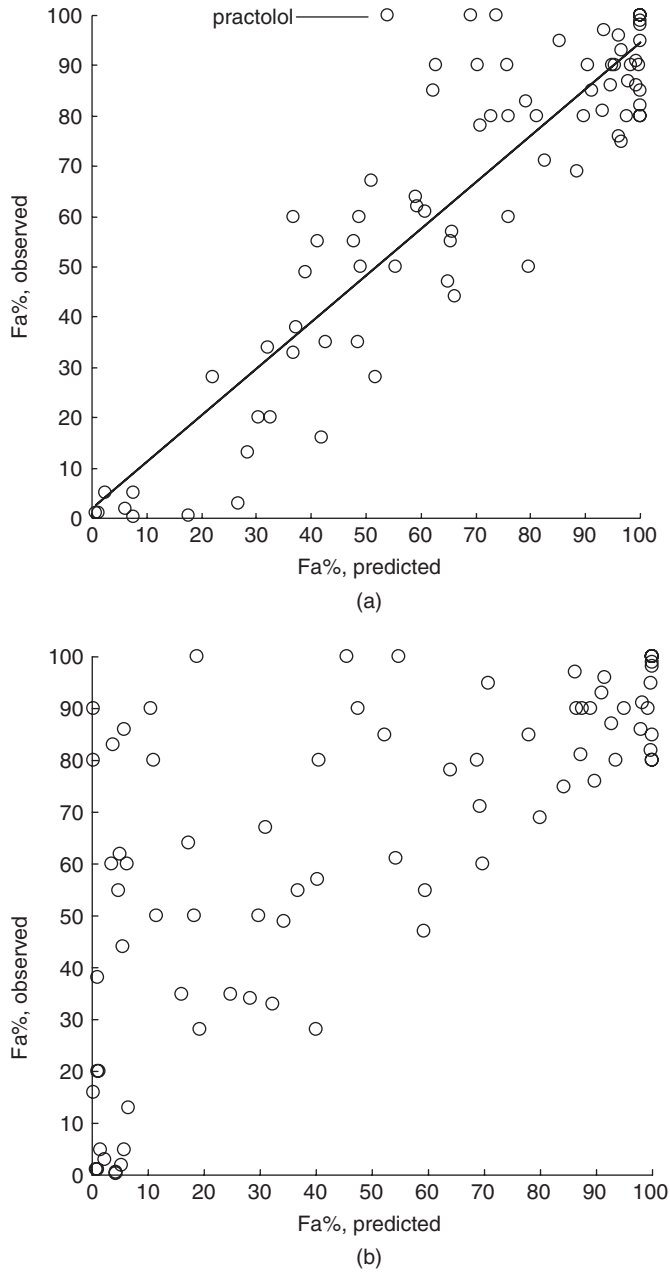

Figure 8.6 Fa% prediction from PAMPA data (a) with and (b) without correction for the paracellular pathway contribution. *Source:* Adapted from Reference 6 with permission.

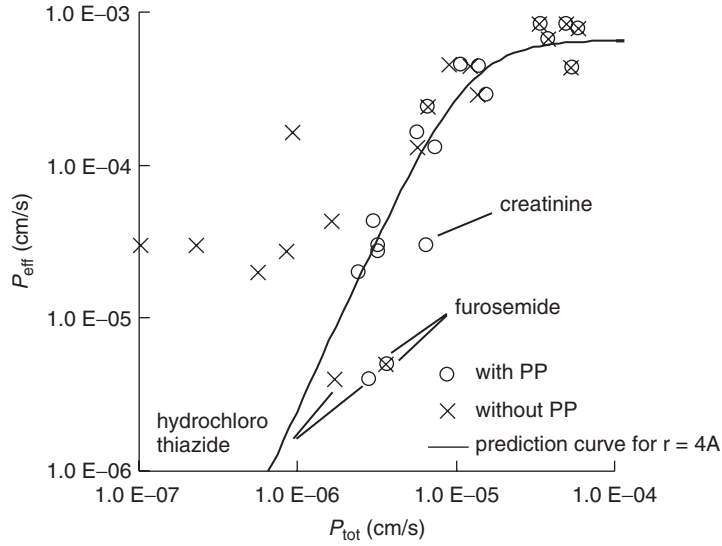

Figure 8.7 Human P_{eff} prediction from PAMPA data with and without the correction for the paracellular pathway contribution (PP: paracellular pathway correction). *Source:* Adapted from Reference 38 with permission.

8.4.3 P_{eff} for UWL Limited Cases[2]

Only a limited number of experimental P_{eff} values for highly lipophilic drugs are available in the literature. In addition, these P_{eff} values were measured in the absence of bile micelles. Therefore, the following equation was used to back-calculate P_{eff} from Fa% for highly lipophilic drugs. In the case of solubility-permeability-limited absorption, P_{eff} can be back-calculated from Fa, $S_{dissolv}$, and dose strength (Dose) as

$$P_{eff} = \frac{\text{Fa} \times \text{Dose}}{\text{DF} \cdot \frac{2}{R_{GI}} \cdot V_{GI} \cdot S_{dissolv} \cdot T_{si}} \tag{8.4}$$

The Fa values at high dose strength (>5 mg/kg) were excluded from the analysis since particle drifting in the UWL would possibly reduce the effective thickness of the UWL (Section 4.7.2). DF = 1.7, R_{GI} = 1.5 cm, T_{si} = 3.5 h, and V_{GI} = 250 ml were used for the calculation of P_{eff} from the clinical Fa values.

Both P_{UWL} and P_{eff} estimated by Equations 4.24 and 4.2, respectively, showed good correlation with *in vivo* P_{eff} estimated by Equation 8.4 (Fig. 8.10). However, no relationship was observed with the apparent Caco-2 permeability (data not shown). This result further supports the fact that P_{eff} of these compounds with

[2]Estimation of P_{UWL} is not important for permeability-limited cases with Fa% < 90%, as epithelial membrane permeability is the rate-limiting step for these cases. However, P_{UWL} affect Fa% for solubility-permeability-limited cases. Therefore, before moving onto the validation for solubility-permeability-limited cases, the validation of P_{UWL} is discussed here.

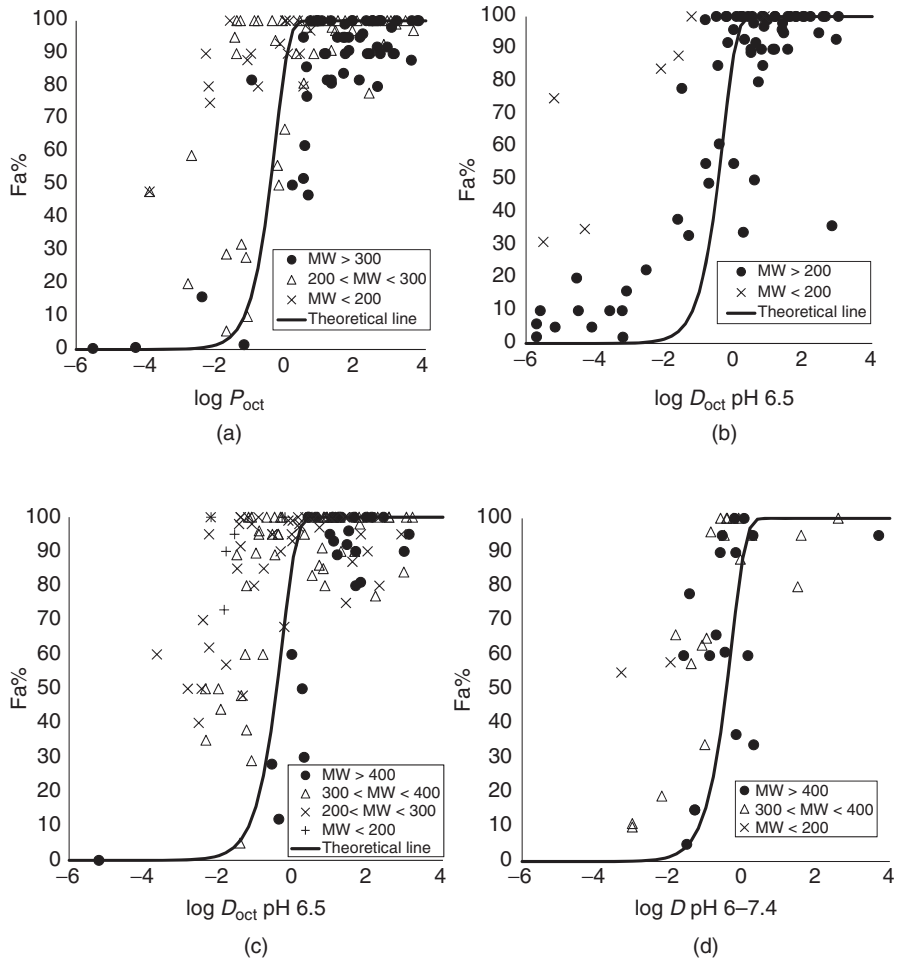

Figure 8.8 Relationship between experimental log D_{oct} and Fa% in humans. (a) Undissociable, (b) monoacid, (c) monobase, and (d) zwitter ion. Low solubility drugs and transporter substrates are excluded from the analysis.

low solubility was mainly determined by the UWL but not by the epithelial membrane. In addition, this result also suggests that bile-micelle binding reduces P_{UWL} permeability in humans (cf. Eq. 4.24) (cf. the reduction of P_{UWL} by bile-micelle binding has been demonstrated using rat and *in vitro* models [45, 46]).

8.4.4 Chemical Structure to P_{eff}, Fa%, and Caco-2 Permeability

Prediction of Fa% and P_{eff} from the chemical structures of drugs has been investigated using the mechanistic models by Obata et al. [25, 48], followed by Reynolds et al. [41]. Calculated log P_{oct}, pK_a, and MW were put into the mechanistic models for the prediction of Fa% and P_{eff} (Chapter 4) (corresponding to PPS I).

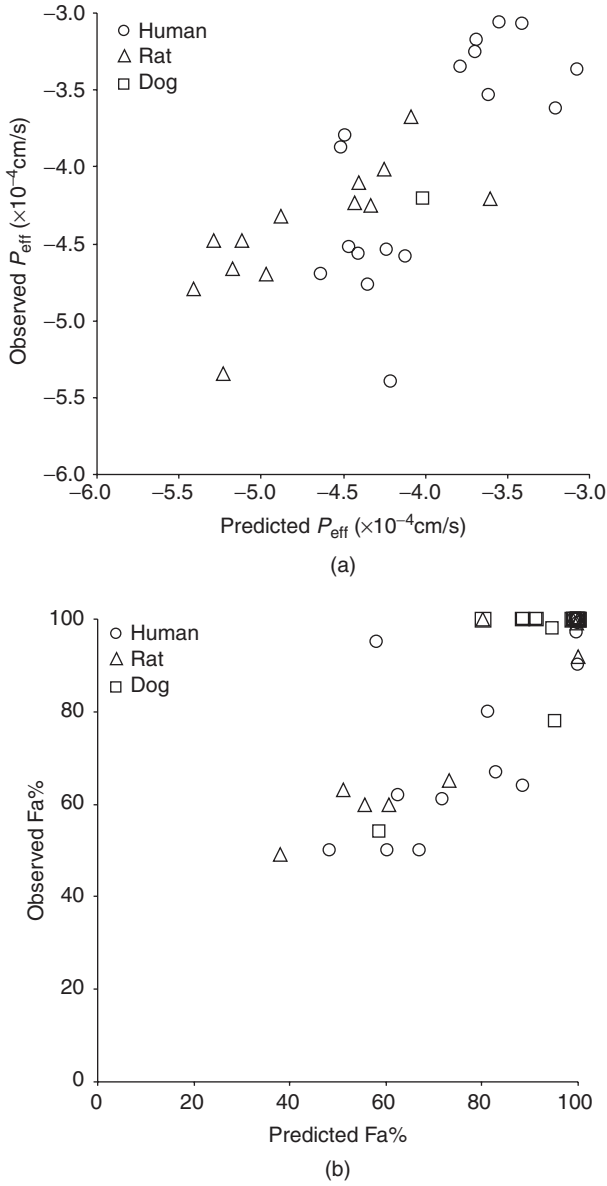

Figure 8.9 Fa and P_{eff} prediction from experimental $\log P_{\mathbf{oct}}$ and pK_a. $P_{trans,0}$ was predicted from $\log P_{oct}$ by Equation 4.34, which was independently derived from the Caco-2 data. Other model equations and physiological parameters were the same as those used in previous independent validation (e.g., DF = 1.7). *Source:* Adapted from Reference 44 with permission.

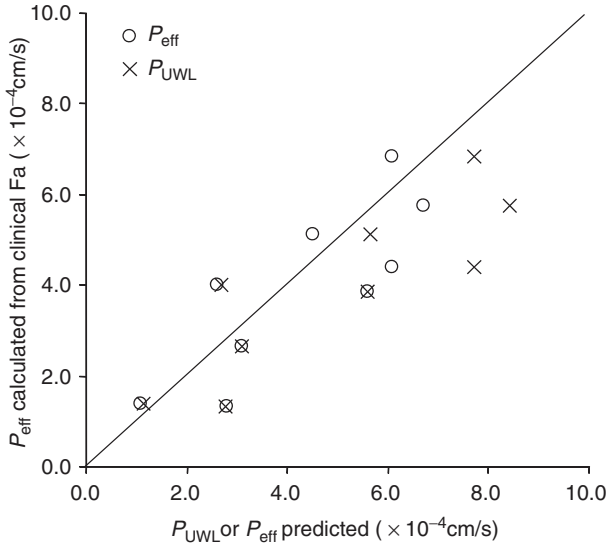

Figure 8.10 Correlation between simulated and observed P_{UWL}. *Source:* Adapted from Reference 47 with permission.

Figure 8.11 shows the predicted and observed Fa% and P_{eff}%. Drugs with low solubility and transporter substrates were excluded from the analysis.

There are many investigations to predict Fa% and P_{eff} from the chemical structure using empirical regression models [49–51]. As the main focus of this book is mechanistic modeling, empirical models are not discussed in this book. When multiple regression is used, the possibility of overlearning should be carefully examined. Even when an independent test set data is separately used for validation, the training set and the test set can share structurally similar compounds. These empirical models should be used for a compound that is within the chemical space of the validation data set.

8.5 VALIDATION FOR DISSOLUTION-RATE AND SOLUBILITY-PERMEABILITY-LIMITED CASES (WITHOUT THE STOMACH EFFECT)

8.5.1 Fa% Prediction Using *In Vitro* Dissolution Data

As discussed in Section 3.2, accurate estimation of k_{diss} from the solubility and other parameters of a drug is not an easy task. The estimation errors of each component of k_{diss} accumulatively propagate to the error in the k_{diss} value. Therefore, a practical approach would be to obtain k_{diss} directly from the *in vitro* dissolution experiment and use it for biopharmaceutical modeling (corresponding to PPS IIB). For this purpose, an *in vitro* dissolution test should be performed

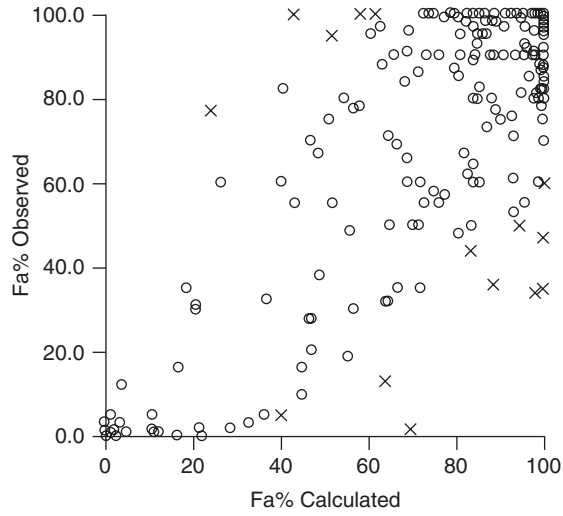

Figure 8.11 Prediction of Fa% from calculated $\log P_{oct}$. *Source:* Adapted from Reference 25 with permission.

under a sink condition. To obtain k_{diss}, the initial linear slope of the dissolved amount–time data is divided by the dose, or Equation 8.5 can be fitted to the dissolved amount–time curve. When a nonsink condition is used, the estimation error for k_{diss} can become significant, as a saturated concentration is quickly achieved [52].

$$\frac{\mathrm{d}X_t}{\mathrm{d}t} = -k_{\text{diss}} \cdot X_{t=0}^{2/3} \cdot X_t^{1/3} \left(1 - \frac{X_{\text{dissolv}}}{V_{\text{fluid}} S_{\text{dissolv}}}\right) \tag{8.5}$$

$$k_{\text{diss}} = \frac{3 D_{\text{eff}} S_{\text{surface}}}{r_{\text{p}} h} = k'_{\text{diss}} S_{\text{surface}}$$

$$= k''_{\text{diss}} D_{\text{eff}} S_{\text{surface}} \left(k'_{\text{diss}} = \frac{3 D_{\text{eff}}}{r_{\text{p}} h}, k''_{\text{diss}} = \frac{3}{r_{\text{p}} h}\right) \tag{8.6}$$

Fa% predictability of this approach was investigated by Takano et al. [53] for structurally diverse BCS II drugs. Fa% of undissociable compounds, free acids, and free bases (with the high pH stomach) were used for validation. By combined use of the simple *in silico* P_{UWL} prediction and one-compartment GI model, the Fa% values of BCS II drugs were appropriately predicted (Fig. 8.12).

In this pivotal investigation by Takano et al. [53, 54], the following points were concluded:

1. It is critical to consider the effect of the UWL on P_{eff}. Without this, in more than half of the cases, Fa% is significantly overestimated, suggesting that

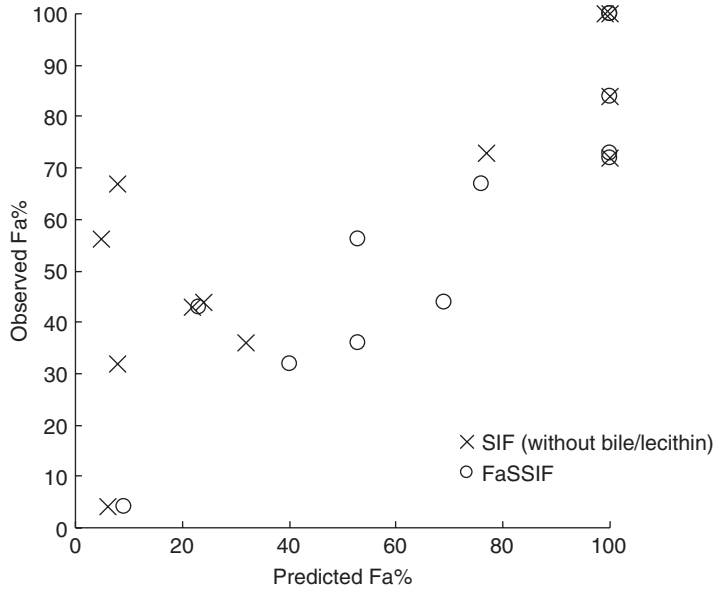

Figure 8.12 Prediction of Fa% using k'_{diss} value obtained from the mini-paddle dissolution test with FaSSIF [53].

the majority of BCS class II drugs are categorized as solubility—UWL-permeability limited, rather than dissolution-rate limited. Caco-2 permeability was found to be inappropriate to be used for drugs with low solubility.

2. The use of a simulated intestinal fluid with bile micelles (FaSSIF) is critical for appropriate Fa% prediction. The use of a simple buffer without bile micelles resulted in significant underestimation of Fa%.
3. A speed of 50 rpm in the minipaddle method (corresponds to 10–25 rpm in a compendium dissolution test) gave an appropriate agitation strength, whereas 25 and 100 rpm under- and overestimated Fa%, respectively.

It should be noted that in this investigation, each drug formulation was added to the vessel after gently crushing the drug products. Therefore, the disintegration process was not reflected in the results.

8.5.2 Fa% Prediction Using *In Vitro* Solubility and Permeability Data

The most frequent use of biopharmaceutical modeling in drug discovery is to estimate *in vivo* Fa% from solubility, particle size, and *in vitro* permeability data for drug candidates with low solubility (corresponds to PPSII A). Therefore, this process is discussed in detail in this section [12]. It should be noted that this discussion became possible after the permeability model had been validated, as discussed in the earlier sections.

TABLE 8.3 Drugs Used to Validate PPSII Type Simulation for DRL and SL Cases

Drug	MW	z^a	pK_a	log P_{oct}	Solubility, mg/ml			Caco-2, $\times 10^{-6}$ cm/s	References
					pH 6.5	FaSSIF	FeSSIF		
Acyclovir	225	0	–	−1.7	2.5	2.5[d]	–	0.38	42, 55, 56
Albendazole	265	0	4.2	3.1	0.00055	0.0021	–	–	57, 58
Aprepitant	534	0	4.2[b]	4.8	0.0008	0.021[e]	–	–	59, 60
Atovaquone	367	0	–	5.1	0.00043	0.0024	–	–	61, 62
AZ0865	366	0	6.1	4.2	0.00185	0.0057	–	–	63
Carbamazepine (anhydrate)	236	0	–	1.8	0.120	0.185, 0.220	–	–	64, 65
Carbamazepine (Dihydrate)	236	0	–	1.8	0.08[f]	0.013	–	–	—
Celecoxib	381	0	–	(>) 3	0.0032	0.0462	0.103	–	66
Chlorothiazide	265	0	–	−0.24	0.73	0.87	0.83	0.92	8, 26, 67
Cilostazole	369	0	–	2.7	0.0063	0.0064, 0.008[e]	0.014[e]	-	68
Cinnarizine	369	+	7.45	5.7	0.0014	0.013, 0.021[e], 0.013[f], 0.021[e,f]	–	–	58
Danazol	337	0	–	4.5	0.0002	0.018, 0.020[e]	0.047	–	47, 69, 70
Digoxin	780	0	–	1.3	0.016	0.017	–	1.3	55, 71, 72
Dipyridamole	505	0	6.2	3.9	0.006	0.017, 0.024[e]	–	–	53, 69
Efavirentz	316	0	–	4.1	0.01	0.194	–	–	53
EMD57033	425	0	—	2.7	0.0047	0.0075	—	—	73
Felodipine	384	0	–	4.3	0.00086	0.077[e]	–	–	69, 74
Fenofibrate	362	0	–	5.2	0.0002	0.014	0.037	–	75, 76
FTI-2600	448	0	–	3.2	0.0037	0.033[e]	–	–	77
Ganciclovir	255	0	–	−1.7	4.3	4.3[d]	–	0.23	55, 78
Gefitinib	447	+	7.2	4.1	0.0041	0.085, 0.083[f]	–	–	79, 80
Glibenclamide	494	–	5.9	3.1	0.0045	0.0046, 0.0027[f]	–	–	58
Griseofulvin	353	0	–	2.5	0.01	0.015, 0.018[e]	–	–	47, 69, 70

(*continued*)

TABLE 8.3 (*Continued*)

Drug	MW	z^a	pK_a	log P_{oct}	Solubility, mg/ml			Caco-2, $\times 10^{-6}$ cm/s	References
					pH 6.5	FaSSIF	FeSSIF		
Irbesartan	429	–	4.4	4.0[c]	0.11	0.21, 0.11[f]	0.29	127	67,81–83
Indomethacin	358	–	4.2	4.3	0.22	0.59, 0.74[e]	—	—	58
Ivermectine	875	0	–	3.2	0.0007	0.12	–	–	53
Ketoconazole	531	+	6.5	4.3	0.012	0.021, 0.027[e]	–	–	26, 53, 62
Lobucavir	265	0	–	−1.2	0.8	0.8[d]	–	0.88	55, 78
LY-2157299	369	0	4.34	1.73	0.082	1.8	–	–	84
N74	353	–	–	3.1	0.041	0.12	–	–	85
Nifedipine	346	0	–	3.2	0.013	0.031[e]	–	–	86
Nitrendipine	360	0	–	3.3	0.004	0.016	–	–	53
Panadiplon	335	0	–	1.2[b]	0.077	0.085*d*, *e*	0.13[e]	–	87
Phenitoin	252	0	–	2.5	0.039	0.043	0.059	–	69
Pranlukast	491	–	3.4	4.2[b]	0.0033	0.088, 0.086[f]	0.8, 0.8[f]	25	67, 88
Spironolactone	417	0	–	3.3	0.03	0.042	–	–	53
Tolfenamic acid	262	–	4.8	5.7	0.027	0.063, 0.040[f]	–	–	58

[a] Dominant charge at pH 6.5 (>50% dissociated cases were assigned as + or −).
[b] Calculated value (ACD/Labs Software V8.14).
[c] Calculated from pK_a and log $D_{pH7.4}$.
[d] Estimated from blank buffer solubility and log P_{oct}.
[e] For dogs.
[f] Estimated from the solubility ratio of anhydrate and dehydrate at pH 1.2.

TABLE 8.4 Simulated and Observed Fa% by PPSII Type Simulation for DRL and SL Cases

Drug	Species	State	Dose, mg	d50[a],μm	Dn	Do	Pn	Predicted Fa%	Type	Observed Fa%	Method[b]	References
Acyclovir	Human	Fasted	200	50[a]	353.3	0.6	0.3	27	PL	29	(VI)	89–91
Acyclovir	Human	Fasted	400	50	353.3	1.2	0.3	23	SL-E	21	(VI)	
Acyclovir	Human	Fasted	800	50	353.3	2.5	0.3	13	SL-E	12	(VI)	
Albendazole	Human	Fasted	1400	10	1.9	5142.8	46	1.9	SL-U	2.7	(II)	92, 93
Aprepitant	Dog	Fasted	20	0.2	9434.5	51.4	48.1	82	SL-U	57	(III)	59, 94
Aprepitant	Dog	Fasted	20	2	94.3	51.4	6.6	21	SL-U	33	(II)	
Aprepitant	Dog	Fasted	20	5	15.1	51.4	3.7	12	SL-U	28	(II)	
Aprepitant	Dog	Fasted	20	26	0.6	51.4	2.7	7	SL-U	18	(II)	
Atovaquone	Human	Fasted	500	0.3	1468.2	1607.1	242.1	33	SL-U	39	(VI)	95–98
Atovaquone	Human	Fasted	1000	0.3	1468.2	3214.2	311.3	23	SL-U	30	(VI)	
Atovaquone	Human	Fasted	1500	0.3	1468.2	4821.3	344.2	18	SL-U	17	(VI)	
AZ0865	Human	Fasted	100	2.5	87.2	134.4	20.1	27	SL-U	49	(II), (IV), (V)	63
Carbamazepine (form I)	Dog	Fasted	40	14	126.6	10.7	11.0	78	SL-U	87	(II), (IV)	65, 99
Carbamazepine(Dihydrate)	Dog	Fasted	40	13	99.4	15.8	11.4	68	SL-U	90	(II), (IV)	
Carbamazepine (form I)	Dog	Fasted	200	14	126.6	53.3	26.3	60	SL-U	62	(II), (IV)	
Carbamazepine(dihydrate)	Dog	Fasted	200	13	99.4	78.8	27.0	49	SL-U	30	(II), (IV)	
Carbamazepine (Tagretol)	Dog	Fasted	200	2.5	2688.0	78.8	40.1	63	SL-E	90	(II), (IV)	
Carbamazepine (Tagretol)	Dog	Fasted	200	150	1.2	49.0	9.0	21	SL-U	48	(II), (IV)	
Carbamazepine (Tagretol)	Human	Fasted	200	2.5	7267.7	8.3	48.9	100	SL-U	100	(III)	
Carbamazepine (Tagretol)	Human	Fasted	400	150	2.0	16.7	15.9	55	SL-U	70	(III)	
Celecoxib	Human	Fasted	5	2	279.4	0.8	4.1	98	PL	94	(III), (VI)	100, 101
Celecoxib	Human	Fasted	25	2	279.4	4.2	4.7	75	SL-U	87	(III), (VI)	
Celecoxib	Human	Fasted	50	2	279.4	8.3	5.8	63	SL-U	69	(III), (VI)	
Celecoxib	Human	Fasted	100	2	279.4	16.7	9.1	58	SL-U	67	(III), (VI)	
Celecoxib	Human	Fasted	200	2	279.4	33.4	14.3	53	SL-U	86	(III), (VI)	

(*continued*)

TABLE 8.4 (*Continued*)

Drug	Species	State	Dose, mg	d50[a],μm	Dn	Do	Pn	Predicted Fa%	Type	Observed Fa%	Method[b]	References
Celecoxib	Human	Fasted	400	2	279.4	66.8	21.3	46	SL-U	51	(III), (VI)	
Celecoxib	Human	Fasted	600	2	279.4	100.2	25.9	40	SL-U	72	(III), (VI)	
Celecoxib	Human	Fasted	900	2	279.4	150.3	30.4	34	SL-U	55	(III), (VI)	
Celecoxib	Human	Fasted	1200	2	279.4	200.4	33.3	30	SL-U	44	(III), (VI)	
Celecoxib	Human	Fed	200	2	1378.5	12.5	17.1	88	SL-U	107	(III), (VI)	
Celecoxib	Human	Fed	400	2	1378.5	25.0	25.2	82	SL-U	81	(III), (VI)	
Chlorothiazide	Human	Fasted	50	50	96.1	0.4	0.6	47	PL	56	(I)	102, 103
Chlorothiazide	Human	Fasted	500	50	96.1	4.4	0.6	17	SL-E	15	(I)	
Chlorothiazide	Human	Fed	500	50	97.6	3.9	0.7	19	SL-E	29	(I)	
Cilostazole	Dog	Fasted	100	0.22	21,476.3	675	401.1	76	SL-U	100	(III), (VI)	68, 104, 105
Cilostazole	Dog	Fasted	100	13	6.2	675	29.8	9	SL-U	20	(III), (VI)	
Cilostazole	Dog	Fasted	100	2.4	180.5	675	88.1	27	SL-U	21	(III), (VI)	
Cilostazole	Dog	Fed	100	0.22	25,318.8	321.4	240.8	82	SL-U	95	(III), (VI)	
Cilostazole	Dog	Fed	100	13	7.3	321.4	17.8	11	SL-U	32	(III), (VI)	
Cilostazole	Dog	Fed	100	2.4	212.7	321.4	53.9	31	SL-U	75	(III), (VI)	
Cilostazole	Human	Fasted	50	10	17.8	60.3	20.8	47	SL-U	40	(II)	
Cilostazole	Human	Fasted	100	10	17.8	120.5	22.9	31	SL-U	31	(II)	
Cilostazole	Human	Fasted	200	10	17.8	241.1	29.0	22	SL-U	25	(II)	
Cinnarizine	Dog	Fasted	25	25	0.8	64.3	3.1	7	SL-U	5	(IV), (VI)	106, 107
Cinnarizine	Human	Fasted	25	25	0.7	14.8	4.8	24	SL-U	27	(IV)	
Cinnarizine	Human	Fasted	25	60	0.1	14.8	4.8	9	DRL	13	(IV)	
Danazol	Dog	Fasted	2	5	11.9	5.4	2.4	43	SL-U	30	(II)	59, 108–111
Danazol	Dog	Fasted	20	5	11.9	54	3.3	11	SL-U	12	(II)	
Danazol	Dog	Fasted	20	229	0	54	2.3	0.35	DRL	2	(II)	
Danazol	Dog	Fasted	200	0.16	11,582.9	540	127.2	43	SL-U	77	(II)	

Danazol	Dog	Fasted	200	10	3	540	8.3	3	SL-U	4.8	(II)	
Danazol	Human	Fasted	100	4.46	7.7	42.9	4	15	SL-U	18	(II), (III)	
Danazol	Human	Fasted	200	4.46	7.7	85.7	5.6	12	SL-U	14	(II), (III)	
Danazol	Human	Fed	100	4.46	111.9	13.7	6.4	52	SL-U	58	(II), (III)	
Digoxin	Human	Fasted	0.5	7	65.8	0.2	1	62	PL	78	(II)	112
Digoxin	Human	Fasted	0.5	13	19.1	0.2	1	60	PL	96	(II)	
Digoxin	Human	Fasted	0.5	102	0.3	0.2	1	10	DRL	37	(II)	
Dipyridamole	Human	Fasted	50	75	0.3	22.7	8	16	DRL	36	(IV), (VI)	113–115
Dipyridamole	Dog	Fasted	75	75	0.2	166	4.6	3	SL-U	11	(IV)	
Efavirentz	Human	Fasted	600	3	444.4	23.9	20	75	SL-U	82	(III)	116, 117
Efavirentz	Human	Fasted	1200	3	444.4	47.7	27.4	65	SL-U	59	(III)	
EMD57033	Dog	Fasted	30	15	3.3	216.0	9.7	8	SL-U	10	(II)	73
Felodipine	Dog	Fasted	3	8	17.9	2.1	2.4	66	SL-U	72	(II)	74
Felodipine	Dog	Fasted	3	125	0.1	2.1	2.3	4	DRL	5	(II)	
Fenofibrate	Human	Fasted	145	0.4	811	79.9	28.6	50	SL-U	70	Other[c]	118–120
Fenofibrate	Human	Fasted	200	2.2	26.8	110.2	8.9	15	SL-U	51	Other	—
Fenofibrate	Human	Fed	67	2.2	364	11.6	7.6	63	SL-U	84	Other	—
Fenofibrate	Human	Fed	145	0.4	11,010.5	25.2	57.8	100	SL-U	79	Other	—
Fenofibrate	Human	Fed	200	2.2	364	34.7	16.5	57	SL-U	72	Other	—
FTI-2600	Dog	Fasted	30	1	931	49.7	21.4	55	SL-U	28	(II)	77
Ganciclovir	Human	Fasted	500	50	574.1	0.9	0.2	18	PL	5.6	(VI)	121
Ganciclovir	Human	Fasted	750	50	574.1	1.3	0.2	14	SL-E	4.5	(VI)	—
Ganciclovir	Human	Fasted	1000	50	574.1	1.8	0.2	10	SL-E	4.5	(VI)	—

(*continued*)

TABLE 8.4 (Continued)

Drug	Species	State	Dose, mg	d50[a],μm	Dn	Do	Pn	Predicted Fa%	Type	Observed Fa%	Method[b]	References
Ganciclovir	Human	Fasted	1250	50	574.1	2.2	0.2	9	SL-E	2.6	(VI)	—
Gefitinib	Human	Fasted	250	30	1.6	22.7	4	21	SL-U	39	(III), (IV), (VI)	80, 122, 123
Glibenclamide	Human	Fasted	5	50	0.3	8.4	16.8	22	DRL	45	(I)	—
Griseofulvin	Dog	Fasted	2	7	35.8	6	7.5	81	SL-U	85	(II)	59, 124, 125
Griseofulvin	Dog	Fasted	20	118	0.1	60	7.4	7	SL-U	2.9	(II)	
Griseofulvin	Dog	Fasted	20	7	35.8	60	10.7	28	SL-U	46.9	(II)	—
Griseofulvin	Human	Fasted	125	4	181.8	64.3	28.8	57	SL-U	45	(III)	—
Griseofulvin	Human	Fasted	500	4	181.8	257.1	78.5	49	SL-U	43	(I)	—
Indomethacin	Dog	Fasted	25	150	1.5	2.3	4.4	59	DRL	46	(IV),(VI129	126, 127
Irbesartan	Human	Fasted	25	20	39.8	0.9	9.4	100	PL	99	(II), (VI)	128–130
Irbesartan	Human	Fasted	50	20	39.8	1.8	9.5	100	SL-U	83	(II), (VI)	
Irbesartan	Human	Fasted	100	20	39.8	3.7	9.9	100	SL-U	75	(II), (VI)	—
Irbesartan	Human	Fasted	150	20	39.8	5.5	10.2	91	SL-U	71	(II), (VI)	—
Irbesartan	Human	Fasted	200	20	39.8	7.3	10.6	86	SL-U	64	(II), (VI)	—
Irbesartan	Human	Fasted	300	20	39.8	11	11.6	78	SL-U	78	(II), (VI)	—
Irbesartan	Human	Fasted	600	20	39.8	22	15.8	69	SL-U	59	(II), (VI)	—
Irbesartan	Human	Fasted	900	20	39.8	33.1	19.8	65	SL-U	54	(II), (VI)	—
Irbesartan	Human	Fed	25	20	62.2	0.6	8.1	100	PL	83	(II), (VI)	—
Irbesartan	Human	Fed	300	20	62.2	6.7	9.5	85	SL-U	90	(II), (VI)	—
Ivermectine	Human	Fasted	6	25	1.2	0.4	2.8	52	DRL	54	(II), (III)	53, 131–133
Ivermectine	Human	Fasted	12	25	1.2	0.8	2.8	52	DRL	52	(II), (III)	
Ivermectine	Human	Fasted	15	25	1.2	1	2.8	52	DRL	51	(II), (III)	—
Ivermectine	Human	Fasted	30	25	1.2	1.9	2.8	53	DRL	53	(II), (III)	—
Ivermectine	Human	Fasted	60	25	1.2	3.9	2.8	43	SL-U	46	(II), (III)	—

Ivermectine	Human	Fasted	90	25	1.2	5.8	2.9	36	SL-U	30	(II), (III)	—
Ivermectine	Human	Fasted	120	25	1.2	7.7	2.9	31	SL-U	35	(II), (III)	—
Ketoconazole	Human	Fasted	200	200	0.1	73.5	11.1	5	DRL	6	(II)	115, 134
Ketoconazole	Dog	Fasted	200	200	0	400	6.3	2	SL-U	3.3	(IV)	—
Lobucavir	Human	Fasted	20	50	105	0.2	0.7	51	PL	48	(VI)	78
Lobucavir	Human	Fasted	70	50	105	0.7	0.7	51	PL	53	(VI)	—
Lobucavir	Human	Fasted	200	50	105	1.9	0.7	31	SL-E	42	(VI)	—
Lobucavir	Human	Fasted	400	50	105	3.9	0.7	21	SL-E	28	(VI)	—
Lobucavir	Human	Fasted	700	50	105	6.7	0.7	14	SL-E	14	(VI)	—
LY-2157299	Dog	Fasted	500	10	363.1	14.8	3.3	30	SL-E	20	(II)	84
N74	Dog	Fasted	10	120	0.5	4.5	5.4	35	DRL	29	(II)	85
Nitrendipine	Human	Fasted	20	10	12.1	9.6	7.3	65	SL-U	76	(II)	53, 135
Nifedipine	Dog	Fasted	10	50	1.0	17.4	6.3	29	SL-U	39	(II)	136
Nifedipine	Dog	Fasted	30	30	2.7	52.3	6.9	19	SL-U	31	(II)	137
Nifedipine	Dog	Fasted	40	10	24.0	69.7	11.3	27	SL-U	34	Other[e]	138
Panadiplon	Dog	Fasted	10	9	161.5	6.4	7.7	81	SL-U	84	(VI)	87
Panadiplon	Dog	Fasted	10	25	20.9	6.4	7.3	77	SL-U	77	(VI)	
Panadiplon	Dog	Fasted	10	100	1.3	6.4	7.1	51	SL-U	25	(VI)	
Panadiplon	Dog	Fed	10	9	176.3	3.6	5.6	84	SL-U	100	(VI)	
Panadiplon	Dog	Fed	10	25	22.9	3.6	5.4	81	SL-U	91	(VI)	
Panadiplon	Dog	Fed	10	100	1.4	3.6	5.3	56	DRL	35	(VI)	
Phenitoin	Human	Fasted	280	4	819.7	50.2	81.3	95	SL-U	81	(II), (VI)	139–142
Phenitoin	Human	Fasted	200	50	5.2	35.9	22	56	SL-U	60	(II), (VI)	
Phenitoin	Human	Fasted	350	190	0.4	62.8	21.2	18	SL-U	14	(II), (VI)	—
Phenitoin	Human	Fed	350	190	0.4	38.5	16.9	21	DRL	31	(II), (VI)	—
Pranlukast	Human	Fasted	50	2	309.6	4.4	0.7	18	SL-E	20	Other[d]	143–146
Pranlukast	Human	Fasted	100	2	309.6	8.8	0.7	11	SL-E	13	Other	

(*continued*)

TABLE 8.4 (Continued)

Drug	Species	State	Dose, mg	d50[a],μm	Dn	Do	Pn	Predicted Fa%	Type	Observed Fa%	Method[b]	References
Pranlukast	Human	Fasted	300	2	309.6	26.3	0.8	5	SL-E	7.2	Other	
Pranlukast	Human	Fasted	600	2	309.6	52.6	0.8	3	SL-E	5	Other	
Pranlukast	Human	Fed	112.5	2	9408.9	0.9	0.1	8	PL	12	Other	
Pranlukast	Human	Fed	225	2	9408.9	1.8	0.1	5	SL-E	11	Other	
Pranlukast	Human	Fed	300	2	9408.9	2.4	0.1	4	SL-E	11	Other	
Pranlukast	Human	Fed	337.5	2	9408.9	2.7	0.1	4	SL-E	7.1	Other	
Pranlukast	Human	Fed	450	2	9408.9	3.6	0.1	3	SL-E	12	Other	
Pranlukast	Human	Fed	562.5	2	9408.9	4.5	0.1	2	SL-E	9.8	Other	
Pranlukast	Human	Fed	675	2	9408.9	5.4	0.1	2	SL-E	7.6	Other	
Spironolactone	Human	Fasted	200	10	80.8	36.7	21.2	64	SL-U	58	(III)	147, 148
Tolfenamic acid	Human	Fasted	200	6	159.5	24.5	24.5	81	SL-U	60	(VI)	149–151
Tolfenamic acid	Human	Fasted	100	18	17.7	12.2	12.4	77	SL-U	82	(VI)	
Tolfenamic acid	Human	Fasted	200	18	17.7	24.5	13.7	60	SL-U	59	(VI)	
Tolfenamic acid	Human	Fasted	400	18	17.7	49	17.8	48	SL-U	61	(VI)	
Tolfenamic acid	Human	Fasted	800	18	17.7	98	31	44	SL-U	68	(VI)	

[a]For acyclovir, chlorothiazide, ganciclovir, and lobucavir, the particle size was assumed to be 50~μm. Predicted Fa% did not depend on the particle size. For cinnarizine, EMD57033, dipyridamole, gefitinib, indomethacin, ivermectine, ketoconazole, N74, nifedipine, and nitrendipine, the particle size was estimated from the dissolution data.

[b]The method used to estimate Fa% (see text for detail): (I), Fa% reported in the literature; (II), relative bioavailability of solution versus solid form formulation; (III) relative bioavailability in the fasted versus the fed state (especially when Do $<$ 1 at the fed state); (IV) relative bioavailability with the low/high pH in the stomach when Do $<$ 1 in the stomach (for basic drugs) (IV); (V), dose-normalized relative bioavailability at Do $<$ 1 versus Do $>$ 1 when the terminal elimination half-life is consistent; (VI), from absolute bioavailability (F) and hepatic clearance using $\mathrm{Fa} = F/(1 - \mathrm{CL_h}/Q)$ (VI).

[c]Estimated using the PK of acid parent drug.

[d]Estimated from the total metabolite amount in urine and the unchanged drug in the feces.

[e]Powder versus solid dispersion.

Drugs with low solubility for which the effect of the stomach on Fa% is negligible are the simplest ones to simulate Fa%. Undissociable and free acid drugs are such cases. In addition, Fa% of free base drugs in high pH stomach cases (such as when coadministered with antacids) was also included, to increase the number of model drugs. As the effect of the stomach is negligible, a simple Fa% equation ($Fa_{SS.corr}$) was used for validation (Section 5.3.5).[3] In total, 29 structurally diverse drugs were used as model drugs (Table 8.3). Fa% data at several doses and particle sizes in humans and dogs were collated from the literature (Table 8.4). In the original investigation, a total of 110 Fa% data were used. In addition, several test set drugs were newly added in this book [LY-2157299, nabumetone, AZ0865, nitrendipine, celecoxib, acyclovir (800 mg, human fed), N74, nifedipine, indomethacin].

As typical input data solubility in biorelevant media (FaSSIF, FeSSIF), molecular weight, experimental log P_{oct}, experimental pK_a, Caco-2 permeability, dose, and particle size were used. For clarification, the mechanistic model equations used for this investigation are summarized as follows (see Chapter 2 for details):

- Fa%[4]

$$\mathrm{Fa} = 1 - \exp\left(-\frac{1}{\frac{1}{k_{\mathrm{diss}}} + \frac{k_{\mathrm{perm}}}{Do}} T_{\mathrm{si}}\right) = 1 - \exp\left(-\frac{1}{\frac{1}{\mathrm{Dn}} + \frac{\mathrm{Do}}{\mathrm{Pn}}}\right) \quad \text{if } \mathrm{Do} < 1, \mathrm{Do} = 1$$

$$\mathrm{Pn} = k_{\mathrm{perm}} T_{\mathrm{si}}, \mathrm{Dn} = k_{\mathrm{diss}} T_{\mathrm{si}}, \mathrm{Do} = \frac{\mathrm{Dose}}{S_{\mathrm{dissolv}} V_{\mathrm{GI}}}$$

- Dissolution

$$k_{\mathrm{diss}} = \frac{3 D_{\mathrm{eff}} S_{\mathrm{surface}}}{\rho} \sum^{i} \frac{f_i}{r_{\mathrm{p},i}^2}$$

$$f_{\mathrm{mono}} = \frac{S_{\mathrm{blank}}}{S_{\mathrm{dissolv}}}$$

$$D_{\mathrm{mono}}(\mathrm{cm}^2/\mathrm{s}) = 9.9 \times 10^{-5} \mathrm{MW}^{-0.453}$$

$$D_{\mathrm{eff}} = D_{\mathrm{mono}} \cdot f_{\mathrm{mono}} + D_{\mathrm{bm}}(1 - f_{\mathrm{mono}})$$

[3] Occams razor. See Section 8.2.
[4] Plus correction factors (Section 5.3.5).

- Permeation

$$k_{\text{perm}} = \frac{2\text{DF}}{R_{\text{GI}}} P_{\text{eff}}$$

$$P_{\text{eff}} = \frac{\text{PE}}{\frac{1}{P'_{\text{ep}}} + \frac{1}{P_{\text{UWL}}}}$$

$$= \frac{\text{PE}}{\frac{1}{f_{\text{mono}}\ (f_0 P_{\text{trans,0}} + P_{\text{para}}) \cdot \text{VE}} + \frac{1}{\frac{D_{\text{eff}}}{h_{\text{UWL}}} + P_{\text{WC}}}}$$

$$P_{\text{trans,0}}(\text{cm/s}) = 2.36 \times 10^{-6} {P_{\text{oct}}}^{1.1}$$

$$P_{\text{para}}(\text{cm/s}) = 3.9 \times 10^{-4} \cdot \frac{1}{\text{MW}^{1/3}} \cdot \text{RK}\left(\frac{\text{MW}^{1/3}}{8.46}\right)\left(f_0 + \sum_{z\,(z \neq 0)} f_z \frac{2.39z}{1 - \text{e}^{-2.39z}}\right)$$

$$h_{\text{UWL}} = h_{\text{fam}} \cdot \left(1 - \text{RK}\left(\frac{r_{\text{p,mean}}}{R_{\text{mucus}}}\right)\right) + h_{\text{pd}} - \frac{1}{2} h_{\text{pd}} R_{\text{SA}} \quad R_{\text{SA}} \leq 1$$

$$h_{\text{UWL}} = h_{\text{fam}} \cdot \left(1 - \text{RK}\left(\frac{r_{\text{p,mean}}}{R_{\text{mucus}}}\right)\right) + \frac{1}{2}\frac{h_{\text{pd}}}{R_{\text{SA}}} \qquad R_{\text{SA}} > 1$$

$$R_{\text{SA}} = \frac{3 \cdot C_{\text{pd}} \cdot h_{\text{pd}} Dose}{\cdot} V_{\text{GI}} \cdot \rho \sum_i \frac{f_i}{r_{\text{p},i}}$$

$$\text{RK}(x) = (1 - x)^2 (1 - 2.104\ x + 2.09\ x^3 - 0.95\ x^5) x < 1$$

The following drug parameters were used (see Chapters 2 and 7 for details):

- S_{dissolv}: The solubility values in FaSSIF and FeSSIF [152]. The pH of FeSSIF was set to 6.5 according to the recent update [88, 153]. TCs of 3, 5, 15, and 18 mM were used for fasted humans, fasted dogs, fed humans, and fed dogs, respectively. TC/PC ratio was 4:1. When the solubility value for dogs was not available, it was estimated from human FaSSIF or FeSSIF data correcting for the bile-micelle concentration.
- S_{surface}: Calculated by the Mooney–Stella equation and HH equation (Section 3.2.6).

- D_{bm}: 0.13, 0.56, 1.12, and 1.14×10^{-6} cm^2/s for 3, 5, 15, and 18 mM TC, respectively (Section 3.1.2). D_{bm} at 3 mM TC was multiplied threefold for P_{UWL} calculation [154].
- ρ: 1.2 g/cm^3.
- P_{ep}: In the case of lipophilic drugs (log $D_{oct,pH\ 6.5} > 2$), P_{ep} was estimated from log P_{oct}, pK_a, and MW because their permeability is expected to be UWL limited, and the Caco-2 study with a standard condition often underestimates the permeability of highly lipophilic drugs (Section 7.9.8). In the case of log $D_{oct,pH\ 6.5} < 2$, Caco-2 permeability was used if available in the literature.
- r_p: Assumed log-normal distribution with ln 2 standard deviation ($\Sigma f_i / r_{p,i}$ and $\sum f_i / r_{p,i}^2$ becomes ca. $1.4/r_{p,mean}$ and $3.3/r_{p,mean}^2$, respectively). When the particle size data is not available, it is back-estimated from the *in vitro* dissolution data.

The following physiological parameters were used (see Chapter 6 for details): DF = 1.7 (independently obtained from human P_{eff}–Fa% relationship), VE = 10 and h_{fam} = 15 μm for both humans and dogs; PE = 3 and 1, R_{GI} = 1.5 and 0.5 cm, and T_{si} = 3.5 and 2 h, $P_{WC} = 0.23$ and 0.29×10^{-4} cm/s, V_{GI} = 130 and 18.6 ml for humans and dogs, respectively. V_{GI} in the fed state was set 1.2-fold larger than that in the fasted state [67]. R_{mucus}, C_{pd}, and h_{UWL} were assumed to be the same in humans and dogs and were set to 2.9, 2.2, and 300 μm, respectively. Because R_{mucus} and C_{pd} are not available in the literature, they are optimized in the original investigation [12].[5]

The results were shown in Figure 8.13. In approximately 80% of the cases, the difference in simulated and observed error was within twofold, suggesting that the GUT framework has practical predictability for drug discovery but not for drug development.

The majority of drugs with low solubility (Do > 1) used in this study was categorized as SL-U (Fig. 8.14) but not DRL. This point is discussed later in Section 10.2.2.

Permeation resistance from the UWL has often been ignored in oral absorption simulation, and infinite fast permeation has sometimes been assumed. However, when permeation resistance from the UWL was ignored, Fa% of the SL-U cases were overestimated. This is in good agreement with the previous findings [53, 54, 59].

Interestingly, in many articles regarding the BCS, it was speculated that BCS II cases would be dissolution-rate limited and that *in vitro–in vivo* correlation

[5]Therefore, strictly speaking, this simulation is not a "prediction" for the cases in the original paper when the particle drifting effect is significant (i.e., SL-U, dose > 5 mg/kg, d_p < 5 μm). However, the number of Fa% data (> 11) is much larger than that of fitted parameter (two). Other cases can be taken as "prediction," as all the physiological data were independently determined and no fitting is employed. The data for the drugs newly added in this book can be interpreted as the independent test set.

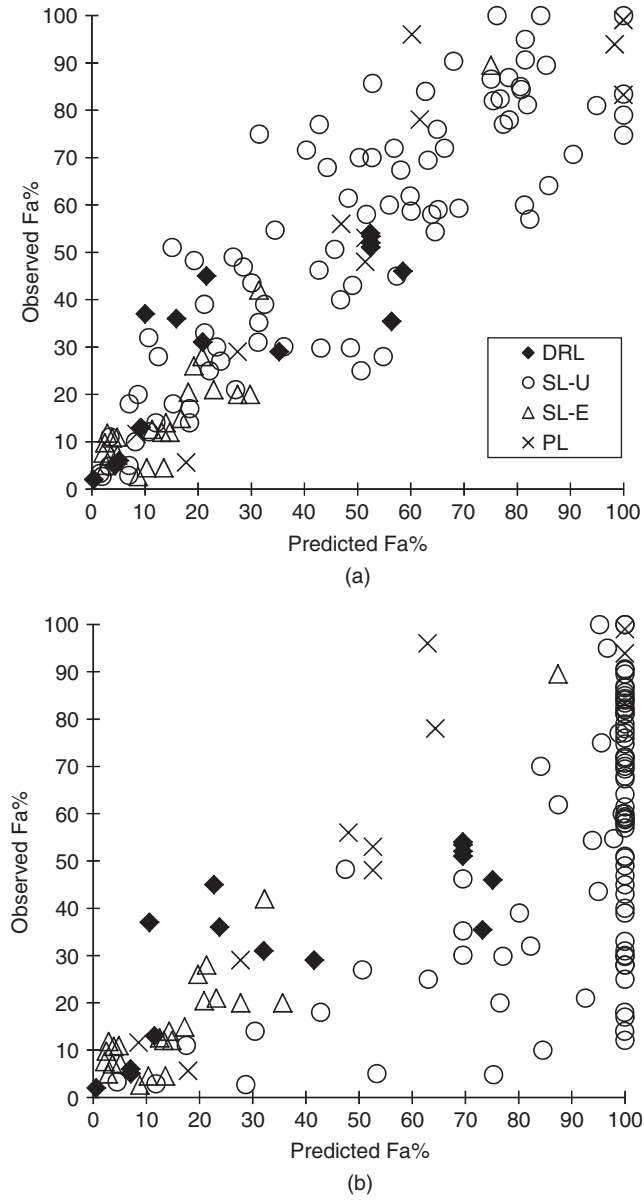

Figure 8.13 Simulated and observed Fa% for drugs with low solubility. (a) UWL considered and (b) UWL neglected.

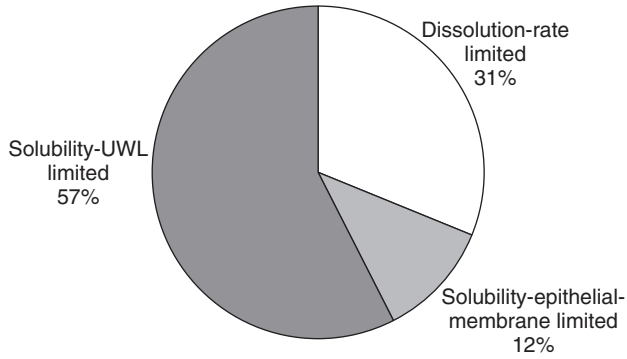

Figure 8.14 Percentage of DRL, SL-E, and SL-U (Do > 1 cases).

should be anticipated for this class. However, the result of this study suggested that the majority of BCS II drugs are likely to be solubility–permeability limited rather than dissolution-rate limited, especially, when the dose is larger than 20 mg.

8.6 VALIDATION FOR DISSOLUTION-RATE AND SOLUBILITY-PERMEABILITY-LIMITED CASES (WITH THE STOMACH EFFECT)

8.6.1 Difference Between Free Base and Salts

Since pH in the stomach is lower than that in the small intestine, a base drug shows higher solubility in the stomach than in the small intestine. Therefore, in the case of a basic drug, the drug molecule once dissolved in the stomach can precipitate out in the small intestine. However, the precipitation mechanism is different depending on the solid form of the active pharmaceutical ingredient (API), that is, free base or salt [2].

8.6.2 Simulation Model for Free Base

As a simpler case, the oral absorption of a free base drug is first discussed in this section [155]. The gastric pH provides a favorable environment to dissolve a free base. However, because the gastric emptying rate follows first-order kinetics, a portion of drug particles exits from the stomach into the small intestine before completely dissolving in the stomach.[6] As the gastric fluid (which contains both dissolved drug molecules and undissolved drug particles) pours into the small intestine, the pH is neutralized, and the dissolved drug concentration (C_{dissolv}) in the small intestine becomes transiently higher than the equilibrium solubility of a

[6]If the solid surface pH of a free base were not taken into account, the dissolution rate in the stomach would be overestimated.

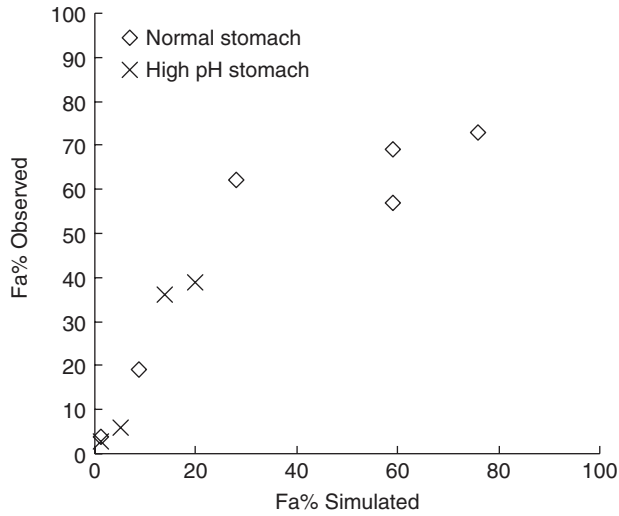

Figure 8.15 Simulated versus observed Fa% for free bases. *Source:* Adapted from Reference 159 with permission.

drug in the small intestine. Owing to the negative concentration gradient around the particles, the particles grow in the small intestine (Fig. 3.17a). This particle growth reduces C_{dissolv} in the small intestine [156]. Therefore, in biopharmaceutical modeling, both the dissolution rate in the stomach and the particle growth rate in the intestine have to be simulated appropriately.

The Nernst–Brunner (NB) equation can be used for both the dissolution and particle growth of API [156].[7] The API particles dissolve or grow depending on the concentration gradient (ΔC) around a particle, that is, ΔC is positive for dissolution and negative for particle growth. Appropriate estimation of the solid surface solubility of a free base is one of the key factors for appropriate simulation. For free base drugs, the solid surface solubility of a drug can become significantly smaller than the bulk solubility in the stomach (>100-fold) (Fig. 3.16). The Mooney–Stella equation can be used to calculate the solid surface pH (Section 3.2.6). The solid surface pH can also be experimentally obtained (Section 7.6.3.3) [157, 158]. In addition, the NB equation has to be modified as Equation 3.53 to differentiate the solid surface solubility from bulk solubility.

To model the pH change between the stomach and the small intestine, a compartment model is required. In addition, the position of undissolved particles will affect the concentration reduction rate in the small intestine. Therefore, biopharmaceutical modeling was performed using the S1I7C1 model.

[7]Particle growth is the reverse process of dissolution.

8.6.3 Simulation Results

Albendazole, aprepitant, dipyridamol, gefitinib, and ketoconazole were used as model drugs to validate this mechanism (all free base APIs (not salts)). Fa% of these drugs was appropriately simulated (Fig. 8.15). On the basis of the simulation results, it was suggested that the dissolution patterns in the gastrointestinal tract were significantly different depending on the dose–solubility ratio in the stomach. The oral absorption patterns of free bases can be roughly categorized into the following two types:

- When the dose number in the stomach is greater than 1 ($Do_{stomach} > 1$), saturated solubility is rapidly achieved in the stomach and further dissolution does not occur (Figs. 8.16 and 8.17). Therefore, most of the drug particles reach the small intestine before being completely dissolved (Fig. 8.18), and the regrowth of these particles rapidly reduces $C_{dissolv}$ in the small intestine.
- When the dose number in the stomach is less than 1 ($Do_{stomach} < 1$), saturated solubility is not achieved in the stomach (Fig. 8.16). However, some portions of drugs reach the small intestine before being completely dissolved in the stomach. The effect of stomach pH on Fa% is larger than that for $Do_{stomach} > 1$ cases (Section 13.1). Since both the dissolution rate in the stomach and the concentration reduction rate in the small intestine become faster as the particle size of a drug is reduced, it was theoretically suggested that there is an optimal particle size to effectively utilize the stomach fluid to dissolve a weak base drug. The relatively large particle sizes of dipyridamol, ketoconazole, and gefitinib might be explained by this mechanism.

8.7 SALTS

After dosing a salt form, a free form (not the salt) precipitates out in the small intestine (Figs. 3.17 and 3.18). The precipitation of the free base is initiated by a nucleation process, and then the nuclei particles grow and $C_{dissolv}$ is reduced in the small intestine. The model equations to simulate nucleation are discussed in Section 3.3. The categorization of precipitation patterns is discussed later in Section 11.1.

Owing to the lack of appropriate *in vitro* precipitation models [63], the validation of the GUT framework for salts has not been achieved yet. As a first step to handle nucleation, the classical nucleation theory has been introduced to the GUT framework [2, 160]. However, this approach should be validated carefully in the future. Currently (as of 2011), none of the commercial software can handle the nucleation process.

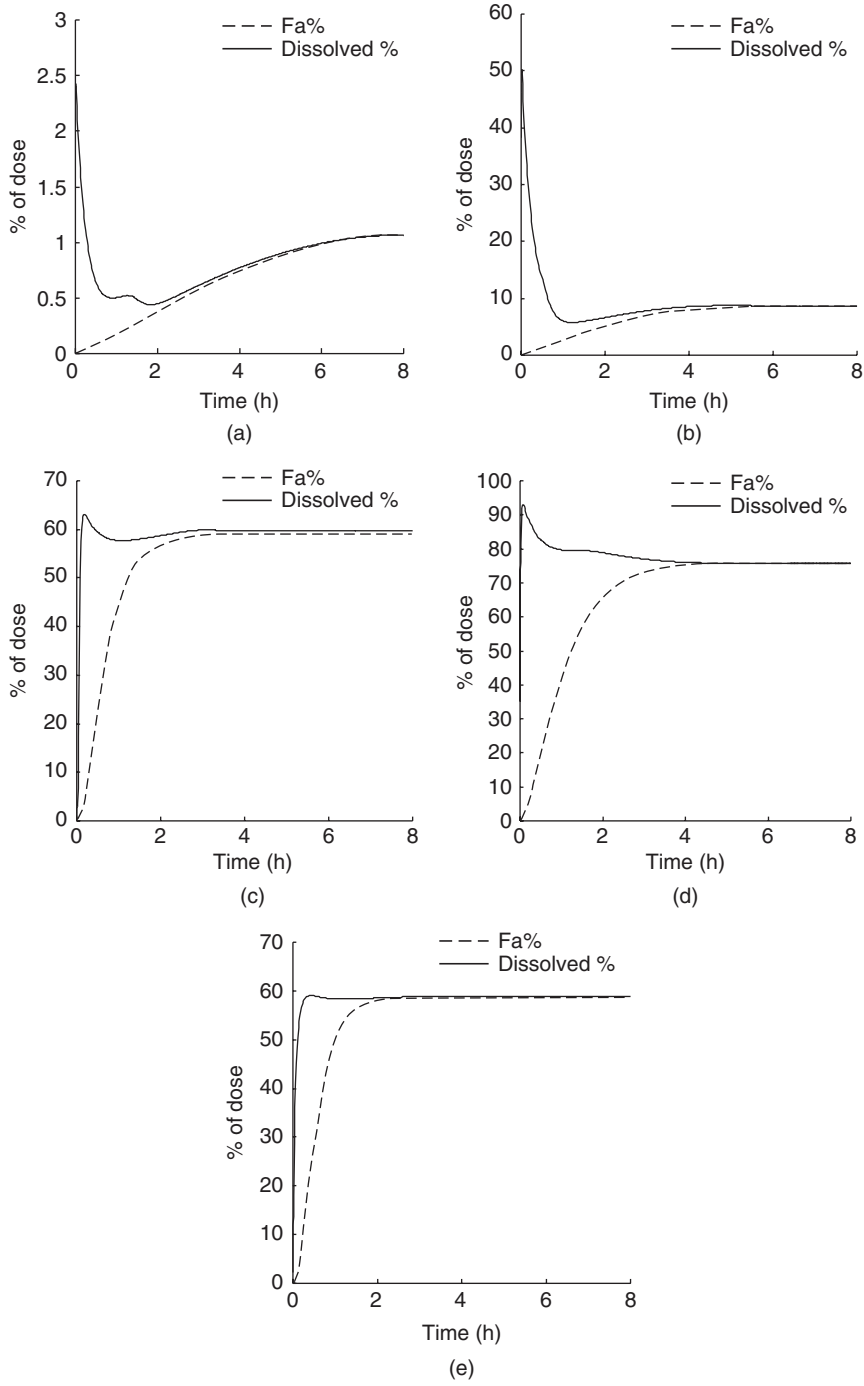

Figure 8.16 Simulated dissolved %. (a) Albendazole, (b) arepitant, (c) dipyridamole, (d) gefitinib, and (e) ketoconazole. *Source:* Adapted from Reference 159 with permission.

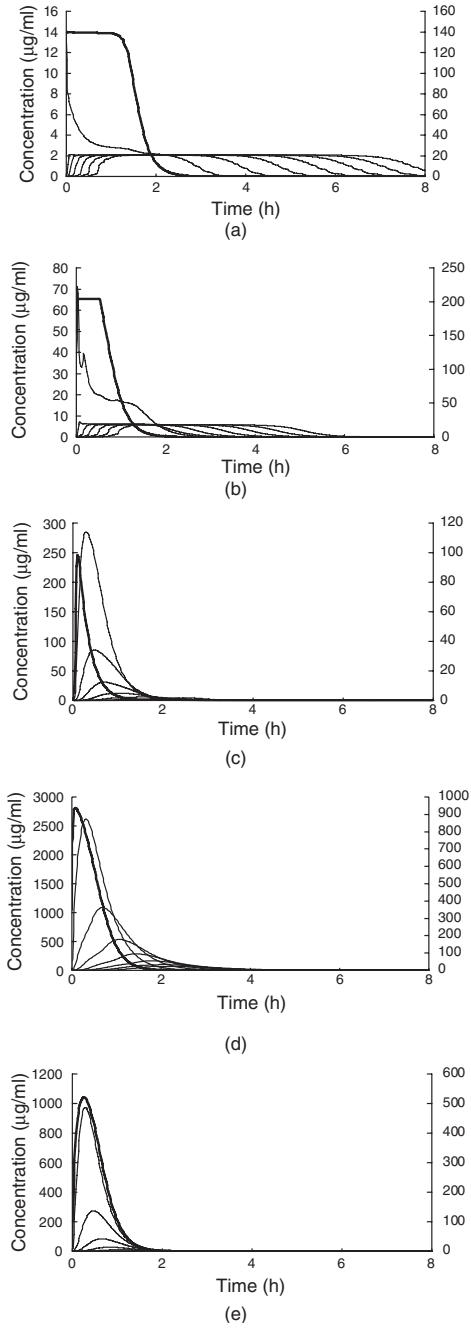

Figure 8.17 Simulated GI concentration. The lines from the left to the right: stomach (bold line), intestine compartments (1 to 7, proximal to distal). Axis: RHS stomach, LHS intestine. (a) Albendazole, (b) arepitant, (c) dipyridamole, (d) gefitinib, and (e) ketoconazole. *Source:* Adapted from Reference 159 with permission.

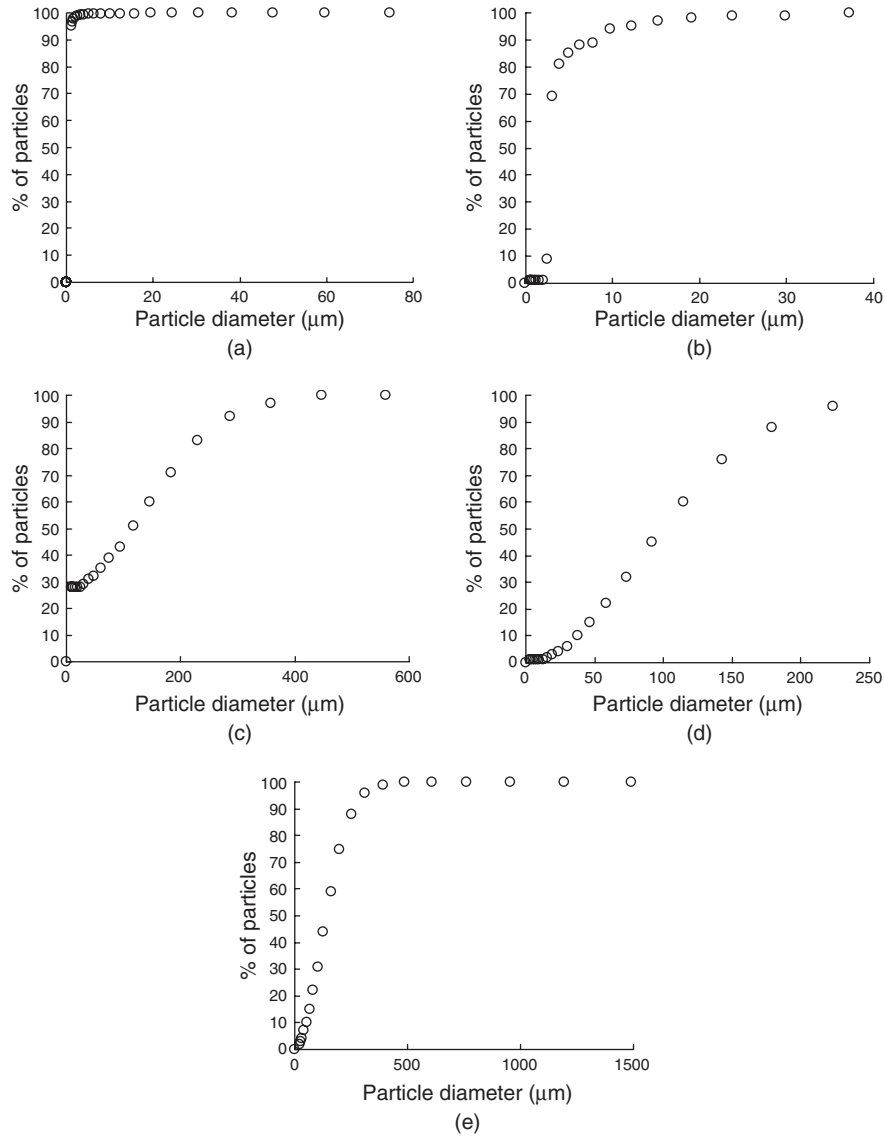

Figure 8.18 Simulated percentage of drug particles exiting stomach as undissolved. (a) Albendazole, (b) arepitant, (c) dipyridamole, (d) gefitinib, and (e) ketoconazole. *Source:* Adapted from Reference 159 with permission.

TABLE 8.5 BCS-Based Assessment of the Feasibility of Biopharmaceutical Modeling

BCS Class	API form/ APermeation Pathway	Prediction Process Step[a] I	II A	II B	III	IV
BCS I		Δ[b]– ◯	◯[b]	◯[b]	◎[b]	◎[b]
BCS II (dissolution limited)	Neutral	×[b]	Δ	◯	◯	◎
	Free acid	×	Δ	◯	◯	◎
	Free base	×	× – Δ	Δ	Δ	◎
	Salts	×	×	× – Δ	Δ	◯
BCS II (solubility limited)	Neutral	×	◯	◯	◯	◎
	Free acid	×	◯	◯	◯	◎
	Free base	×	× – Δ	× – Δ	Δ	◯
	Salts	×	×	×	Δ	Δ
BCS III (permeability limited)	Passive	×	◯	◯	◯	◎
	Active	×	Δ	Δ	Δ	◯
BCS IV	—	×	×	×	Δ	◯
Special formulations[c]	—	×	×	×	Δ	◯

[a] See text.
[b] ×, Poor predictability; Δ, marginal predictability; ◯, reasonable predictability (e.g., with in twofold error with 70% probability); ◎, Excellent predictability.
[c] SEDDS, solid dispersion, nano API particle, controlled release, etc.

8.8 RELIABILITY OF BIOPHARMACEUTICAL MODELING

As per the above discussions, the predictability of biopharmaceutical modeling is guesstimated based on the BCS (Table 8.5). BCS categorizes drugs into four classes based on the permeability and dose number. The theoretical basis of BCS is discussed in the next chapter. BCS is quite useful to navigate the strategy in drug discovery and development. BCS has been used as a common language among disciplines. Therefore, the BCS system is used as guidance for the reliability of biopharmaceutical modeling [2].

REFERENCES

1. Volgyi, G., Baka, E., Box, K.J., Comer, J.E., Takacs-Novak, K. (2010). Study of pH-dependent solubility of organic bases. Revisit of Henderson-Hasselbalch relationship. *Anal. Chim. Acta*, 673, 40–46.
2. Sugano, K. (2009). Introduction to computational oral absorption simulation. *Expert Opin. Drug Metab. Toxicol*, 5, 259–293.
3. Zhao, Y., Le, J., Abraham, M.H., Hersey, A., Eddershaw, P.J., Luscombe, C.N., Boutina, D., Beck, G., Sherborne, B., Cooper, I., Platts, J.A. (2001). Evaluation

of human intestinal absorption data and subsequent derivation of a quantitative structure-activity relationship (QSAR) with the Abraham descriptors. *J. Pharm. Sci*., 90, 749–784.

4. Varma, M.V., Obach, R.S., Rotter, C., Miller, H.R., Chang, G., Steyn, S.J., El-Kattan, A., Troutman, M.D. (2010). Physicochemical space for optimum oral bioavailability: contribution of human intestinal absorption and first-pass elimination. *J. Med. Chem*., 53, 1098–1108.
5. Zmuidinavicius, D., Didziapetris, R., Japertas, P., Avdeef, A., Petrauskas, A. (2003). Classification structure-activity relations (C-SAR) in prediction of human intestinal absorption. *J. Pharm. Sci*., 92, 621.
6. Sugano, K., Takata, N., Machida, M., Saitoh, K., Terada, K. (2002). Prediction of passive intestinal absorption using bio-mimetic artificial membrane permeation assay and the paracellular pathway model. *Int. J. Pharm*., 241, 241–251.
7. Shimizu, R., Sukegawa, T., Tsuda, Y., Itoh, T. (2008). Quantitative prediction of oral absorption of PEPT1 substrates based on *in vitro* uptake into Caco-2 cells. *Int. J. Pharm*., 354, 104–110.
8. Saitoh, R., Sugano, K., Takata, N., Tachibana, T., Higashida, A., Nabuchi, Y., Aso, Y. (2004). Correction of permeability with pore radius of tight junctions in Caco-2 monolayers improves the prediction of the dose fraction of hydrophilic drugs absorbed by humans. *Pharm. Res*., 21, 749.
9. Bretschneider, B., Brandsch, M., Neubert, R. (1999). Intestinal transport of beta-lactam antibiotics: analysis of the affinity at the H+/peptide symporter (PEPT1), the uptake into Caco-2 cell monolayers and the transepithelial flux. *Pharm. Res*., 16, 55–61.
10. Ranadive, S.A., Chen, A.X., Serajuddin, A.T. (1992). Relative lipophilicities and structural-pharmacological considerations of various angiotensin-converting enzyme (ACE) inhibitors. *Pharm. Res*., 9, 1480–1486.
11. Tam, K.Y., Avdeef, A., Tsinman, O., Sun, N. (2010). The permeation of amphoteric drugs through artificial membranes–an in combo absorption model based on paracellular and transmembrane permeability. *J. Med. Chem*., 53, 392–401.
12. Sugano, K. (2011). Fraction of a dose absorbed estimation for structurally diverse low solubility compounds. *Int. J. Pharm*., 405, 79–89.
13. Williams, P.E., Brown, A.N., Rajaguru, S., Francis, R.J., Walters, G.E., McEwen, J., Durnin, C. (1989). The pharmacokinetics and bioavailability of cilazapril in normal man. *Br. J. Clin. Pharmacol*., 27 Suppl 2, 181S–188S.
14. Cilazapril. Interview form. http://www.info.pmda.go.jp.
15. Wessel, M.D., Jurs, P.C., Tolan, J.W., Muskal, S.M. (1998). Prediction of human intestinal absorption of drug compounds from molecular structure. *J. Chem. Inf. Comput. Sci*., 38, 726–735.
16. Faropenem. Interview form. http://www.info.pmda.go.jp.
17. Lappin, G., Shishikura, Y., Jochemsen, R., Weaver, R.J., Gesson, C., Houston, B., Oosterhuis, B., Bjerrum, O.J., Rowland, M., Garner, C. (2010). Pharmacokinetics of fexofenadine: evaluation of a microdose and assessment of absolute oral bioavailability. *Eur. J. Pharm. Sci*., 40, 125–131.
18. Bagli, M., Hoflich, G., Rao, M.L., Langer, M., Baumann, P., Kolbinger, M., Barlage, U., Kasper, S., Moller, H.J. (1995). Bioequivalence and absolute bioavailability of oblong and coated levomepromazine tablets in CYP2D6 phenotyped subjects. *Int. J. Clin. Pharmacol. Ther*., 33, 646–652.

19. Wei, Y., Neves, L.A., Franklin, T., Klyuchnikova, N., Placzek, B., Hughes, H.M., Curtis, C.G. (2009). Vascular perfused segments of human intestine as a tool for drug absorption. *Drug Metab. Dispos*., 37, 731–736.
20. Balon, K., Riebesehl, B.U., Muller, B.W. (1999). Drug liposome partitioning as a tool for the prediction of human passive intestinal absorption. *Pharm. Res*., 16, 882–888.
21. Sugano, K., Artificial membrane technologies to assess transfer and permeation of drugs in drug discovery, in: B. Testa, H. van de Waterbeemd (Eds.) Comprehensive medicinal chemistry II Volume 5 ADME-Tox approach, Elsevier, Oxford, 2007, pp. 453–487.
22. Selvig, K. (1981). Pharmacokinetics of proxyphylline in adults after intravenous and oral administration. *Eur. J. Clin. Pharmacol*., 19, 149–155.
23. Kansy, M., Senner, F., Gubernator, K. (1998). Physicochemical high throughput screening: parallel artificial membrane permeation assay in the description of passive absorption processes. *J. Med. Chem*., 41, 1007–1010.
24. Knauf, H., Mutschler, E. (1984). Pharmacodynamics and pharmacokinetics of xipamide in patients with normal and impaired kidney function. *Eur. J. Clin. Pharmacol*., 26, 513–520.
25. Obata, K., Sugano, K., Saitoh, R., Higashida, A., Nabuchi, Y., Machida, M., Aso, Y. (2005). Prediction of oral drug absorption in humans by theoretical passive absorption model. *Int. J. Pharm*., 293, 183–192.
26. Avdeef, A., Absorption and Drug Development, Wiley-Interscience, NJ, Hoboken, 2003.
27. Lennernaes, H. (2007). Intestinal permeability and its relevance for absorption and elimination. *Xenobiotica*, 37, 1015–1051.
28. Lipka, E., Spahn-Langguth, H., Mutschler, E., Amidon, G.L. (1998). *In vivo* nonlinear intestinal permeability of celiprolol and propranolol in conscious dogs: evidence for intestinal secretion. *Eur. J. Pharm. Sci*., 6, 75–81.
29. Zakeri-Milani, P., Valizadeh, H., Tajerzadeh, H., Azarmi, Y., Islambolchilar, Z., Barzegar, S., Barzegar-Jalali, M. (2007). Predicting human intestinal permeability using single-pass intestinal perfusion in rat. *J. Pharm. Pharm. Sci*., 10, 368–379.
30. Chiou, W.L., Jeong, H.Y., Chung, S.M., Wu, T.C. (2000). Evaluation of using dog as an animal model to study the fraction of oral dose absorbed of 43 drugs in humans. *Pharm. Res*., 17, 135–140.
31. Chiou, W.L., Barve, A. (1998). Linear correlation of the fraction of oral dose absorbed of 64 drugs between humans and rats. *Pharm. Res*., 15, 1792–1795.
32. Knutson, T., Fridblom, P., Ahlstrom, H., Magnusson, A., Tannergren, C., Lennernas, H. (2008). Increased understanding of intestinal drug permeability determined by the LOC-I-GUT approach using multislice computed tomography. *Mol. Pharm*., 6, 2–10.
33. Fagerholm, U., Johansson, M., Lennernaes, H. (1996). Comparison between permeability coefficients in rat and human jejunum. *Pharm. Res*., 13, 1336–1342.
34. Kalantzi, L., Reppas, C., Dressman, J.B., Amidon, G.L., Junginger, H.E., Midha, K.K., Shah, V.P., Stavchansky, S.A., Barends, D.M. (2006). Biowaiver monographs for immediate release solid oral dosage forms: acetaminophen (paracetamol). *J. Pharm. Sci*., 95, 4–14.

35. Takahashi, M., Washio, T., Suzuki, N., Igeta, K., Yamashita, S. (2010). Investigation of the intestinal permeability and first-pass metabolism of drugs in cynomolgus monkeys using single-pass intestinal perfusion. *Biol. Pharm. Bull*., 33, 111–116.

36. Chiou, W.L., Buehler, P.W. (2002). Comparison of oral absorption and bioavailability of drugs between monkey and human. *Pharm. Res*., 19, 868–874.

37. Avdeef, A., Tam, K.Y. (2010). How well can the Caco-2/Madin-Darby canine kidney models predict effective human jejunal permeability? *J. Med. Chem*, 53, 3566–3584.

38. Sugano, K., Nabuchi, Y., Machida, M., Aso, Y. (2003). Prediction of human intestinal permeability using artificial membrane permeability. *Int. J. Pharm*., 257, 245–251.

39. Avdeef, A. (2010). Leakiness and size exclusion of paracellular channels in cultured epithelial cell monolayers-interlaboratory comparison. *Pharm. Res*., 27, 480–489.

40. Avdeef, A., Bendels, S., Di, L., Faller, B., Kansy, M., Sugano, K., Yamauchi, Y. (2007). Parallel artificial membrane permeability assay (PAMPA)-critical factors for better predictions of absorption. *J. Pharm. Sci*., 96, 2893–2909.

41. Reynolds, D.P., Lanevskij, K., Japertas, P., Didziapetris, R., Petrauskas, A. (2009). Ionization-specific analysis of human intestinal absorption. *J. Pharm. Sci*., 98, 4039–4054.

42. Sugano, K., Hamada, H., Machida, M., Ushio, H. (2001). High throuput prediction of oral absorption: Improvement of the composition of the lipid solution used in parallel artificial membrane permeation assay. *J. Biomol. Screen*, 6, 189–196.

43. Sugano, K., Hamada, H., Machida, M., Ushio, H., Saitoh, K., Terada, K. (2001). Optimized conditions of bio-mimetic artificial membrane permeation assay. *Int. J. Pharm*., 228, 181–188.

44. Sugano, K. (2009). Theoretical investigation of passive intestinal membrane permeability using Monte Carlo method to generate drug-like molecule population. *Int. J. Pharm*., 373, 55–61.

45. Poelma, F.G.J., Breas, R., Tukker, J.J., Crommelin, D.J.A. (1991). Intestinal absorption of drugs. The influence of mixed micelles on the disappearance kinetics of drugs from the small intestine of the rat. *J. Pharm. Pharmacol*., 43, 317–324.

46. Amidon, G.E., Higuchi, W.I., Ho, N.F.H. (1982). Theoretical and experimental studies of transport of micelle-solubilized solutes. *J. Pharm. Sci*., 71, 77–84.

47. Sugano, K. (2009). Oral absorption simulation for low solubility compounds. *Chem. Biodivers*., 6, 2014–2029.

48. Sugano, K., Obata, K., Saitoh, R., Higashida, A., Hamada, H. (2006). Processing of biopharmaceutical profiling data in drug discovery. Pharmacokinetic Profiling in Drug Research: Biological, Physicochemical, and Computational Strategies, [LogP2004, Lipophilicity Symposium], 3rd; 2004 Feb 29 Mar 4; Zurich, Switzerland. pp. 441–458.

49. Winiwarter, S., Bonham, N.M., Ax, F., Hallberg, A., Lennernas, H., Karlen, A. (1998). Correlation of human jejunal permeability (*in vivo*) of drugs with experimentally and theoretically derived parameters. A multivariate data analysis approach. *J. Med. Chem*., 41, 4939–4949.

50. Hou, T., Wang, J., Li, Y. (2007). ADME evaluation in drug discovery. 8. The prediction of human intestinal absorption by a support vector machine. *J. Chem. Inf. Model*, 47, 2408–2415.

51. Shen, J., Cheng, F., Xu, Y., Li, W., Tang, Y. (2010). Estimation of ADME properties with substructure pattern recognition. *J. Chem. Inf. Model*., 50, 1034–1041.
52. Fujioka, Y., Kadono, K., Fujie, Y., Metsugi, Y., Ogawara, K.-i., Higaki, K., Kimura, T. (2007). Prediction of oral absorption of griseofulvin, a BCS class II drug, based on GITA model: utilization of a more suitable medium for in-vitro dissolution study. *J. Controlled Release*, 119, 222–228.
53. Takano, R., Sugano, K., Higashida, A., Hayashi, Y., Machida, M., Aso, Y., Yamashita, S. (2006). Oral absorption of poorly water-soluble drugs: computer simulation of fraction absorbed in humans from a miniscale dissolution test. *Pharm. Res*., 23, 1144–1156.
54. Takano, R., Doctoral Thesis, Setsunan University, 2009.
55. Matsson, P., Bergstroem, C.A.S., Nagahara, N., Tavelin, S., Norinder, U., Artursson, P. (2005). Exploring the role of different drug transport routes in permeability screening. *J. Med. Chem*., 48, 604–613.
56. Sawyer, M.H., Webb, D.E., Balow, J.E., Straus, S.E. (1988). Acyclovir-induced renal failure. Clinical course and histology. *Am. J. Med*., 84, 1067–1071.
57. Escher, B., Berger, C., Bramaz, N., Kwon, J.H., Richter, M., Tsinman, O., Avdeef, A. (2008). Membrane-water partitioning, membrane permeability and baseline toxicity. *Environ. Toxicol. Chem*., 27, 909–918.
58. Fagerberg, J.H., Tsinman, O., Sun, N., Tsinman, K., Avdeef, A., Bergstrom, C.A.S. (2010). Dissolution rate and apparent solubility of poorly soluble drugs in biorelevant dissolution media. *Mol. Pharm*., ACS ASAP.
59. Takano, R., Furumoto, K., Shiraki, K., Takata, N., Hayashi, Y., Aso, Y., Yamashita, S. (2008). Rate-limiting steps of oral absorption for poorly water-soluble drugs in dogs; prediction from a miniscale dissolution test and a physiologically-based computer simulation. *Pharm. Res*., 25, 2334–2344.
60. Aprepitant (2009). Aprepitant Interview form. http://www.info.pmda.go.jp.
61. Singh, B.N. (2005). A quantitative approach to probe the dependence and correlation of food-effect with aqueous solubility, dose/solubility ratio, and partition coefficient (Log P) for orally active drugs administered as immediate-release formulations. *Drug Dev. Res*., 65, 55–75.
62. Vertzoni, M., Fotaki, N., Kostewicz, E., Stippler, E., Leuner, C., Nicolaides, E., Dressman, J., Reppas, C. (2004). Dissolution media simulating the intraluminal composition of the small intestine: physiological issues and practical aspects. *J. Pharm. Pharmacol*., 56, 453–462.
63. Carlert, S., Palsson, A., Hanisch, G., von Corswant, C., Nilsson, C., Lindfors, L., Lennernas, H., Abrahamsson, B. (2010). Predicting intestinal precipitation–a case example for a basic BCS class II drug. *Pharm. Res*., 27, 2119–2130.
64. Schwebel, H.J., van Hoogevest, P., Leigh, M.L., Kuentz, M. (2011). The apparent solubilizing capacity of simulated intestinal fluids for poorly water-soluble drugs. *Pharm. Dev. Technol*., 16, 278–286.
65. Kobayashi, Y., Ito, S., Itai, S., Yamamoto, K. (2000). Physicochemical properties and bioavailability of carbamazepine polymorphs and dihydrate. *Int. J. Pharm*., 193, 137–146.
66. Shono, Y., Jantratid, E., Janssen, N., Kesisoglou, F., Mao, Y., Vertzoni, M., Reppas, C., Dressman, J.B. (2009). Prediction of food effects on the absorption of celecoxib based on biorelevant dissolution testing coupled with physiologically based pharmacokinetic modeling. *Eur. J. Pharm. Biopharm*., 73, 107–114.

67. Sugano, K., Kataoka, M., da Costa Mathews, C., Yamashita, S. (2010). Prediction of food effect by bile micelles on oral drug absorption considering free fraction in intestinal fluid. *Eur. J. Pharm. Sci*., 40, 118–124.
68. Jinno, J.-I., Kamada, N., Miyake, M., Yamada, K., Mukai, T., Odomi, M., Toguchi, H., Liversidge, G.G., Higaki, K., Kimura, T. (2006). Effect of particle size reduction on dissolution and oral absorption of a poorly water-soluble drug, cilostazol, in beagle dogs. *J. Controlled Release*, 111, 56–64.
69. Glomme, A., März, J., Dressman, J., Predicting the intestinal solubility of poorly soluble drugs in: B. Testa, S. Krämer, H. Wunderli-Allenspach, G. Folkers (Eds.) Pharmacokinetic Profiling in Drug Research, Wiley-VCH, Zurich, 2006, pp. 259–280.
70. Okazaki, A., Mano, T., Sugano, K. (2008). Theoretical dissolution model of polydisperse drug particles in biorelevant media. *J. Pharm. Sci*., 97, 1843–1852.
71. Alsenz, J., Kansy, M. (2007). High throughput solubility measurement in drug discovery and development. *Adv. Drug Delivery Rev*., 59, 546–567.
72. Dzimiri, N., Fricke, U., Klaus, W. (1987). Influence of derivatization on the lipophilicity and inhibitory actions of cardiac glycosides on myocardial sodium-potassium ATPase. *Br. J. Pharmacol*., 91, 31–38.
73. Schamp, K., Schreder, S.-A., Dressman, J. (2006). Development of an *in vitro*/*in vivo* correlation for lipid formulations of EMD 50733, a poorly soluble, lipophilic drug substance. *Eur. J. Pharm. Biopharm*., 62, 227–234.
74. Scholz, A., Abrahamsson, B., Diebold, S.M., Kostewicz, E., Polentarutti, B.I., Ungell, A.-L., Dressman, J.B. (2002). Influence of hydrodynamics and particle size on the absorption of felodipine in labradors. *Pharm. Res*., 19, 42–46.
75. Hanafy, A., Spahn-Langguth, H., Vergnault, G., Grenier, P., Tubic Grozdanis, M., Lenhardt, T., Langguth, P. (2007). Pharmacokinetic evaluation of oral fenofibrate nanosuspensions and SLN in comparison to conventional suspensions of micronized drug. *Adv. Drug Delivery Rev*., 59, 419–426.
76. Buch, P., Langguth, P., Kataoka, M., Yamashita, S. (2009). IVIVC in oral absorption for fenofibrate immediate release tablets using a dissolution/permeation system. *J. Pharm. Sci*., 98, 2001–2009.
77. Takano, R., Takata, N., Saitoh, R., Furumoto, K., Higo, S., Hayashi, Y., Machida, M., Aso, Y., Yamashita, S. (2010). Quantitative analysis of the effect of supersaturation on *in vivo* drug absorption. *Mol. Pharm*., 7, 1431–1440.
78. Yang, Z., Manitpisitkul, P., Sawchuk, R.J. (2006). *In situ* studies of regional absorption of lobucavir and ganciclovir from rabbit intestine and predictions of dose-limited absorption and associated variability in humans. *J. Pharm. Sci*., 95, 2276–2292.
79. Wilson, C.G., O'Mahony, B., Connolly, S.M., Cantarini, M.V., Farmer, M.R., Dickinson, P.A., Smith, R.P., Swaisland, H.C. (2009). Do gastrointestinal transit parameters influence the pharmacokinetics of gefitinib? *Int. J. Pharm*., 376, 7–12.
80. Gefitinib (2009). Gefitinib Interview form. http://www.info.pmda.go.jp.
81. Tosco, P., Rolando, B., Fruttero, R., Henchoz, Y., Martel, S., Carrupt, P.-A., Gasco, A. (2008). Physicochemical profiling of sartans: a detailed study of ionization constants and distribution coefficients. *Helv. Chim. Acta*, 91, 468–482.
82. Young, A.M., Audus, K.L., Proudfoot, J., Yazdanian, M. (2006). Tetrazole compounds: the effect of structure and pH on Caco-2 cell permeability. *J. Pharm. Sci*., 95, 717–725.
83. Irbesartan (2009). Irbesartan Interview form. http://www.info.pmda.go.jp.

84. Bhattachar, S.N., Perkins, E.J., Tan, J.S., Burns, L.J. (2011). Effect of gastric pH on the pharmacokinetics of a bcs class II compound in dogs: utilization of an artificial stomach and duodenum dissolution model and gastroplus, simulations to predict absorption. *J. Pharm. Sci*., 100(11), 4756–4765.

85. Lehto, P., Kortejarvi, H., Liimatainen, A., Ojala, K., Kangas, H., Hirvonen, J., Tanninen, V.P., Peltonen, L. (2011). Use of conventional surfactant media as surrogates for FaSSIF in simulating *in vivo* dissolution of BCS class II drugs. *Eur. J. Pharm. Biopharm*., 78, 531–538.

86. Clarysse, S., Psachoulias, D., Brouwers, J., Tack, J., Annaert, P., Duchateau, G., Reppas, C., Augustijns, P. (2009). Postprandial changes in solubilizing capacity of human intestinal fluids for BCS Class II drugs. *Pharm. Res*., 26, 1456–1466.

87. Nishihata, T., Ishizaka, M., Yokohama, S., Martino, A.C., Gordon, R.E. (1993). Effects of particle size of bulk drug and food on the bioavailability of U-78875 in dogs. *Drug Dev. Ind. Pharm*., 19, 2679–2698.

88. Kataoka, M., Masaoka, Y., Yamazaki, Y., Sakane, T., Sezaki, H., Yamashita, S. (2003). *In vitro* system to evaluate oral absorption of poorly water-soluble drugs: simultaneous analysis on dissolution and permeation of drugs. *Pharm. Res*., 20, 1674–1680.

89. Steingrimsdottir, H., Gruber, A., Palm, C., Grimfors, G., Kalin, M., Eksborg, S. (2000). Bioavailability of aciclovir after oral administration of aciclovir and its prodrug valaciclovir to patients with leukopenia after chemotherapy. *Antimicrob. Agents Chemother*., 44, 207–209.

90. Vergin, H., Kikuta, C., Mascher, H., Metz, R. (1995). Pharmacokinetics and bioavailability of different formulations of aciclovir. *Arzneim.-Forsch*., 45, 508–515.

91. Acyclovir. Interview form. http://www.info.pmda.go.jp.

92. Rigter, I.M., Schipper, H.G., Koopmans, R.P., Van Kan, H.J.M., Frijlink, H.W., Kager, P.A., Guchelaar, H.J. (2004). Relative bioavailability of three newly developed albendazole formulations: a randomized crossover study with healthy volunteers. *Antimicrob. Agents Chemother*., 48, 1051–1054.

93. Schipper, H.G., Koopmans, R.P., Nagy, J., Butter, J.J., Kager, P.A., Van Boxtel, C.J. (2000). Effect of dose increase or cimetidine co-administration on albendazole bioavailability. *Am. J. Trop. Med. Hyg*., 63, 270–273.

94. Wu, Y., Loper, A., Landis, E., Hettrick, L., Novak, L., Lynn, K., Chen, C., Thompson, K., Higgins, R., Batra, U., Shelukar, S., Kwei, G., Storey, D. (2004). The role of biopharmaceutics in the development of a clinical nanoparticle formulation of MK-0869: a Beagle dog model predicts improved bioavailability and diminished food effect on absorption in human. *Int. J. Pharm*., 285, 135–146.

95. Webpage, The electronic Medicines Compendium Wellvone 750mg, http://www.medicines.org.uk/EMC/medicine/777/SPC/Wellvone+750mg+5ml+oral+suspension/.

96. Rolan, P.E., Mercer, A.J., Weatherley, B.C., Holdich, T., Meire, H., Peck, R.W., Ridout, G., Posner, J. (1994). Examination of some factors responsible for a food-induced increase in absorption of atovaquone. *Br. J. Clin. Pharmacol*., 37, 13–20.

97. Freeman, C.D., Klutman, N.E., Lamp, K.C., Dall, L.H., Strayer, A.H. (1998). Relative bioavailability of atovaquone suspension when administered with an enteral nutrition supplement. *Ann. Pharmacother*., 32, 1004–1007.

98. Dixon, R., Pozniak, A.L., Watt, H.M., Rolan, P., Posner, J. (1996). Single-dose and steady-state pharmacokinetics of a novel microfluidized suspension of atovaquone in human immunodeficiency virus-seropositive patients. *Antimicrob. Agents Chemother*., 40, 556–560.

99. Zhang, X., Lionberger, R.A., Davit, B.M., Yu, L.X. (2011). Utility of physiologically based absorption modeling in implementing Quality by Design in drug development. *AAPS J*., 13, 59–71.

100. Dolenc, A., Kristl, J., Baumgartner, S., Planinsek, O. (2009). Advantages of celecoxib nanosuspension formulation and transformation into tablets. *Int. J. Pharm*., 376, 204–212.

101. Davies, N.M., McLachlan, A.J., Day, R.O., Williams, K.M. (2000). Clinical pharmacokinetics and pharmacodynamics of celecoxib: a selective cyclo-oxygenase-2 inhibitor. *Clin. Pharmacokinet*., 38, 225–242.

102. Welling, P.G., Barbhaiya, R.H. (1982). Influence of food and fluid volume on chlorothiazide bioavailability: comparison of plasma and urinary excretion methods. *J. Pharm. Sci*., 71, 32–35.

103. Dressman, J.B., Fleisher, D., Amidon, G.L. (1984). Physicochemical model for dose-dependent drug absorption. *J. Pharm. Sci*., 73, 1274–1279.

104. Bramer, S.L., Forbes, W.P. (1999). Relative bioavailability and effects of a high fat meal on single dose cilostazol pharmacokinetics. *Clin. Pharmacokinet*., 37, 13–23.

105. Bramer, S.L., Forbes, W.P., Mallikaarjun, S. (1999). Cilostazol pharmacokinetics after single and multiple oral doses in healthy males and patients with intermittent claudication resulting from peripheral arterial disease. *Clin. Pharmacokinet*., 37 Suppl 2, 1–11.

106. Yamada, I., Goda, T., Kawata, M., Ogawa, K. (1990). Use of gastric acidity-controlled beagle dogs in bioavailability studies of cinnarizine. *Yakugaku Zasshi*, 110, 280–285.

107. Ogata, H., Aoyagi, N., Kaniwa, N., Ejima, A., Sekine, N., Kitamura, M., Inoue, Y. (1986). Gastric acidity dependent bioavailability of cinnarizine from two commercial capsules in healthy volunteers. *Int. J. Pharm*., 29, 113–120.

108. Liversidge, G.G., Cundy, K.C. (1995). Particle size reduction for improvement of oral bioavailability of hydrophobic drugs: I. Absolute oral bioavailability of nanocrystalline danazol in beagle dogs. *Int. J. Pharm*., 125, 91–97.

109. Sunesen, V.H., Vedelsdal, R., Kristensen, H.G., Christrup, L., Muellertz, A. (2005). Effect of liquid volume and food intake on the absolute bioavailability of danazol, a poorly soluble drug. *Eur. J. Pharm. Sci*., 24, 297–303.

110. Charman, W.N., Rogge, M.C., Boddy, A.W., Berger, B.M. (1993). Effect of food and a monoglyceride emulsion formulation on danazol bioavailability. *J. Clin. Pharmacol*., 33, 381–386.

111. Lloyd-Jones, J.G. (1977). Danazol plasma concentration in man. *J. Int. Med. Res*., 5 Suppl 3, 18–24.

112. Jounela, A.J., Pentikainen, P.J., Sothmann, A. (1975). Effect of particle size on the bioavailability of digoxin. *Eur. J. Clin. Pharmacol*., 8, 365–370.

113. Bjornsson, T.D., Mahony, C. (1983). Clinical pharmacokinetics of dipyridamole. *Thromb. Res*., 93–104.

114. Russell, T.L., Berardi, R.R., Barnett, J.L., O'Sullivan, T.L., Wagner, J.G., Dressman, J.B. (1994). pH-Related changes in the absorption of dipyridamole in the elderly. *Pharm. Res*., 11, 136–143.

115. Zhou, R., Moench, P., Heran, C., Lu, X., Mathias, N., Faria, T.N., Wall, D.A., Hussain, M.A., Smith, R.L., Sun, D. (2005). pH-dependent dissolution *in vitro* and absorption *in vivo* of weakly basic drugs: development of a canine model. *Pharm. Res*., 22, 188–192.

116. Merck, FDA approval document for sustiva, http://www.accessdata.fda.gov/scripts/cder/drugsatfda/index.cfm.

117. Gao, J.Z., Hussain, M.A., Motheram, R., Gray, D. A. B., Benedek, I.H., Fiske, W.D., Doll, W.J., Sandefer, E., Page, R.C., Digenis, G.A. (2007). Investigation of human pharmacoscintigraphic behavior of two tablets and a capsule formulation of a high dose, poorly water soluble/highly permeable drug (Efavirenz). *J. Pharm. Sci*., 96, 2970–2977.

118. Sauron, R., Wilkins, M., Jessent, V., Dubois, A., Maillot, C., Weil, A. (2006). Absence of a food effect with a 145mg nanoparticle fenofibrate tablet formulation. *Int. J. Clin. Pharmacol. Ther*., 44, 64–70.

119. Zhu, T., Ansquer, J.-C., Kelly Maureen, T., Sleep Darryl, J., Pradhan Rajendra, S. (2010). Comparison of the gastrointestinal absorption and bioavailability of fenofibrate and fenofibric Acid in humans. *J. Clin. Pharmacol*., 50, 914–921.

120. Guivarc'h, P.-H., Vachon, M.G., Fordyce, D. (2004). A new fenofibrate formulation: results of six single-dose, clinical studies of bioavailability under fed and fasting conditions. *Clin. Ther*., 26, 1456–1469.

121. Spector, S.A., Busch, D.F., Follansbee, S., Squires, K., Lalezari, J.P., Jacobson, M.A., Connor, J.D., Jung, D., Shadman, A., Mastre, B., Buhles W., Drew W. L., AIDS Clinical Trials Group, and Cytomegalovirus Cooperative Study Group. (1995). Pharmacokinetic, safety, and antiviral profiles of oral ganciclovir in persons infected with human immunodeficiency virus: a phase I/II study. *J. Infect. Dis*., 171, 1431–1437.

122. Bergman, E., Forsell, P., Persson, E.M., Knutson, L., Dickinson, P., Smith, R., Swaisland, H., Farmer, M.R., Cantarini, M.V., Lennernaes, H. (2007). Pharmacokinetics of gefitinib in humans: the influence of gastrointestinal factors. *Int. J. Pharm*., 341, 134–142.

123. Tashtoush, B.M., Al-Qashi, Z.S., Najib, N.M. (2004). *In vitro* and *in vivo* evaluation of glibenclamide in solid dispersion systems. *Drug Dev. Ind. Pharm*., 30, 601–607.

124. Ahmed, I.S., Aboul-Einien, M.H., Mohamed, O.H., Farid, S.F. (2008). Relative bioavailability of griseofulvin lyophilized dry emulsion tablet vs. immediate release tablet: a single-dose, randomized, open-label, six-period, crossover study in healthy adult volunteers in the fasted and fed states. *Eur. J. Pharm. Sci*., 35, 219–225.

125. Chiou, W.L., Riegelman, S. (1971). Absorption characteristics of solid dispersed and micronized griseofulvin in man. *J. Pharm. Sci*., 60, 1376–1380.

126. Hosny, E.A., El-Sayed, Y.M., Al-Meshal, M.A., Al-Angary, A.A. (1994). Effect of food on bioavailability of bioadhesive-containing indomethacin tablets in dogs. *Int. J. Pharm*., 112, 87–91.

127. Jung, M.S., Kim, J.S., Kim, M.S., Alhalaweh, A., Cho, W., Hwang, S.J., Velaga, S.P. (2010). Bioavailability of indomethacin-saccharin cocrystals. *J. Pharm. Pharmacol*., 62, 1560–1568.

128. Vachharajani, N.N., Shyu, W.C., Mantha, S., Park, J.S., Greene, D.S., Barbhaiya, R.H. (1998). Lack of effect of food on the oral bioavailability of irbesartan in healthy male volunteers. *J. Clin. Pharmacol*., 38, 433–436.

129. Hirlekar, R.S., Sonawane, S.N., Kadam, V.J. (2009). Studies on the effect of water-soluble polymers on drug-cyclodextrin complex solubility. *AAPS PharmSciTech*., 10, 858–863.

130. Irbesartan, Interview form, http://www.info.pmda.go.jp.

131. Guzzo, C.A., Furtek, C.I., Porras, A.G., Chen, C., Tipping, R., Clineschmidt, C.M., Sciberras, D.G., Hsieh, J. Y. K., Lasseter, K.C. (2002). Safety, tolerability, and pharmacokinetics of escalating high doses of ivermectin in healthy adult subjects. *J. Clin. Pharmacol*., 42, 1122–1133.

132. Ivermectine, Interview form, http://www.info.pmda.go.jp.

133. Merck, F. D. A., approval document for ivermectin, in.

134. Lelawongs, P., Barone, J.A., Colaizzi, J.L., Hsuan, A. T. M., Mechlinski, W., Legendre, R., Guarnieri, J. (1988). Effect of food and gastric acidity on absorption of orally administered ketoconazole. *Clin. Pharm*., 7, 228–235.

135. Mikus, G., Fischer, C., Heuer, B., Langen, C., Eichelbaum, M. (1987). Application of stable isotope methodology to study the pharmacokinetics, bioavailability and metabolism of nitrendipine after i.v. and p.o. administration. *Br. J. Clin. Pharmacol*., 24, 561–569.

136. Sugimoto, M., Okagaki, T., Narisawa, S., Koida, Y., Nakajima, K. (1998). Improvement of dissolution characteristics and bioavailability of poorly water-soluble drugs by novel cogrinding method using water-soluble polymer. *Int. J. Pharm*., 160, 11–19.

137. Hoshi, N., Kida, A., Hayashi, T., Murakami, Y. (2007). Development of PVA copolymer capsules II. *Pharm. Tech Jpn*., 23, 75–80.

138. Sugimoto, I., Kuchiki, A., Nakagawa, H., Tohgo, K., Kondo, S., Iwane, I., Takahashi, K. (1980). Dissolution and absorption of nifedipine from nifedipine-polyvinylpyrrolidone coprecipitate. *Drug Dev. Ind. Pharm*., 6, 137–160.

139. Lund, L., Alvan, G., Berlin, A., Alexanderson, B. (1974). Pharmacokinetics of single and multiple doses of phenytoin in man. *Eur. J. Clin. Pharmacol*., 7, 81–86.

140. Mizuno, N., Shinkuma, D., Hamaguchi, T. (2003). Variance of bioavailability of pharmaceutical preparations and analysis of factors affecting it. *Yakugaku Zasshi*, 123, 477–493.

141. Yakou, S., Umehara, K., Sonobe, T., Nagai, T., Sugihara, M., Fukuyama, Y. (1984). Particle size dependency of dissolution rate and human bioavailability of phenytoin in powders and phenytoin-polyethylene glycol solid dispersions. *Chem. Pharm. Bull*., 32, 4130–4136.

142. Hamaguchi, T., Shinkuma, D., Irie, T., Yamanaka, Y., Morita, Y., Iwamoto, B., Miyoshi, K., Mizuno, N. (1993). Effect of a high-fat meal on the bioavailability of phenytoin in a commercial powder with a large particle size. *Int. J. Clin. Pharmacol., Ther. Toxicol*., 31, 326–330.

143. Nakajima, M., Kanamaru, M., Umematsu, T., Tsubokura, S. (1993).. A phase I clinical study of a Leukotriene C4, D4 and E4 receptor antagonist; ONO-1078 in healthy volunteers. *Rynsho Iyaku*, 9 Suppl 1, 3–29.

144. Brocks, D.R., Upward, J.W., Georgiou, P., Stelman, G., Doyle, E., Allen, E., Wyld, P., Dennis, M.J. (1996). The single and multiple dose pharmacokinetics of pranlukast in healthy volunteers. *Eur. J. Clin. Pharmacol*., 51, 303–308.

145. Brocks, D.R., Upward, J., Davy, M., Howland, K., Compton, C., McHugh, C., Dennis, M.J. (1997). Evening dosing is associated with higher plasma concentrations of pranlukast, a leukotriene receptor antagonist, in healthy male volunteers. *Br. J. Clin. Pharmacol*., 44, 289–291.

146. Pranlukast, Interview form, http://www.info.pmda.go.jp.

147. Overdiek, H. W. P. M., Merkus, F. W. H. M. (1986). Influence of food on the bioavailability of spironolactone. *Clin. Pharmacol. Ther*., 40, 531–536.

148. Barber, D., Keuter, J., Kravig, K. (1998). A logical stepwise approach to laser diffraction particle size distribution analysis methods development and validation. *Pharm. Dev. Technol*., 3, 153–161.

149. Pentikaeinen, P.J., Neuvonen, P.J., Backman, C. (1981). Human pharmacokinetics of tolfenamic acid, a new antiinflammatory agent. *Eur. J. Clin. Pharmacol*., 19, 359–365.

150. Neuvonen, P.J., Kivisto, K.T. (1988). Effect of magnesium hydroxide on the absorption of tolfenamic and mefenamic acids. *Eur. J. Clin. Pharmacol*., 35, 495–501.

151. Pedersen, S.B. (1994). Biopharmaceutical aspects of tolfenamic acid. *Pharmacol. Toxicol. (Oxford, UK)*, 75, 22–32.

152. Galia, E., Nicolaides, E., Horter, D., Lobenberg, R., Reppas, C., Dressman, J.B. (1998). Evaluation of various dissolution media for predicting *in vivo* performance of class I and II drugs. *Pharm. Res*., 15, 698–705.

153. Jantratid, E., Janssen, N., Reppas, C., Dressman, J.B. (2008). Dissolution media simulating conditions in the proximal human gastrointestinal tract: an update. *Pharm. Res*., 25, 1663–1676.

154. Li, C.-Y., Zimmerman, C.L., Wiedmann, T.S. (1996). Diffusivity of bile salt/phospholipid aggregates in mucin. *Pharm. Res*., 13, 535–541.

155. Sugano, K. (2010). Computational oral absorption simulation of free base drugs. *Int. J. Pharm*., 398, 73–82.

156. Johnson, K.C. (2003). Dissolution and absorption modeling: model expansion to simulate the effects of precipitation, water absorption, longitudinally changing intestinal permeability, and controlled release on drug absorption. *Drug Dev. Ind. Pharm*., 29, 833–842.

157. Vertzoni, M., Pastelli, E., Psachoulias, D., Kalantzi, L., Reppas, C. (2007). Estimation of intragastric solubility of drugs. *Pharm. Res*., 24, 909–917.

158. Pudipeddi, M., Zannou, E.A., Vasanthavada, M., Dontabhaktuni, A., Royce, A.E., Joshi, Y.M., Serajuddin, A.T.M. (2008). Measurement of surface pH of pharmaceutical solids: a critical evaluation of indicator dye-sorption method and its comparison with slurry pH method. *J. Pharm. Sci*., 97, 1831–1842.

159. Sugano, K. (2010). Computational oral absorption simulation of free base drugs. *Int. J. Pharm*., 398(1–2), 73–82.

160. Sugano, K. (2009). A simulation of oral absorption using classical nucleation theory. *Int. J. Pharm*., 378, 142–145.